NAVAL POSTGRADUATE SCHOOL
Monterey, California

THESIS

DYNAMIC ANALYSIS OF THE LOW POWER ATMOSPHERIC COMPENSATION EXPERIMENT (LACE) SPACECRAFT

by

Wesley F. Walters

Thesis Advisor: Ramesh Kolar

Approved for public release; Distribution is unlimited

DISCLAIMER NOTICE

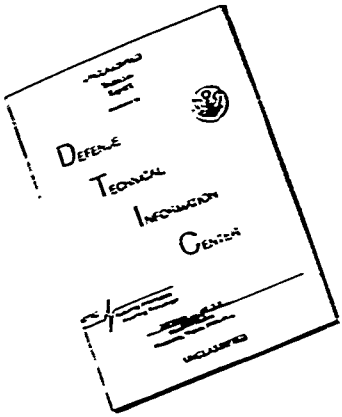

THIS DOCUMENT IS BEST QUALITY AVAILABLE. THE COPY FURNISHED TO DTIC CONTAINED A SIGNIFICANT NUMBER OF PAGES WHICH DO NOT REPRODUCE LEGIBLY.

UNCLASSIFIED

SECURITY CLASSIFICATION OF THIS PAGE

REPORT DOCUMENTATION PAGE

Form Approved OMB No 0704-0188

1a REPORT SECURITY CLASSIFICATION: Unclassified	1b RESTRICTIVE MARKINGS
2a SECURITY CLASSIFICATION AUTHORITY	3 DISTRIBUTION/AVAILABILITY OF REPORT: APPROVED FOR PUBLIC RELEASE; DISTRIBUTION IS UNLIMITED
2b DECLASSIFICATION/DOWNGRADING SCHEDULE	
4 PERFORMING ORGANIZATION REPORT NUMBER(S)	5 MONITORING ORGANIZATION REPORT NUMBERS
6a NAME OF PERFORMING ORGANIZATION: Naval Postgraduate School; 6b OFFICE SYMBOL (If applicable)	7a NAME OF MONITORING ORGANIZATION: Naval Postgraduate School
6c ADDRESS (City, State, and ZIP Code): Monterey, CA 93943-5000	7b ADDRESS (City, State, and ZIP Code): Monterey, CA 93943-5000
8a NAME OF FUNDING/SPONSORING ORGANIZATION; 8b OFFICE SYMBOL (If applicable)	9 PROCUREMENT INSTRUMENT IDENTIFICATION NUMBER
8c ADDRESS (City, State, and ZIP Code)	10 SOURCE OF FUNDING NUMBERS: PROGRAM ELEMENT NO; PROJECT NO; TASK NO; WORK UNIT ACCESSION NO

11 TITLE (Include Security Classification)
DYNAMIC ANALYSIS OF THE LOW POWER ATMOSPHERIC COMPENSATION EXPERIMENT (LACE) SPACECRAFT

12 PERSONAL AUTHOR(S)
WALTERS, WESLEY F.

13a TYPE OF REPORT	13b TIME COVERED	14 DATE OF REPORT (Year, Month Day)	15 PAGE COUNT
Master's Thesis	FROM _____ TO _____	JUNE 1990	218

16 SUPPLEMENTARY NOTATION
The views expressed in this thesis are those of the author and do not reflect the official policy or position of the Department of Defense or the U.S. Government

17 COSATI CODES			18 SUBJECT TERMS (Continue on reverse if necessary and identify by block number)
FIELD	GROUP	SUB GROUP	DYNAMIC ANALYSIS, THERMOELASTIC EFFECTS CHAOTIC VIBRATIONS

19 ABSTRACT (Continue on reverse if necessary and identify by block number)

The Low Power Atmospheric Compensation Experiment (LACE) spacecraft was launched for NRL in February 1990. The LACE flight dynamics experiment will provide on-orbit systems identification of the LACE spacecraft. The experiment is designed to measure modal frequencies, damping ratios and oscillation amplitudes of the LACE spacecraft. The purpose of this study is to develop a finite element model of the LACE spacecraft and conduct a dynamics analysis to determine natural frequencies and mode shapes. Four configurations of the spacecraft are analyzed. This data will be compared with actual orbital data and will provide an opportunity for improvements in the accuracy of computer simulations of flexible structures and multi-body dynamics. Thermoelastic effects due to differential heating are addressed to check the magnitude of deformations that may cause a problem for stability or on-orbit identification. The final phase of this study is to conduct a parametric analysis of the spacecraft boom to investigate the presence of chaotic vibration for combinations of excitation amplitude and frequency.

20 DISTRIBUTION/AVAILABILITY OF ABSTRACT	21 ABSTRACT SECURITY CLASSIFICATION
☒ UNCLASSIFIED/UNLIMITED ☐ SAME AS RPT ☐ DTIC USERS	unclassified
22a NAME OF RESPONSIBLE INDIVIDUAL: RAMESH KOLAR	22b TELEPHONE (Include Area Code): (408) 646-2491; 22c OFFICE SYMBOL: AA/KJ

DD Form 1473, JUN 86 — Previous editions are obsolete — S/N 0102-LF-014-6603

SECURITY CLASSIFICATION OF THIS PAGE: UNCLASSIFIED

Approved for public release; distribution is unlimited.

DYNAMIC ANALYSIS OF THE LOW POWER ATMOSPHERIC COMPENSATION EXPERIMENT (LACE) SPACECRAFT

by

Wesley F. Walters
Major, United States Army
B.S., United States Military Academy, 1977

Submitted in partial fulfillment
of the requirements for the degree of

AERONAUTICAL AND ASTRONAUTICAL ENGINEER

and

MASTER OF SCIENCE IN
ASTRONAUTICAL ENGINEERING

from the

NAVAL POSTGRADUATE SCHOOL
June 1990

Author: Wesley J Walters
Wesley F. Walters

Approved by: Ramesh Kolar
Ramesh Kolar, Thesis Advisor

B.M. Agrawal
Brij Agrawal, Second Reader

E. Roberts Wood, Chairman
Department of Aeronautics and Astronautics

Dean of Faculty
and Graduate Studies

ABSTRACT

The Low Power Atmospheric Compensation Experiment (LACE) spacecraft was launched for NRL in February 1990. The LACE flight dynamics experiment will provide on-orbit systems identification of the LACE spacecraft. The experiment is designed to measure modal frequencies, damping ratios, and oscillation amplitudes of the LACE spacecraft. The purpose of this study is to develop a finite element model of the LACE spacecraft and conduct a dynamics analysis to determine natural frequencies and mode shapes. Four configurations of the spacecraft are analyzed. This data will be compared with actual orbital data and will provide an opportunity for improvements in the accuracy of computer simulations of flexible structures and multi-body dynamics. Thermoelastic effects due to differential heating are addressed to check the magnitude of deformations that may cause a problem for stability or on-orbit identification. The final phase of this study is to conduct a parametric analysis of the spacecraft boom to investigate the presence of chaotic vibration for combinations of excitation amplitude and frequency.

TABLE OF CONTENTS

ACKNOWLEDGEMENTS

I would like to thank Ram Nagulpally, CASA Gifts, Inc., Al Frazier, ABLE-AEC Engineering, and Mike Fisher, NRL, for their technical support and advice. I would like to especially thank my advisor, Professor Ramesh Kolar, for his direction, guidance and help in completing this project. He has helped me to develop an interest in the field of chaotic vibrations and non-linear systems.

I would also like to thank Ann Warner for her hard work and dedication in formatting and typing this document.

Finally, I would like to thank my wife, Suzanne, for her support and understanding during these three years in Monterey.

I. INTRODUCTION

A. PURPOSE

This study is concerned with the modeling and analysis of the Low Power Atmospheric Compensation Experiment (LACE) spacecraft. One of the missions of the LACE spacecraft is to conduct and obtain flight data for on-orbit system identification. The flight dynamics experiment is designed to measure modal frequencies, damping ratios, oscillation amplitude of the LACE spacecraft and vibration intensity generated by boom deployments and retractions. This experiment will provide an opportunity for improvements in the accuracy of computer simulations of large flexible space structures and multi-body dynamics.

It will also provide a mechanism for evaluating influence of magnetic torques, gravity gradient torques and atmospheric drag on the LACE-type structures.

The purpose of this study is to develop a finite element model of the LACE spacecraft using the finite element program Graphical Interactive Element Total System (GIFTS). Dynamic analysis is performed on the model to determine the natural frequencies and mode shapes. Thermoelastic effects due to differential heating are addressed to check if the magnitude of deformations could cause a problem for stability or system

identification. Finally, a parametric analysis is conducted on a model of the spacecraft boom to investigate the possibility of chaotic vibrations that may be induced during the mission.

B. OVERVIEW/BACKGROUND

1. Spacecraft Description

NRL-developed LACE was successfully launched on February 14, 1990, from Cape Canaveral on a DELTA II launch vehicle. The spacecraft incorporates three deployable/retractable booms of maximum length 150 feet. The 2,800 lb. LACE spacecraft is stabilized by a 150 ft. zenith directed gravity gradient boom mounted on top of the spacecraft, a momentum wheel with axis along the pitch axis and a magnetic damper at the tip of the gravity gradient boom. The retroreflector boom is mounted forward and deployed along the velocity vector, while the balance boom is mounted and pointed aft. Figure 1 shows the basic configuration of the spacecraft.

2. Experimental Hardware

The flight dynamics experiment hardware consists of three germanium corner cubes mounted on the lead boom, on the bottom of the bus and on the aft balance boom to serve as targets for the 10.6 micron Firepond laser radar at MIT Lincoln Laboratory, Lexington, Massachusetts. The Firepond laser has a 4 millisecond square wave pulse at a frequency of 62.5 Hz and pulse energy of 3.2 joules. The Firepond laser radar will illuminate the cubes to measure the relative motion

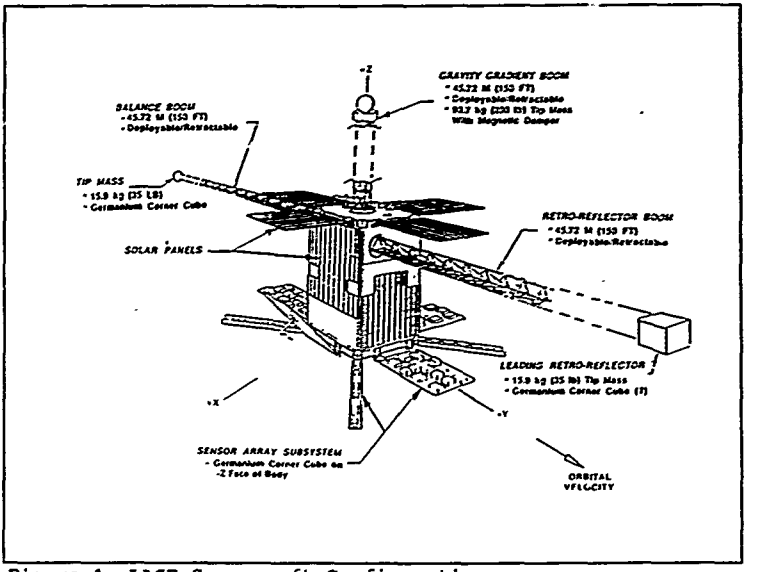

Figure 1. LACE Spacecraft Configuration

of the boom with respect to the main body. Reflections from the corner cubes will give differential Doppler information on the magnitude of the displacement rates due to boom flexure. [Ref. 1]

The Ultra-Violet Plume Instrument (UVPI) will be used to measure the absolute bus rotation rate. It has the capability of resolving angular velocities of $5 * 10^{-5}$ radian/sec. [Ref. 2]

Figure 2 depicts the LACE flight dynamics experiment.

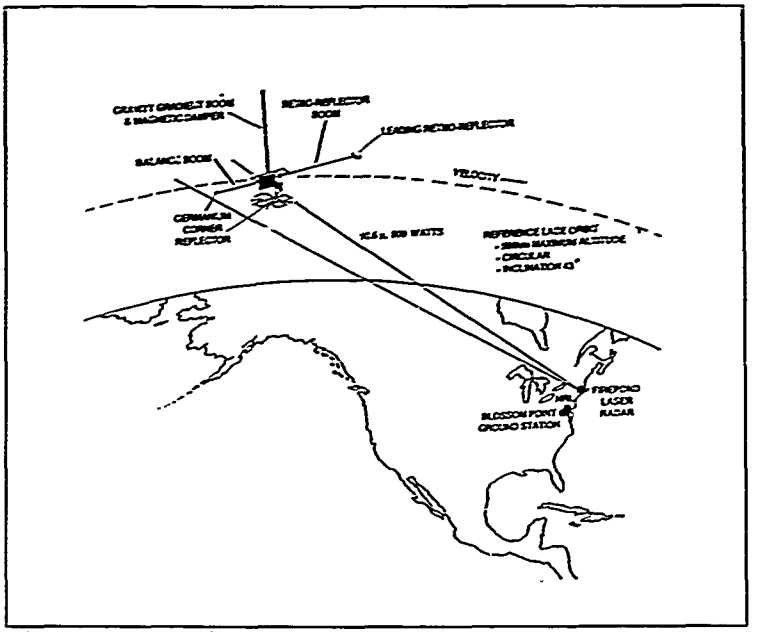

Figure 2. LACE Flight Dynamics Experiment

3. Acquisition Sequence

The recommended acquisition sequence for the LACE spacecraft calls for four different boom deployments. Initially, the gravity gradient will be extended to 75 feet. After the spacecraft has stabilized, the boom will be deployed to 150 feet and the momentum wheel will be spun up. Then the leading (retroreflector) and tracking (balance) booms will be extended to 119.5 feet. The final configuration will have the retroreflector boom and gravity gradient boom extended to 150 feet and the trailing balance boom extended to 75 feet.

4. Orbital Parameters

Table I lists the orbital parameters for LACE.

Table I. LACE ORBITAL PARAMETERS

Altitude	541 km
Period	95.47 min
Inclination	43.087 degrees
Eccentricity	.00108
Semi-major Axis	6919.351 km

C. MOTIVATION

During the past five years, system identification of flexible space structures has emerged as an important problem. Many proposed space missions will involve large space structures that are very flexible, contain thousands of structural elements and have special mission requirements, such as pointing accuracies. Some of these structures include space defense platforms, solar power stations and manned laboratories, such as the space station. These structures may require some type of active control to carry out ongoing maneuvers, suppress and control vibration and achieve accurate and reliable pointing. An obstacle to meeting some of these objectives can be attributed to the inability to analytically model the structural dynamics of these highly flexible structures with a high degree of confidence or precision. Typically, such information is also required in the design of vibration suppression and control systems.

The inability to model dynamics of large flexible structures is caused by four factors:

1. Because of launch costs, large space structures are constructed out of very light composites and cannot support their weight in gravity. This prevents ground-based testing.

2. New composite materials will result in modeling uncertainty of the material properties.

3. Complications arise from the combination of very high flexibility and large thermal gradients.

4. On-orbit structure will be exposed to harsh space environments which include particle radiation, solar effects, gravitational anomalies, extreme temperatures and near vacuum. The structure may undergo physical parameter changes. [Ref. 3]

General purpose structural modeling and multi-body dynamics computer programs such as GIFTS and TREETOPS, respectively, can be used to define and investigate complex space structures. However, there is no assurance that optimum structural models can be generated with these programs. It is envisioned that the on-orbit data received from LACE can be used to improve these computer models.

D. THESIS OUTLINE

This study contains eight chapters. The second chapter provides a discussion of the theoretical basis adopted by GIFTS to develop a finite element model and provide dynamic analysis. Chapter III describes the development of the simple beam model and complex finite element model of the LACE spacecraft. Chapter IV provides the natural frequencies and

mode shapes of the spacecraft. In Chapter V a thermoelastic analysis is conducted on the LACE spacecraft boom to determine the effects of differential heating. Chapter VI discusses multi-body dynamics and describes a multi-body program called TREETOPS. Chapter VII gives a description and a method to identify chaotic vibrations. A parametric analysis of the LACE spacecraft boom modeled as a single degree of freedom system is provided to determine if chaotic vibrations may be induced. The model uses experimental data for stiffness, mass and damping and examines the behavior for possible chaos in the system. Chapter VIII contains conclusions and scope for future research.

II. THEORETICAL FORMULATION

A. FINITE ELEMENT METHOD

The finite element method is a numerical procedure to compute the response of complex structures. The basic unit of this analysis, the discrete finite element, is a geometrically simplified representation of a small part of the physical structure. The finite element method views the complete complex structure as an assembly of a finite number of these finite discrete elements (beams, rods, plates, etc.), each of whose properties and deformation responses are simple, as compared to the complete structure. The division of the discrete elements is natural, in general, and follows the way the actual structure is built (truss members, frames, etc.). The elements interconnect at nodes where the elements meet and move in unison only after compatibility requirements are met. This assures that adjacent elements will not overlap or separate.

Each node has six degrees of freedom with three deflections and three rotations. Based on how the elements are connected at the rods, the computed properties of the individual elements are determined and assembled to obtain the equivalent, but more complex properties of the entire assembled model. The structural model created can then be used

to predict the behavior of the real structure. In this study, the structural model will be used to determine the structure's natural frequencies and mode shapes. The finite element types used to model the LACE spacecraft include rod, beam and plate/shell elements. These elements will be discussed further in accordance with the theory adopted used by GIFTS.

1. Rod Elements

Rod elements are pin-jointed truss members that are capable of carrying axial forces only. Figure 3 shows a typical rod element.

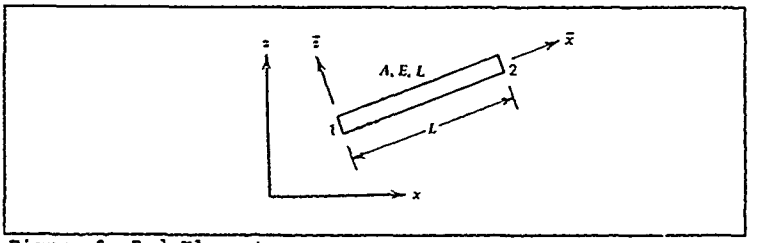

Figure 3. Rod Elements

The element is located in the (x-y-z) coordinate system, which is also known as the reference or global coordinate system. Coordinates along the element are the local or element coordinate system ($\bar{x}$-$\bar{y}$-$\bar{z}$).

The following derivations can be found in more detail in Allen and Haisler [Ref. 4: section 7.2]. The element stiffness matrix, derived from the principle of virtual work, in local coordinate system, is defined by the equation

$$[\bar{K}] = \frac{AE}{L}\begin{bmatrix} 1 & -1 \\ -1 & 1 \end{bmatrix} \qquad (1)$$

The matrix $[\bar{K}]$ represents the truss element stiffness matrix in the local coordinate system.

Figure 4 shows the rod element oriented at a positive angle θ relative to the global axis.

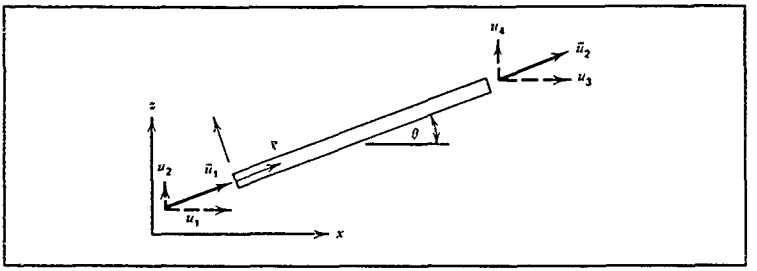

Figure 4. Rod Element at θ

Element and global displacements at nodes 1 and 2 are related by

$$\begin{Bmatrix} \bar{u}_1 \\ \bar{u}_2 \end{Bmatrix} = \begin{bmatrix} \cos\theta & \sin\theta & 0 & 0 \\ 0 & 0 & \cos\theta & \sin\theta \end{bmatrix} \begin{Bmatrix} u_1 \\ u_2 \\ u_3 \\ u_4 \end{Bmatrix} \qquad (2)$$

or

$$\{\bar{u}\} = [T]\{u\} \tag{3}$$

where

$$[T] = \begin{bmatrix} \cos\theta & \sin\theta & 0 & 0 \\ 0 & 0 & \cos\theta & \sin\theta \end{bmatrix} \tag{4}$$

Using the strain energy equation and the matrix product transpose rule, the following relations are derived:

$$u = \frac{1}{2}\{\bar{u}\}[\bar{K}]\{\bar{u}\}$$

$$= \frac{1}{2}\{u\}[K]\{u\} \tag{5}$$

where

$$[K] = [T]^T[\bar{K}][T] \tag{6}$$

Therefore, using equations (1) and (6), [K] is transformed to the global coordinate system to obtain

$$K = \frac{AE}{L}\begin{bmatrix} c^2 & cs & -c^2 & -cs \\ cs & s^2 & -cs & -s^2 \\ -c^2 & -cs & c^2 & cs \\ -cs & -s^2 & cs & s^2 \end{bmatrix} \tag{7}$$

where $c = \cos\theta$ and $s = \sin\theta$.

2. Beam Elements

Beam elements are characterized as members that are capable of resisting bending. The beam element will carry axial forces, shear forces and bending moments. Figure 5 depicts a typical planar beam finite element.

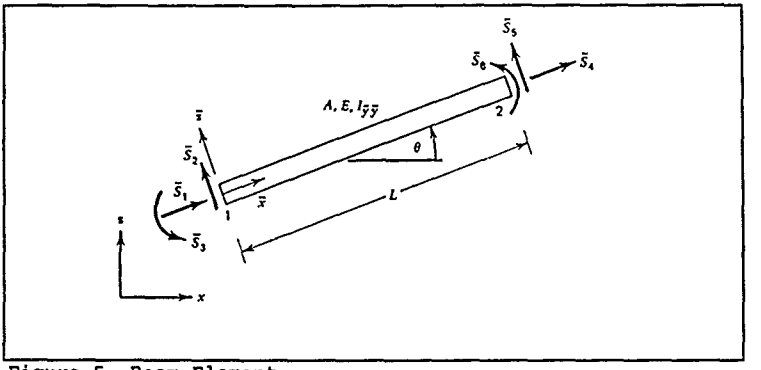

Figure 5. Beam Element

The following can be found in more detail in Allen and Haisler [Ref. 4: section 7.3.]

The stiffness matrix is defined by the equation

$$[\bar{K}] = \begin{bmatrix} \frac{EA}{L} & 0 & 0 & \frac{-EA}{L} & 0 & 0 \\ 0 & \frac{12EI}{L^3} & \frac{6EI}{L^2} & 0 & \frac{-12EI}{L^3} & \frac{6EI}{L^2} \\ 0 & \frac{6EI}{L^2} & \frac{4EI}{L} & 0 & \frac{-6EI}{L^2} & \frac{2EI}{L} \\ \frac{-EA}{L} & 0 & 0 & \frac{EA}{L} & 0 & 0 \\ 0 & \frac{-12EI}{L^3} & \frac{-6EI}{L^3} & 0 & \frac{12EI}{L^3} & \frac{-6EI}{L^2} \\ 0 & \frac{6EI}{L^2} & \frac{2EI}{L} & 0 & \frac{-6EI}{L^2} & \frac{4EI}{L} \end{bmatrix} \qquad (8)$$

where $I = I_{yy}$.

In order to assemble the stiffness matrices, they must be transformed to global coordinates. The local-global transformation, as before, is given by

$$[T] = \begin{bmatrix} c & s & 0 & 0 & 0 & 0 \\ -s & c & 0 & 0 & 0 & 0 \\ 0 & 0 & 1 & 0 & 0 & 0 \\ 0 & 0 & 0 & c & s & 0 \\ 0 & 0 & 0 & -s & c & 0 \\ 0 & 0 & 0 & 0 & 0 & 1 \end{bmatrix} \qquad (9)$$

where $c = \cos\theta$ and $s = \sin\theta$.

The remainder of the finite element formulation is similar to the previous section on rod elements. The stiffness matrix in global coordinates is constructed using equations (6), (8) and (9).

3. Plate Bending Theory

A flat plate, like a beam, supports transverse loads and offers resistance to bending. Figure 6 shows stresses that act on a homogeneous linearly elastic plate.

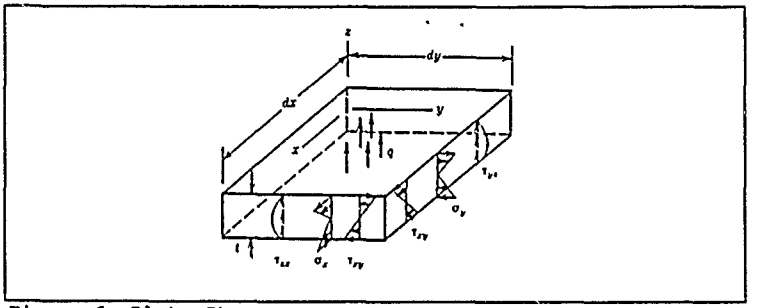

Figure 6. Plate Stresses

The normal stresses σ_x and σ_y vary linearly with z and contribute to bending moments M_x and M_y.

The normal stress σ_z is negligible when compared with σ_x, σ_y and τ_{xy}. The transverse shear stresses τ_{yz} and τ_{zx} vary quadratically with z. Plate bending in this analysis refers to external loads perpendicular to the xy plane and applied moments. [Ref. 5]

The stresses shown in Figure 6 result in the following equations [Ref. 5] for bending moments M and transverse shears Q.

$$M_x = \int_{-t/2}^{t/2} \sigma_x z dz \qquad M_y = \int_{-t/2}^{t/2} \sigma_y z dz \qquad M_{xy} = \int_{-t/2}^{t/2} \tau_{xy} z dz \quad \text{(10a)}$$

$$Q_x = \int_{-t/2}^{t/2} \tau_{zx} dz \qquad Q_y = \int_{-t/2}^{t/2} \tau_{yz} dz \quad \text{(10b)}$$

Stresses σ_x and σ_y are greatest at the surface $z=\pm t/2$, while τ_{xy} is maximum at the midsurface. Transverse shear stresses τ_{yz}, τ_{zx} are small compared to σ_x, σ_y and τ_{xy}, and are not considered in the classical Kirchhoff plate theory.

In what follows, Kirchhoff's plate theory [Ref. 5] is briefly reviewed, which forms the basis for the GIFTS formulation.

As transverse loads are applied to the plate, the points on the midsurface move only in the z direction. Under loads, normals to the midsurface are assumed to remain normal before and after deformation. Figure 7 shows a differential element of a thin plate before and after loading. As shown, the line OP is perpendicular to the midsurface before and after loading.

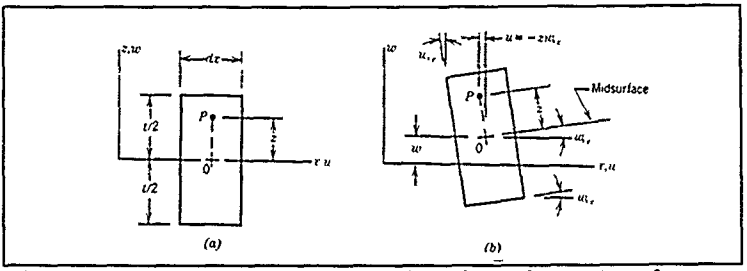

Figure 7. Differential Element of a Thin Plate a) Before Loading b) After Loading

From Figure 7, with $\frac{\partial w}{\partial x}$ and $\frac{\partial w}{\partial y}$ being assumed as small angles, the following relations apply:

$$u = -z\frac{\partial w}{\partial x} \quad \text{hence} \quad \epsilon_x = \frac{\partial u}{\partial x} = -z\frac{\partial^2 w}{\partial x^2}$$

$$v = -z\frac{\partial w}{\partial y} \qquad \epsilon_y = \frac{\partial v}{\partial y} = -z\frac{\partial^2 w}{\partial y^2} \qquad (11)$$

$$\gamma_{xy} = \frac{\partial u}{\partial y} + \frac{\partial v}{\partial x} = -2z\frac{\partial^2 w}{\partial x \partial y}$$

These are the strain displacement relations in accordance with classical Kirchhoff's plate theory applied to a thin plate.

By using stress-strain relations, the moment-curvature relations may be derived. Neglecting thermal expansion and assuming isotropic material, stress-strain relations are given by:

$$\begin{Bmatrix}\sigma_x\\ \sigma_y\\ \tau_{xy}\end{Bmatrix} = \frac{E}{(1-\nu^2)}\begin{bmatrix}1 & \nu & 0\\ \nu & 1 & 0\\ 0 & 0 & \frac{1-\nu}{2}\end{bmatrix}\begin{Bmatrix}e_x\\ e_y\\ \gamma_{xy}\end{Bmatrix} \qquad (12)$$

By substituting equation (11) into equation (12) and substituting the result into equation (10a), the following is obtained:

$$\{M\} = -[D_k]\{\kappa\} \qquad (13)$$

where the moments and curvatures are

$$\{M\} = \lfloor M_x\ M_y\ M_{xy} \rfloor^T \quad ; \quad \{\kappa\} = \lfloor \frac{\partial^2 w}{\partial x^2}\ \frac{\partial^2 w}{\partial y^2}\ 2\frac{\partial^2 w}{\partial x \partial y} \rfloor \qquad (14)$$

and

$$[D_k] = D\begin{bmatrix}1 & \nu & 0\\ \nu & 1 & 0\\ 0 & 0 & \frac{(1-\nu)}{2}\end{bmatrix} \qquad (15)$$

where $D = \frac{Et^3}{12(1-\nu^2)}$. D is called the flexural rigidity of the plate and is analogous to bending stiffness EI of a beam.

The next step is to formulate the element stiffness matrix using the virtual work equation:

$$\delta W_{int} = \int_v \frac{1}{2}\{\delta e\}^T [E]\{\delta e\}\, dv \qquad (16)$$

where

$$\{e\}^T = \left\lfloor -z\frac{\partial^2 w}{\partial x^2} \; -z\frac{\partial^2 w}{\partial y^2} \; -2z\frac{\partial^2 w}{\partial x \partial y} \right\rfloor$$

and where [E] is given by equation (12). δw_{int} and δe are the internal virtual work and virtual strains respectively.

For plates, using the strain-displacement relations,

$$\delta w_{int} = \int_A \frac{1}{2} \{\kappa\}^T [D_b] \{\kappa\} \, dA, \text{ where } \{\kappa\}^T = \left\lfloor \frac{\partial^2 w}{\partial x^2} \frac{\partial^2 w}{\partial y^2} \frac{\partial^2 w}{\partial x \partial y} \right\rfloor \quad (17)$$

For an element having N nodes, displacements W is interpolated as

$$W = \underset{1x3N}{\lfloor N \rfloor} \{d\} \quad (18)$$

where the nodal degrees of freedom are given by

$$\{d\} = \left\lfloor w_1 \frac{\partial w}{\partial x_1} \frac{\partial w}{\partial y_1} \ldots w_N \frac{\partial w}{\partial x_N} \frac{\partial w}{\partial y_N} \right\rfloor^T$$

Equation (18) is differentiated to yield curvatures

$$\{\kappa\} = \underset{3x3N}{[B]} \{d\} \quad (19)$$

On substituting equation (19) into equation (17) yields

$$\delta w_{int} = \{\delta d\}^T [K] \{d\} \quad (20)$$

where the element stiffness matrix [K] is identified as

$$\underset{3Nx3N}{[K]} = \int_A [B]^T [D_b] [B] \, dA \quad (21)$$

B. FREE VIBRATION OF MULTI-DEGREE-OF-FREEDOM SYSTEMS

Craig [Ref. 6] provides a good overview of multi-degree-of-freedom (MDOF) systems.

The equation of motion for a free undamped MDOF system can be written as

$$[m]\{\ddot{u}\} + [K]\{u\} = \{0\} \tag{22}$$

where [m] and [K] are (NxN) matrices and {u(t)} is a Nx1 vector of generalized displacement coordinates. The solution of the differential equation gives harmonic motion given by

$$u = u_o \cos(wt-\alpha) \tag{23}$$

Substituting equation (23) into (22) yields the eigenvalue problem

$$([K] - w^2[m])\{u\} = 0 \tag{24}$$

For non-trivial solution,

$$|K - w^2 m| = 0 \tag{25}$$

Equation 25 is recognized as the characteristic equation for the free vibration response. The resulting polynomial in w^2 yields the roots or the eigenvalues which correspond to the natural frequencies of the system.

Corresponding to each eigenvalue, w_r^2, there will be an eigenvector or natural mode u_r, where

$$u_r = \begin{Bmatrix} u_1 \\ u_2 \\ \cdot \\ \cdot \\ \cdot \\ u_N \end{Bmatrix} \quad r = 1,2,\ldots,N \tag{26}$$

Typically, these modes may be scaled by a process called normalization and results in modal vectors called normal modes. A mode that has been scaled to have a unique amplitude will be designated as ϕ_r and will be dimensionless. The modal vector corresponding to w_r can be written

$$\mu_r = c_r \phi_r \tag{27}$$

where c_r is a scaling constant whose units are such that $\phi_r^T m \phi_r$ has the dimension of mass.

There are three procedures for normalizing modes for MDOF systems. [Ref. 6]

1. Scale the r^{th} mode so that $(\phi_i)_r=1$ at a specified coordinate i.
2. Scale the r^{th} mode so that $(\phi_i)_r=1$, where $|(\phi_i)_r|=\max_j|(\phi_j)_r|$,
3. Scale the r^{th} mode so that the generalized mass is defined by

$$m_r = \phi_r^T m \phi_r \tag{28}$$

The generalized stiffness for the r^{th} mode is

$$K_r = \phi_r^T k \phi_r \tag{29}$$

By expressing equation (24) for the r^{th} mode and premultipling by ϕ_r^T, the generalized stiffness-mass relations are obtained as

$$K_r = w_r^2 m_r \tag{30}$$

C. NUMERICAL EVALUATION OF MODES AND FREQUENCIES OF MDOF SYSTEMS

This section discusses the procedure used by GIFTS to obtain numerical solution to large eigenproblems. The LACE spacecraft in its fully deployed state was modeled by over 16,000 degrees of freedom. The dynamic analysis of this structure involves determining the natural frequencies and the corresponding natural modes by solving the equation

$$(K - w_i^2)\,\phi_i = 0 \tag{31}$$

Vector iteration methods are simple and elegant for obtaining eigenpairs. The specific method used by GIFTS is the subspace iteration method. The subspace iteration solution is very effective in the calculation of the lowest eigenvalue and corresponding eigenvectors of systems with large bandwidth and which are too large for the high-speed storage of the computer. [Ref. 7]

Bathe [Ref. 8] establishes three steps for the subspace iteration method.

1. Establish q starting iteration vectors, q>p, where p is the number of eigenvalues and vectors to be calculated.

2. Use simultaneous inverse iteration on the q vectors and Ritz analysis to extract the best eigenvalue and eigenvector approximations from the q iteration vectors.

3. After convergence, the Sturm sequence check is used to verify that the required eigenvalues and corresponding eigenvectors have been calculated.

The objective of the subspace iteration method is to solve for the lowest p eigenvalues and eigenvectors satisfying

$$K\Phi = M\Phi\Lambda \tag{32}$$

where Λ =diagonal (λ_i) and $\Phi = [\phi_1, \ldots \phi_p]$. The eigenvectors must also satisfy the orthogonality conditions

$$\Phi^T K \Phi = \Lambda \; ; \; \Phi^T M \Phi = I \tag{33}$$

Detailed derivations of the subspace iteration method are shown in Bathe [Ref. 8]. The subspace iteration algorithm shown below finds an orthogonal basis of vectors in E_{L+1} subspace.

$$K\bar{X}_{L+1} = MX_L \tag{34}$$

for L=1,2,..., and with iterations from E_L to E_{L+1}. Next, projections of the operators K and M onto K_{L+1} are computed:

$$K_{L+1} = \bar{X}_{L+1}^T K \bar{X}_{L+1} \tag{35}$$

$$M_{L+1} = \bar{X}_{L+1}^T M \bar{X}_{L+1} \tag{36}$$

By solving for the eigensystem of projected operators

$$K_{L+1} Q_{L+1} = M_{L+1} Q_{L+1} \Lambda_{L+1} \tag{37}$$

where Q is an orthogonal matrix, improved approximation for the eigenvectors is found by

$$X_{L+1} = \bar{X}_{L+1} Q_{L+1} \tag{38}$$

It may be noted that $\Lambda_{L+1} \dashrightarrow \Lambda$ and $X_{L+1} \dashrightarrow \phi$ as $L \dashrightarrow \infty$.

The first step of the subspace iteration is to generate the starting iteration vectors in X_1. The following algorithm is used to select the starting iteration vector. The first column in MX_1 is the diagonal of M. The other columns are unit vectors with entries +1 at coordinates with the smallest k_n/m_n ratio.

The subspace iteration method requires a measure to compute convergence. Assuming that in (L-1) and L iterations, eigenvalue approximations $\lambda_i^{(L)}$ and $\lambda_i^{(L+1)}$, i=1,...p, have been calculated. The measure for convergence, then, is

$$\frac{|\lambda_i^{(L+1)} - \lambda_i^{(L)}|}{\lambda_i^{(L+1)}} \leq tol \quad ; \quad i = 1, \ldots p. \tag{39}$$

where tol may be 10^{-2S}, when eigenvalues shall be accurate to 2S digits.

Since equations (32) and (33) can be satisfied by any eigenpairs, there must be a way to verify the calculations. Once the convergence is satisfied in equation (39), with s being at least equal to 3, a check may be performed to make sure that the smallest eigenvalues and corresponding eigenvectors have been calculated. The Sturm sequence property is used to provide this check. This property is derived from the following analysis. [Ref. 8] By using the Gauss elimination solution, the stiffness matrix can be factorized as

$$K = LDL^T \tag{40}$$

where L is a lower unit triangular matrix and D is the diagonal matrix.

Let $K-\mu M$ be factorized into LDL^T. In the decomposition of $K-\mu M$, the number of negative elements in D is equal to the number of eigenvalues smaller than μ. Because of this property, by assuming a shift μ and checking whether μ is smaller or larger than the required eigenvalue, successive iterations can reduce the interval in which the eigenvalue must be. A summary of subspace iteration solution is shown in Table II.

Table II. SUMMARY OF SUBSPACE ITERATION

Operation	Calculation	Number of Operations: $m = m_K = m_M$	Number of Operations: $m = m_K$, $m_M = 0$	Required Storage
Factorization of K	$K = LDL^T$	$\frac{1}{2}nm^2 + \frac{1}{2}nm$	$\frac{1}{2}nm^2 + \frac{1}{2}nm$	
Subspace iteration	$K\bar{X}_{k+1} = Y_k$	$nq(2m + 1)$	$nq(2m + 1)$	
	$K_{k+1} = \bar{X}_{k+1}^T Y_k$	$\frac{1}{2}nq(q + 1)$	$\frac{1}{2}nq(q + 1)$	
	$\bar{Y}_{k+1} = M\bar{X}_{k+1}$	$nq(2m + 1)$	nq	
	$M_{k+1} = \bar{X}_{k+1}^T \bar{Y}_{k+1}$	$\frac{1}{2}nq(q + 1)$	$\frac{1}{2}nq(q + 1)$	Algorithm is effectively implemented as out-of-core solver
	$K_{k+1}Q_{k+1} = M_{k+1}Q_{k+1}\Lambda_{k+1}$		$O(q^3)$ neglected	
	$Y_{k+1} = \bar{Y}_{k+1}Q_{k+1}$	nq^2	nq^2	
Sturm sequence check	$\bar{K} = K - \mu M$	$n(m + 1)$	n	
	$\bar{K} = LDL^T$	$\frac{1}{2}nm^2 + \frac{1}{2}nm$	$\frac{1}{2}nm^2 + \frac{1}{2}nm$	
Error estimates	$\frac{\|K\phi_i^{(q+1)} - \lambda_i^{(q+1)}M\phi_i^{(q+1)}\|_2}{\|K\phi_i^{(q+1)}\|_2}$	$4nm + 5n$	$2nm + 5n$	
Total for solution of p lowest eigenvalues and associated eigenvectors, assuming that ten iterations are required and $q = \min\{2p, p + 8\}$		$nm^2 + nm(4 + 4p) + 5np + 20nq(2m + q + \frac{1}{2})$	$nm^2 + nm(3 + 2p) + 5np + 20nq(m + q + \frac{1}{2})$	

III. LACE FINITE ELEMENT MODEL

A. GIFTS CAPABILITIES

GIFTS has several capabilities which facilitate the modeling of large complex structures. Some of these capabilities include:

1. automatic model generation
2. model editing, display and information
3. automatic load and boundary conditions
4. vibrational mode extraction
5. substructuring
6. thermal stress analysis

Element types that can be used include:

1. rods and beams
2. plates/shells
3. solid elements and axisymmetric elements [Ref. 9]

The elements can be selected from a library of options. The materials can be created by the user or from a library of defined materials. GIFTS also allows users to define anisotropic materials.

Static and dynamic analysis can be performed on the model. The dynamic analysis provides free vibrations and mode shapes. These vibrational mode shapes can be displayed on the screen. For structures that undergo thermal loading, deflections and

stresses can be calculated by computing thermal (pseudo-forces) forces to simulate the thermal effects.

GIFTS also has the capability for substructuring and multi-level substructuring. Large models may be divided into substructures. Certain areas of a substructure may be modeled as a second level substructure to allow economic modeling and reduce computational costs.

B. SIMPLE FINITE ELEMENT MODEL OF LACE

Initially, the LACE spacecraft is modeled as a point mass with three attached beam members. The three dimensional triangular trusses are modeled as solid circular beams. To ensure that this beam had the same bending characteristics, the following bending stiffness relations was used from A&C-Able Engineering [Ref. 10].

$$\textit{flexural rigidity } (EI) = 1.5\,\pi E R^4 e^2 \qquad (41)$$

where

- e = maximum bending strain of longerons when completely coiled ($e = d/2R = F/E$)
- F = coiling stress of longerons
- d = longeron diameter
- E = Young's modulus of longeron material
- R = boom radius

with

- e = .015
- R = 5.0 inches
- E = 8.0×10^6 psi

This results in EI = 5.3×10^6 lbs-in^2.

From this relation, I is seen to be .663 which results in a solid circular beam with a radius of .9583 inches. The beam is with 10 elements for a 150 foot truss and 5 elements for a 75 ft. truss. This model is used in GIFTS with the appropriate tip masses to determine the natural frequencies and mode shapes. The results will be shown and discussed in the next chapter. A listing of the file to generate the model is given in Appendix A.

C. COMPLEX FINITE ELEMENT MODEL OF LACE

1. Main Spacecraft Body

The on-orbit configuration of the LACE spacecraft is shown in Figure 8. From the figure, it can be seen that the LACE spacecraft consists of structural panels, solar panels, sensor panels, truss elements and various beam types.

The primary structure of LACE consists of a frame type structure consisting of channel section stringers, tee-section stringers, z-section doublers, and angle-section members. The primary structure also consists of honeycomb panels. Figures 9a and 9b show the basic configuration of the primary structure.

The secondary structure of the LACE spacecraft consists of the fixed and deployable solar array substrate, deployable sensor panels and deployable sensor arms. Figure 10 shows the LACE spacecraft secondary structure.

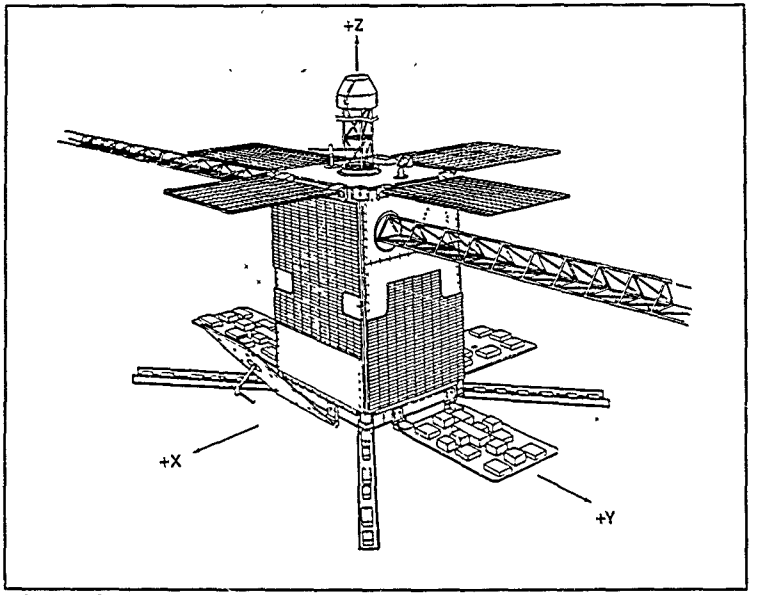

Figure 8. LACE Spacecraft On-Orbit Configuration

The primary frame members are made of aluminum, AL6061-T6. Table III shows the material characteristics of AL6061-T6 used in GIFTS.

Table III. AL6061-T6 CHARACTERISTICS

Yield Stress	1.8 E4 psi
Young's Modulus	9.9 E6 psi
Poisson's Ratio	.33
Mass Density	2.5382 E-4 lbs-sec^2/in^4

The honeycomb panels consist of .05 thick face sheets consisting of aluminum, AL6061-T6. The core of the panels are 1/4 -5052 -.003, with a density of .01552 lbs-sec^2/in^4.

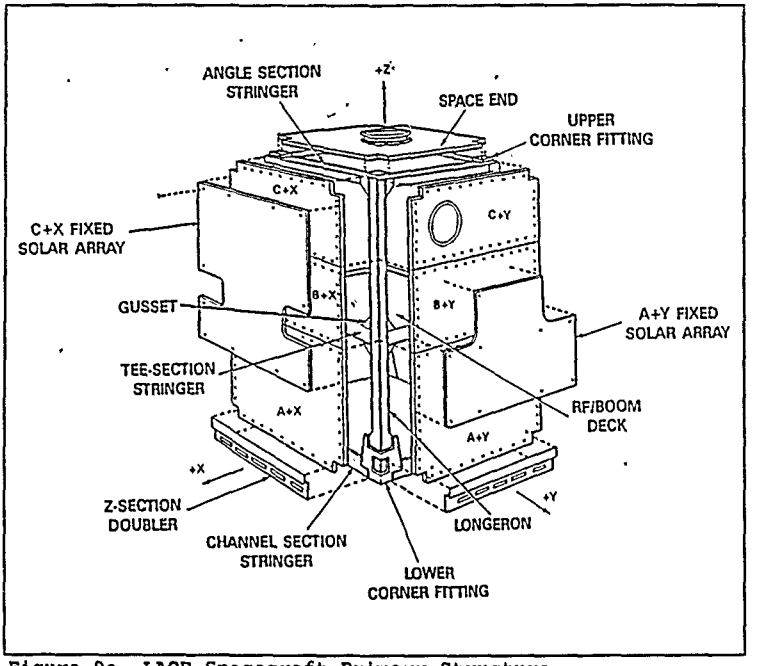

Figure 9a. LACE Spacecraft Primary Structure

Figures 11a and 11b show the primary and secondary honeycomb panel structure and dimensions.

The primary panels are one inch thick with a .9 inch core. The solar array panels are .5 inches thick with a .4 inch core and the deployable sensor panels are .75 inches thick with a core of .65. The deployable sensor arms are channel beams with .125 inch thick aluminum, AL6061-T6.

The honeycomb panels are modeled as aluminum panels, AL6061-T6, with appropriate conversions to account for

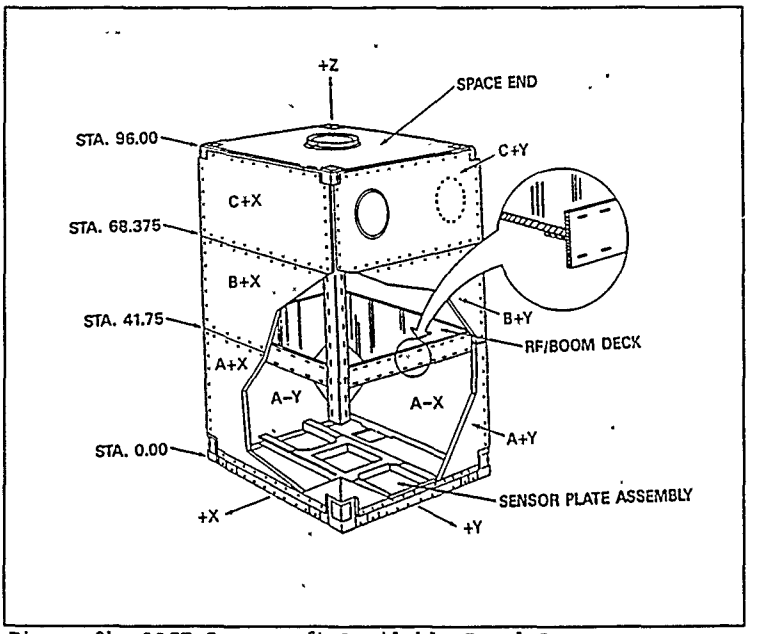

Figure 9b. LACE Spacecraft Available Panel Area

equivalent stiffness and weight. The panel stiffness for a honeycomb panel is given by [Ref. 11]

$$D = \frac{Eth^2}{2\ (1 - \nu^2)} \qquad (42)$$

where

E = Young's modulus
t = face thickness of the panel
h = core thickness
υ = Poisson's ratio

The stiffness for each honeycomb panel is calculated using the above formula.

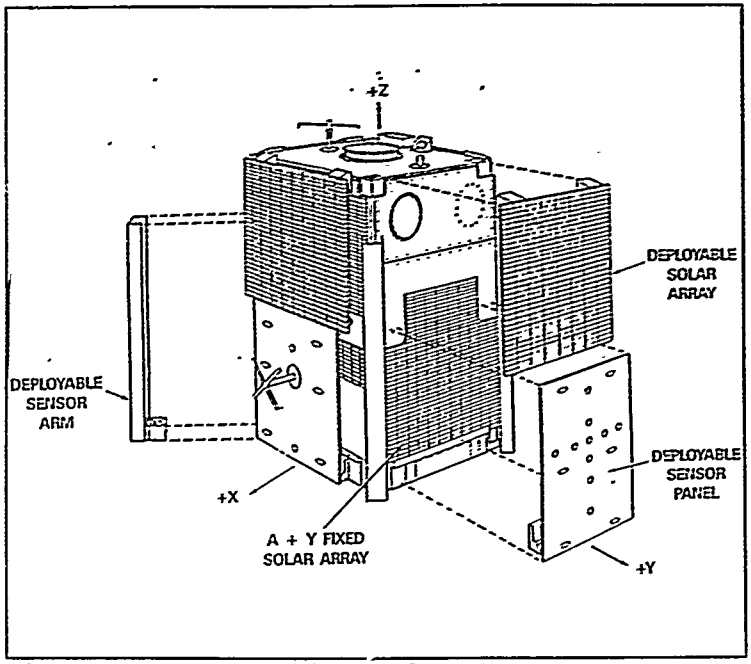

Figure 10. LACE Spacecraft Secondary Structure

Using the stiffness, an equivalent thickness is calculated, using the flexural rigidity formula for isotropic materials.

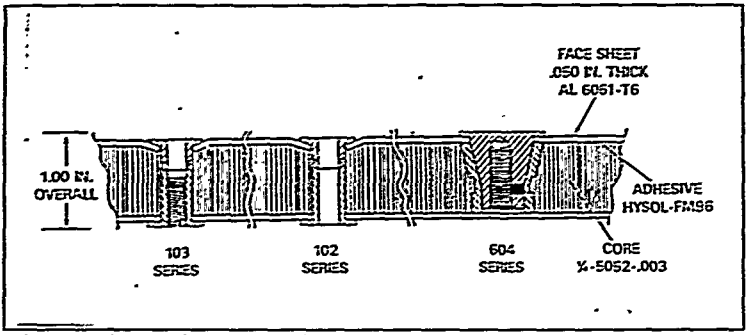

Figure 11a. Primary Panel

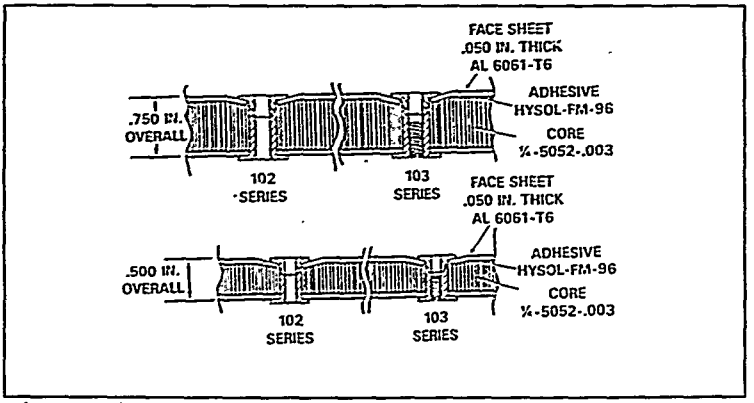

Figure 11b. Secondary Panels

$$D = \frac{E\,t^3}{12\,(1-\nu^2)} \qquad (43)$$

The mass of the honeycomb panels is computed and used with the new thickness to determine volume and density. These calculations are presented in Appendix B. Table IV summarizes

the new parameters used to model the honeycomb panels as aluminum panels with appropriate stiffness and mass.

Table IV. THICKNESS AND DENSITY PARAMETERS

	Thickness (in)	Density ($lbs\text{-}sec^2/in^4$)
Primary Panels	.624	5.364×10^{-5}
Solar Panels	.3634	8.1915×10^{-5}
Sensor Panels	.502	6.22×10^{-5}

The finite elements model of the main body of the LACE spacecraft is shown in Figure 12. The associated file to generate the model is given in Appendix C.

The LACE spacecraft has several sensors and components. Even though the spacecraft is essentially a rigid body, the mass of the components was modeled as accurately as possible according to the mesh size of the grids. Appendix D contains the component placements and mass distributions.

2. Spacecraft Trusses

The automatic deployable lattice booms are manufactured by AEC-Able Engineering Company, Inc. They are designed for applications that require high dimensional stability and high ratio of bending stiffness to weight. Figure 13 shows the principal parts of the continuous longeron boom and the retraction geometry. The longerons are continuous along the length and are connected to the batten frames with pivot fittings. Six diagonals provide shearing strength and stiffnesses. When the boom is twisted, tension increases on three of the diagonals, causing batten members to buckle and

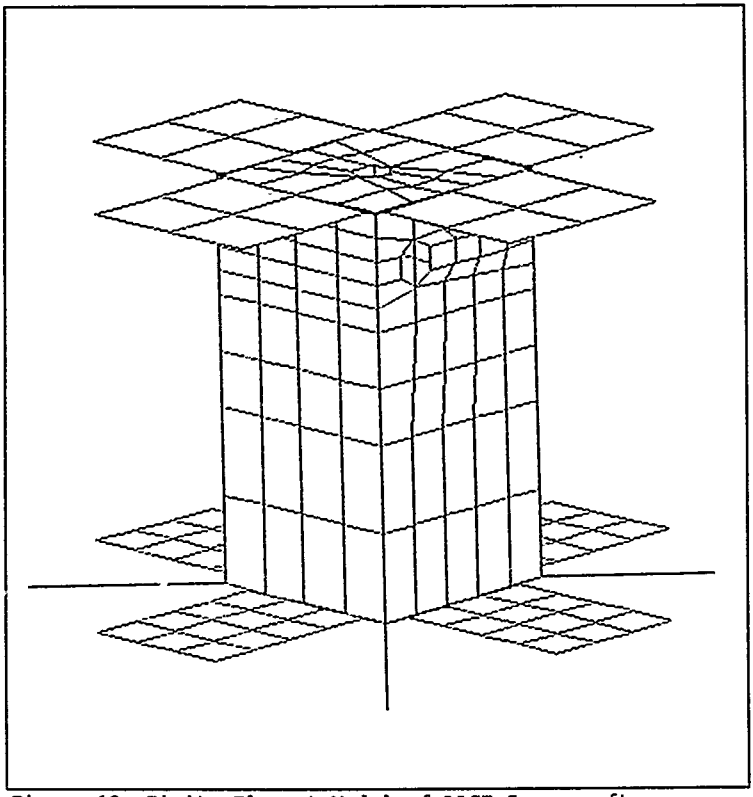

Figure 12. Finite Element Model of LACE Spacecraft

shorten. As twisting increases, the longerons rotate about the pivots and assume a helical configuration. In the retracted position the longerons are coiled in flat helices while battens lie on top of each other.

The longerons and battens are modeled as circular beams while the diagonals are modeled as rod elements. The battens

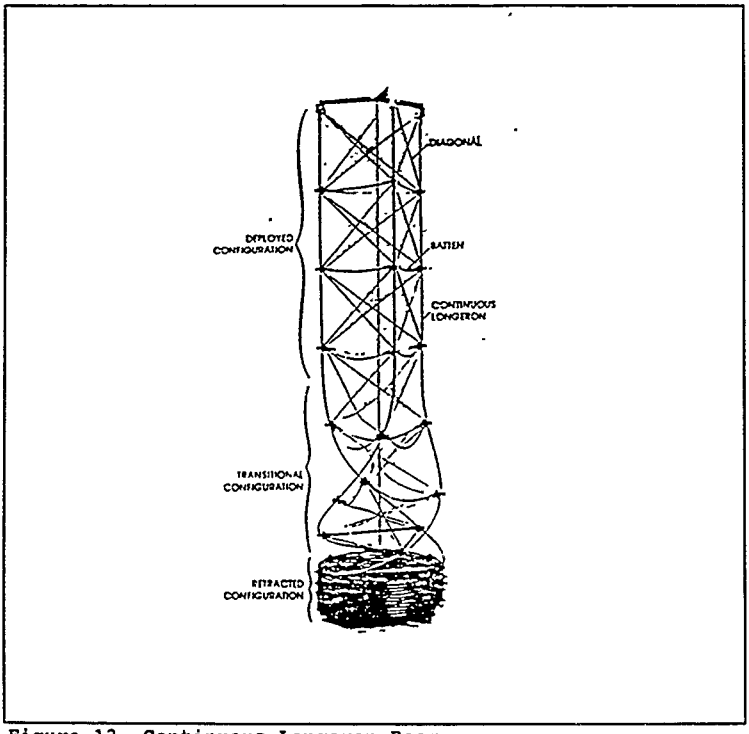

Figure 13. Continuous Longeron Boom

are oval-shaped and attached to the longeron by pivot joints, but for simplification the battens are modeled as circular and the joints are not modeled. Listed in Table V are the dimensions and properties of the truss. When fully retracted the triangular batten frames lie within a 10 inch diameter circle.

Figure 14 shows a cross-sectional view of the truss and its dimensions.

Table V. TRUSS PROPERTIES AND DIMENSIONS

Longeron and Batten Diameter	.150 inches
Diagonal Diameter	.050 inches
Material Type	S-glass epoxy
Density	.075 lbs/in^3
Young's Modulus	E=8.0 x 10^6 psi

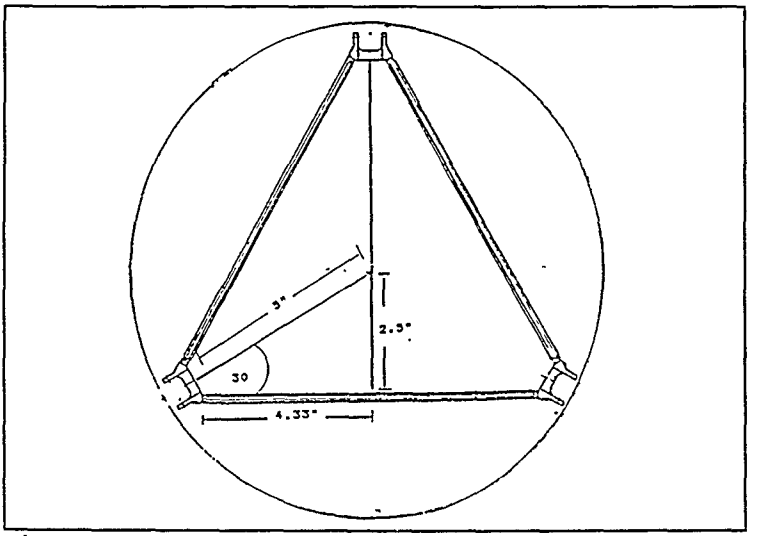

Figure 14. Cross-Sectional View and Dimensions of Longeron Structure

The booms of the spacecraft are ideal for substructuring. The 150-foot boom results in over 5,000 unknowns, when modeled as three-dimensional beam-truss elements. The substructuring technique is used in modeling when the number of unknowns may be reduced substantially. Initially, substructuring and multi-level substructuring

techniques were used to model the trusses, reducing the computational time considerably.

The first substructure was a 15-foot section of the truss. Ten of these substructures were joined together to construct the 150-foot boom. This multi-level substructure was attached to the main body of the spacecraft, thus forming a super element to the main body. This reduced the complete model from over 16,000 unknowns to about 2,500 unknowns. This was an attempt to capture the dynamics of the LACE spacecraft more accurately.

However, the use of substructuring generated large negative masses in the mass matrix. Kamel *et al.* [Ref. 12] provide a detailed formulation of the constrained substructuring techniques. As only the executable version of GIFTS program was available, and the objective was to obtain dynamic characteristics, it was decided to pursue modeling the whole structure.

The limitations of the program or the methodology adopted there is being pursued as well. The supplier of software is looking into the problem. The input files used to generate the multi-level substructuring model of LACE and typical negative mass elements are attached in Appendix E.

The listing of the file to create the trusses and attachment to the spacecraft is in Appendix F.

IV. RESULTS OF DYNAMIC ANALYSIS

For linear behavior, resonance occurs when the frequency of excitation equals the natural frequency. In order to avoid the ill-effects of large amplitude vibration at resonance, the natural frequency must be known and compared with potential excitation frequencies. The gravity gradient pitch vibration frequency is 2.3×10^{-4} Hz and is widely separated from the lowest modes of the finite element models.

Table V presents computed values for the first four modes of three different models of the LACE spacecraft.

Table V NATURAL FREQUENCIES OF THREE LACE MODELS

Mode	GIFTS Beam Model (Hz)	NASTRAN [Ref 1] Beam Model (Hz)	GIFTS Complex Model (Hz)
1	.01930	.01935	.0216
2	.04825	.04729	.0516
3	.05454	.0536	.0588
4	.1738	.1106	.1253

Initially, the NASTRAN beam model was developed by Naval Research Laboratories (NRL). The present beam model was developed as described in the previous chapter. The first three modes agree within 2%, however the present fourth mode appears to be an anomaly. The GIFTS complex model is consistently 10% higher than the NASTRAN model. The NASTRAN model appears to yield fairly good data in the lower modes.

This discrepancy may be attributed to the modeling uncertainties and approximation of the geometric and stiffness distributions. The detailed modeling of NASTRAN was not available. It may be noted that there is no excitation frequencies at those computed frequencies. Further, complex modeling is recommended when higher modes and frequencies are required. The simple model may not capture these higher modes and even skip some modes. The higher modes assume importance, especially, for very flexible structures and in the design of control systems for vibration control and suppression. Figures 15 to 20 show the mode shapes and frequencies for the NASTRAN model while Figures 21 to 26 show the data for the GIFTS beam model. Figures 27 to 30 show the GIFTS complex model of the spacecraft. Appendix F contains the frequency and mode shapes of the LACE spacecraft in three configurations as it deploys to its final state.

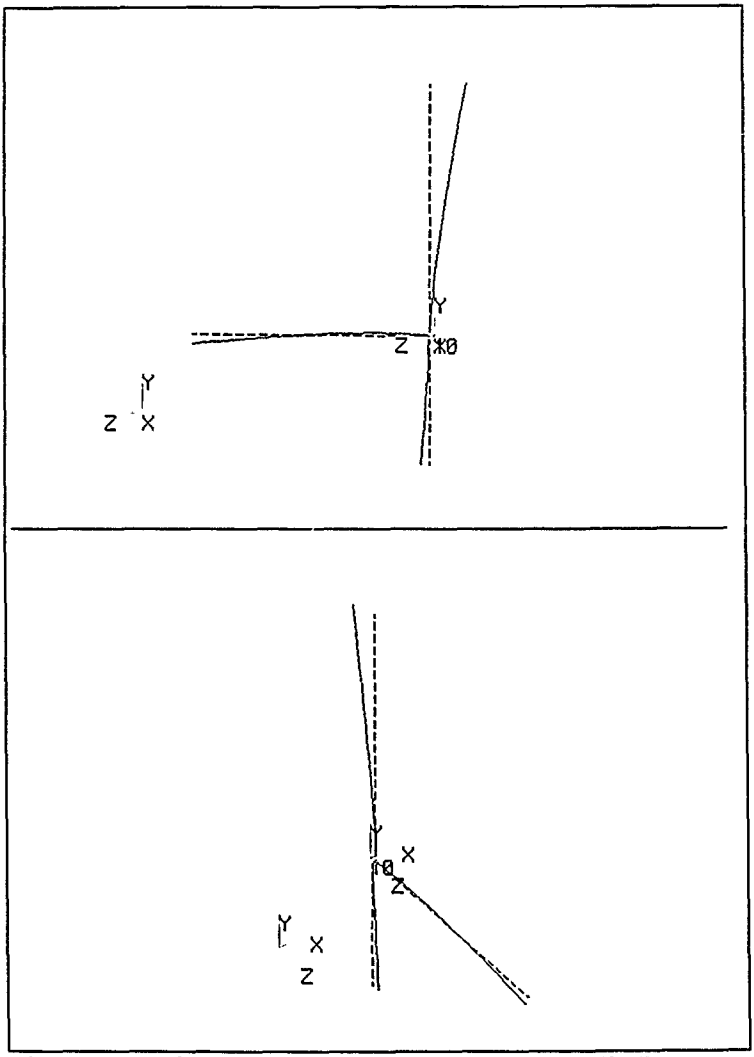

Figure 15. Mode 1, υ = .01935 Hz, NASTRAN BEAM MODEL

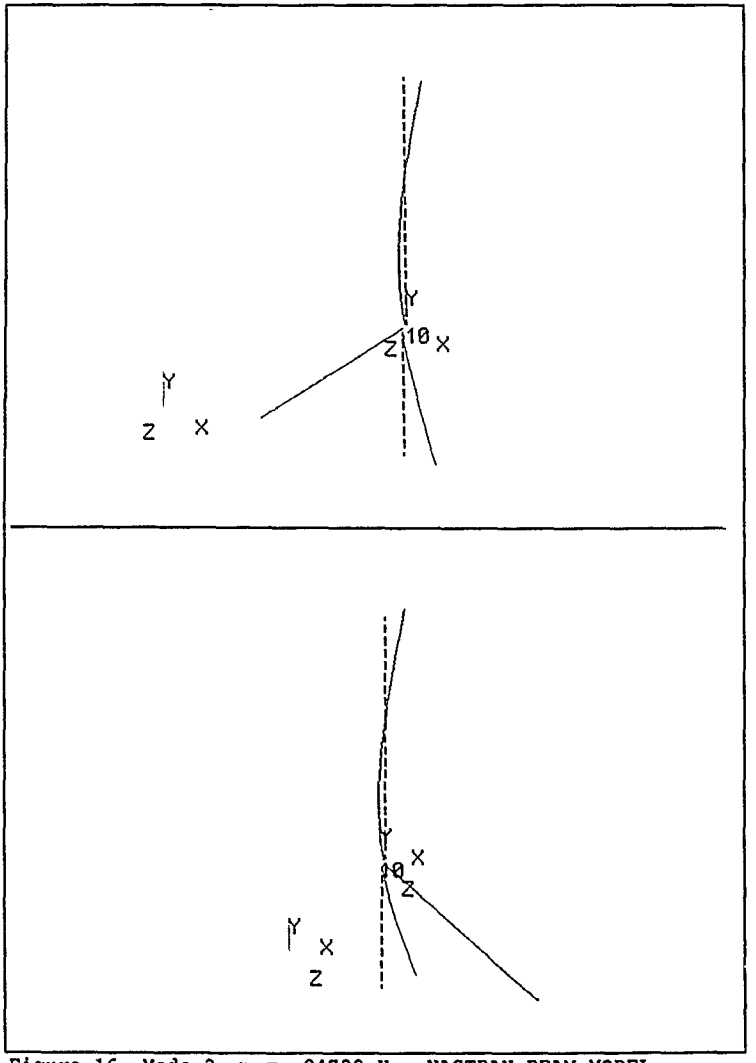

Figure 16. Mode 2, υ = .04729 Hz, NASTRAN BEAM MODEL

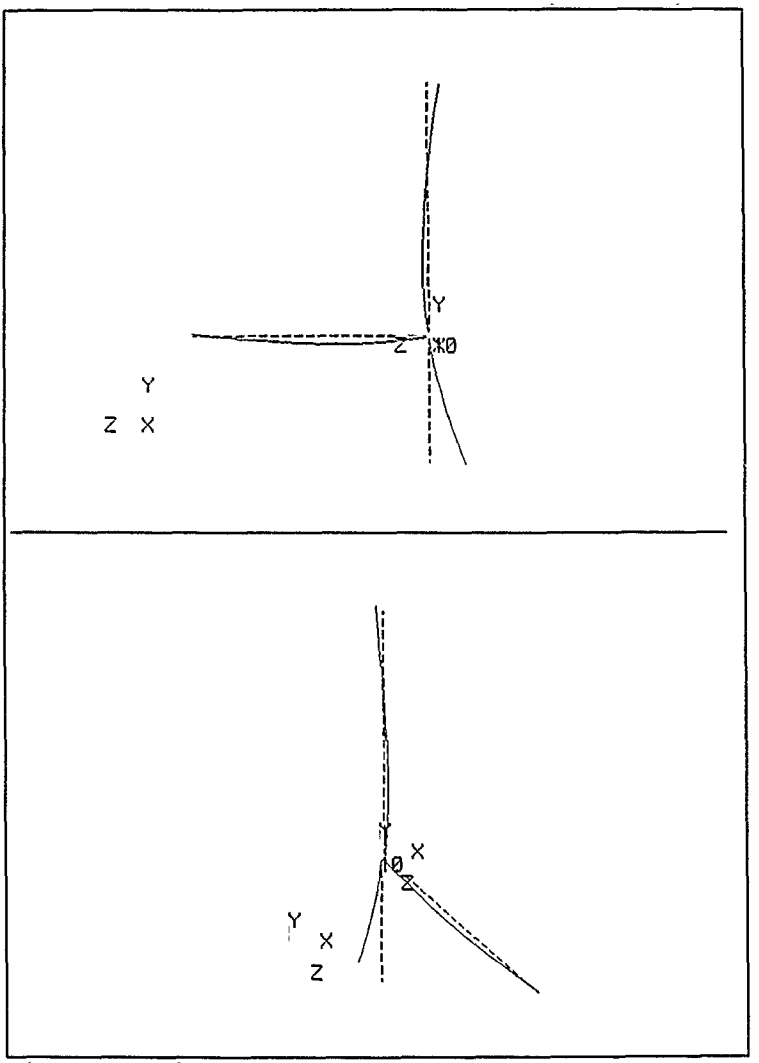

Figure 17. Mode 3, υ = .05362 Hz, NASTRAN BEAM MODEL

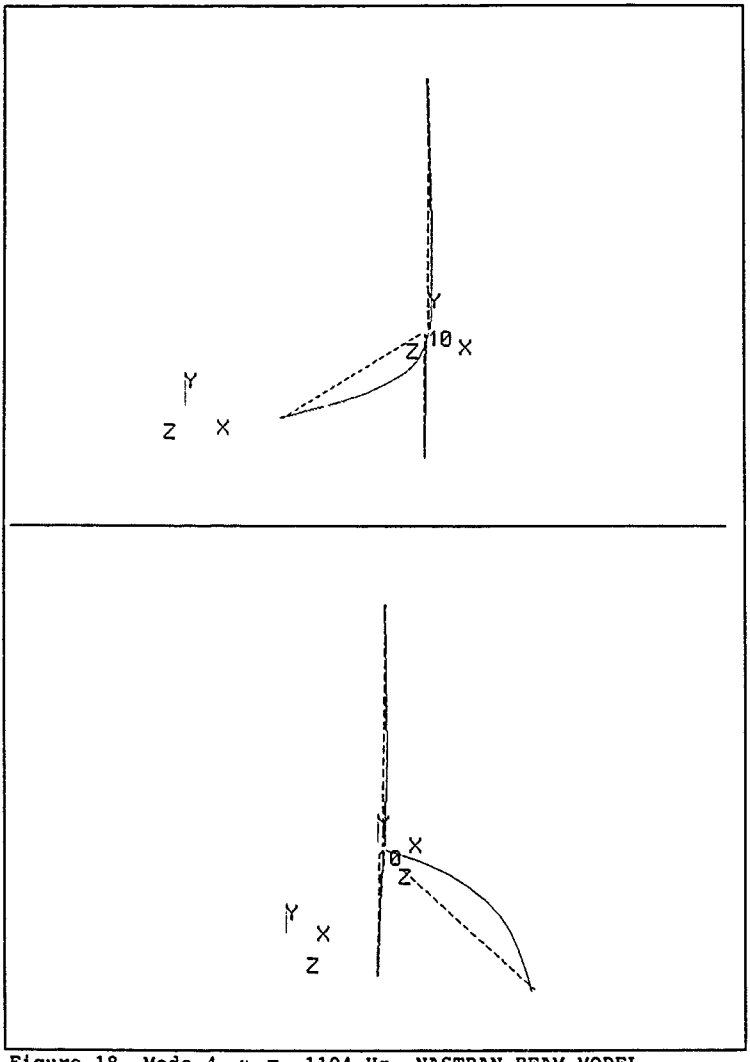

Figure 18. Mode 4, υ = .1104 Hz, NASTRAN BEAM MODEL

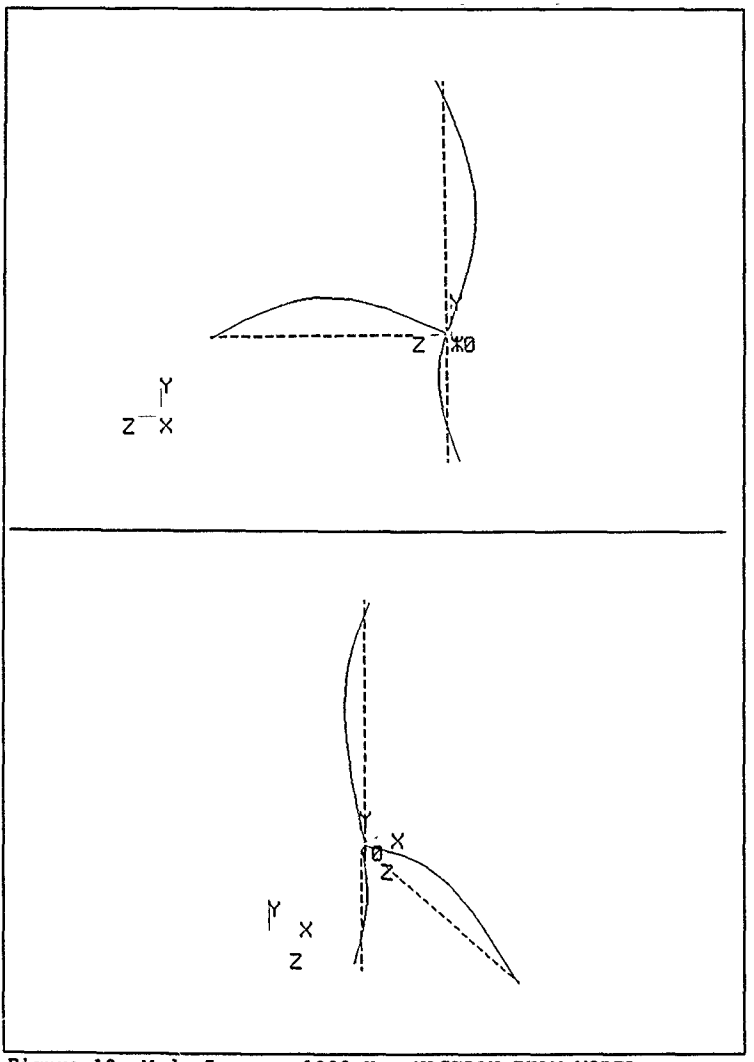

Figure 19. Mode 5, υ = .1808 Hz, NASTRAN BEAM MODEL

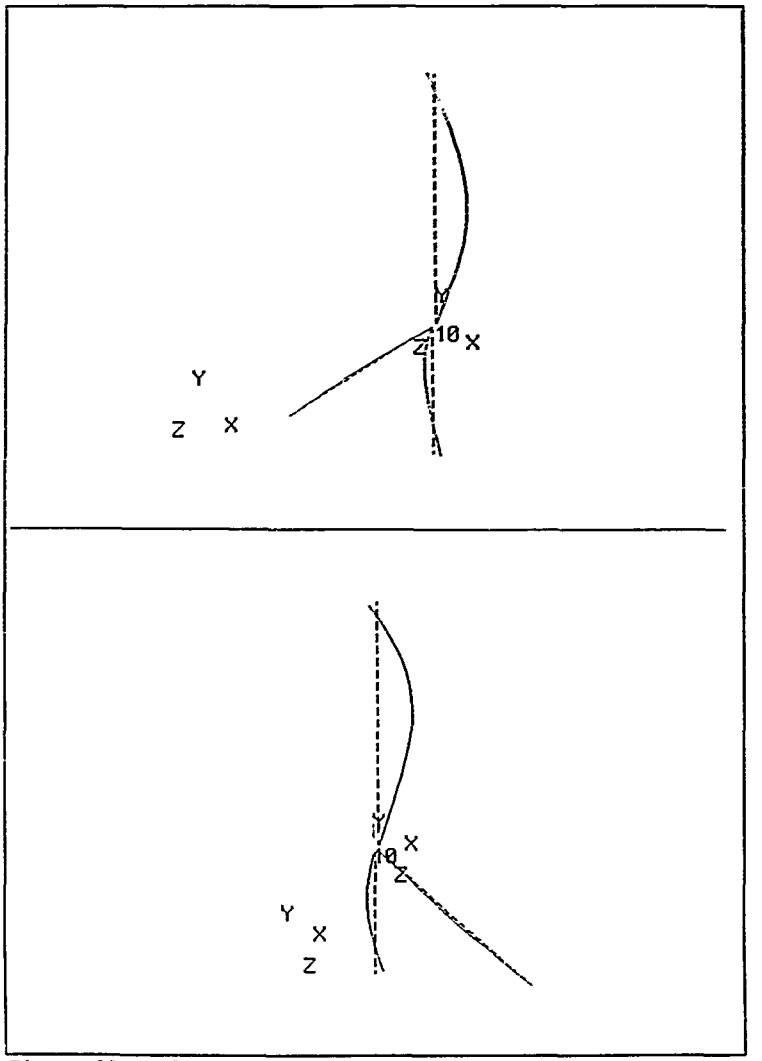

Figure 20. Mode 6, υ = .2019 Hz, NASTRAN BEAM MODEL

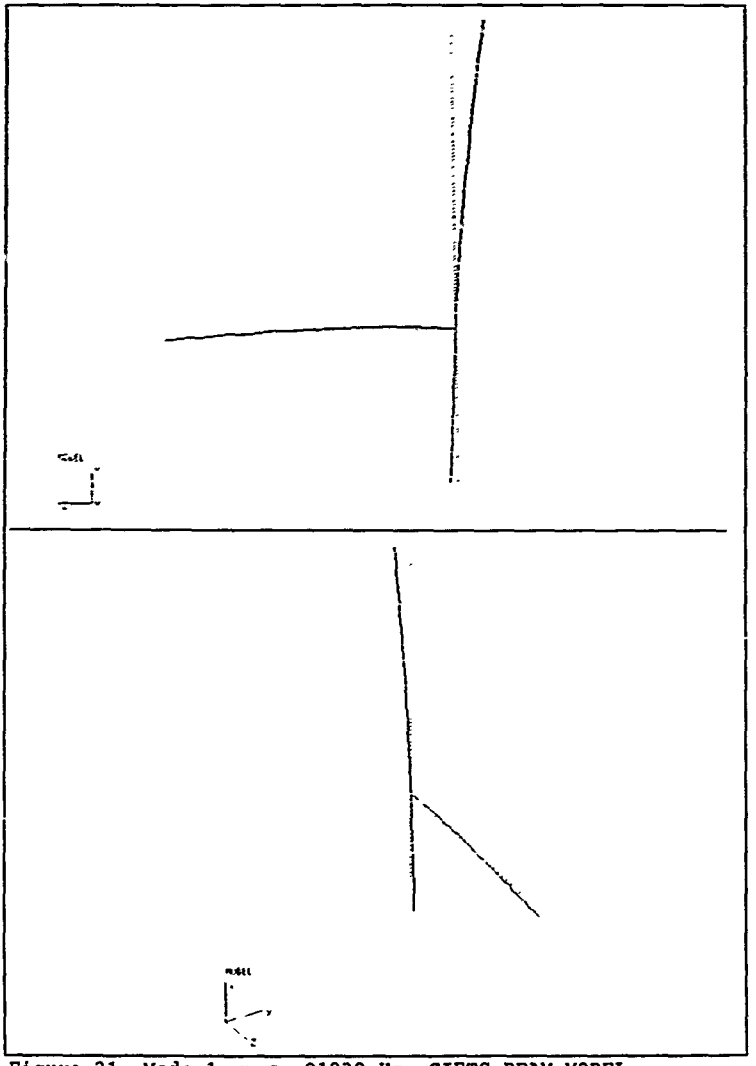

Figure 21. Mode 1, υ = .01930 Hz, GIFTS BEAM MODEL

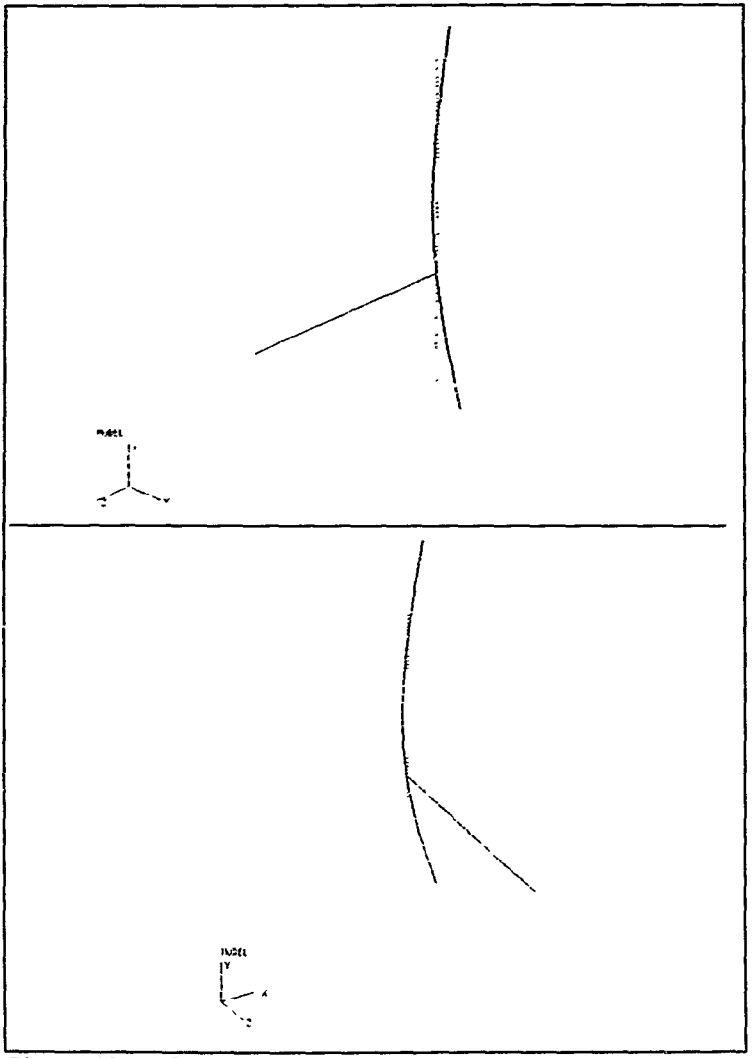

Figure 22. Mode 2, υ = .04825 Hz, GIFTS BEAM MODEL

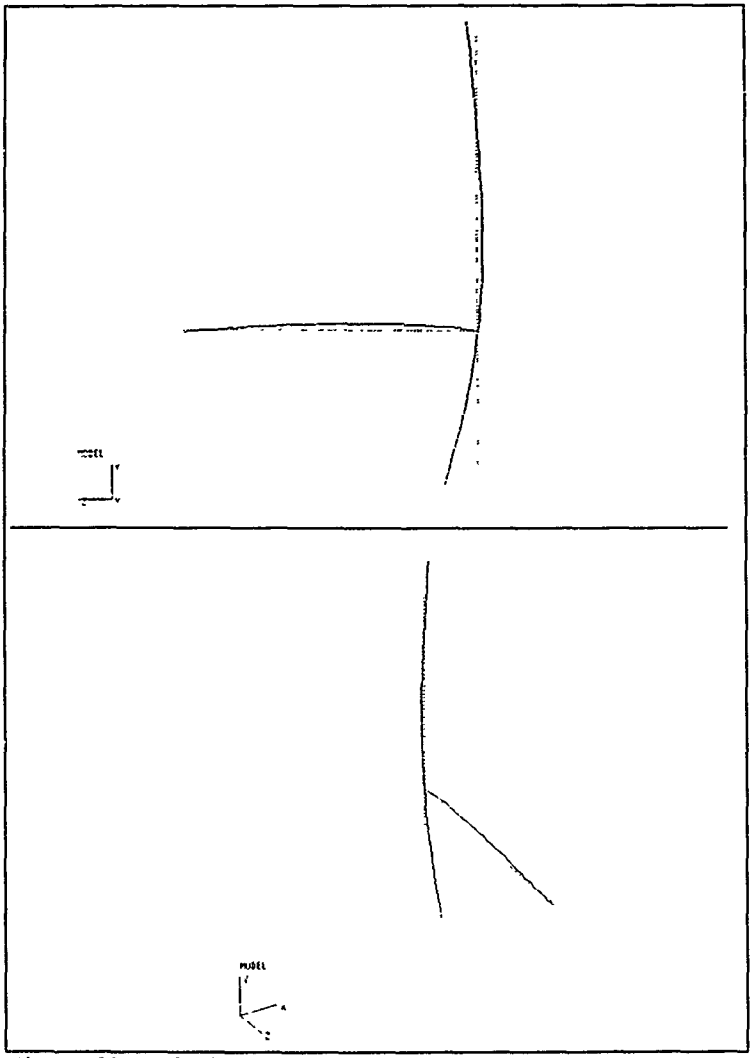

Figure 23. Mode 3, υ = .05459E Hz, GIFTS BEAM MODEL

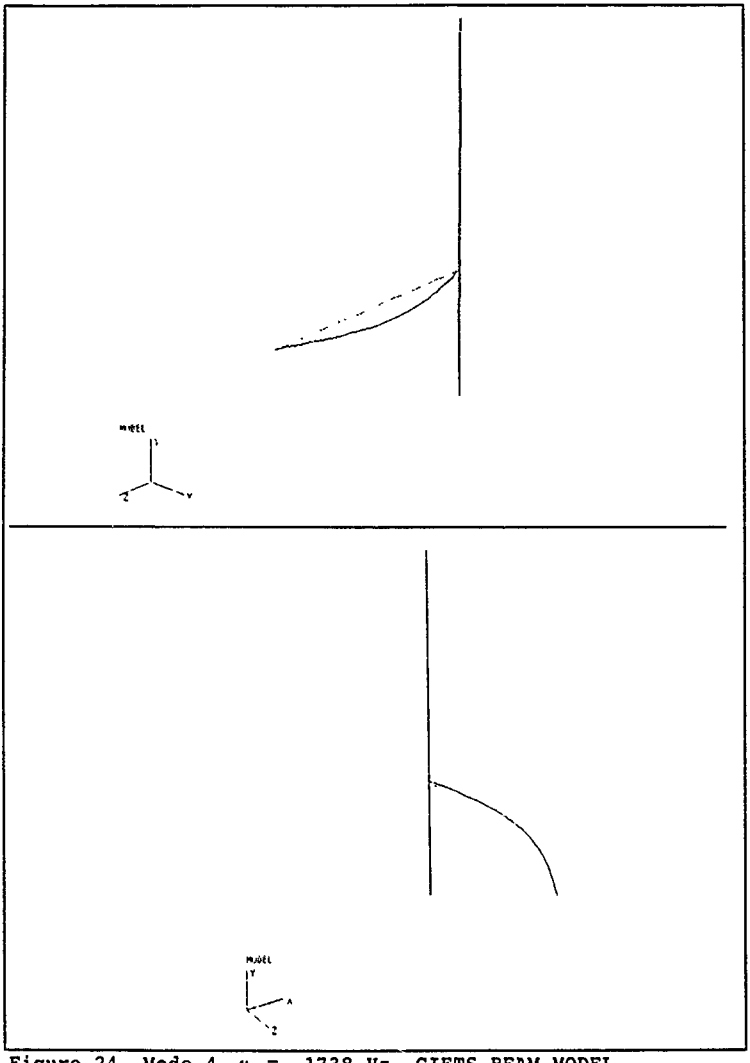

Figure 24. Mode 4, υ = .1738 Hz, GIFTS BEAM MODEL

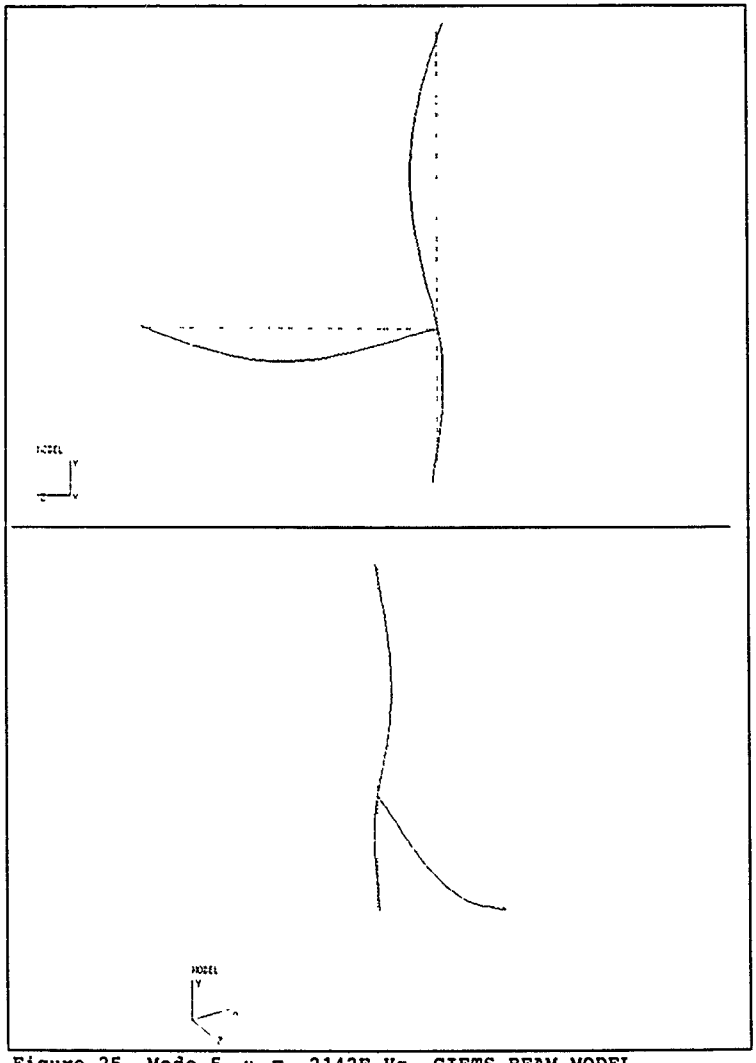

Figure 25. Mode 5, υ = .2142E Hz, GIFTS BEAM MODEL

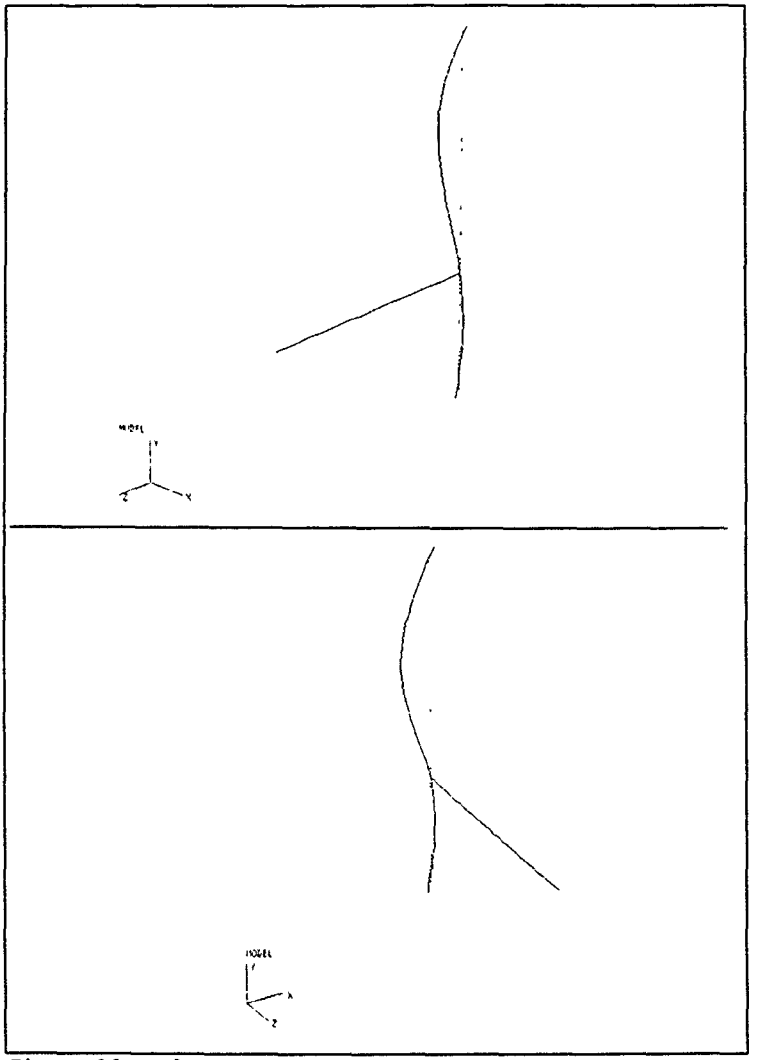

Figure 26. Mode 6, υ = .2349 Hz, GIFTS BEAM MODEL

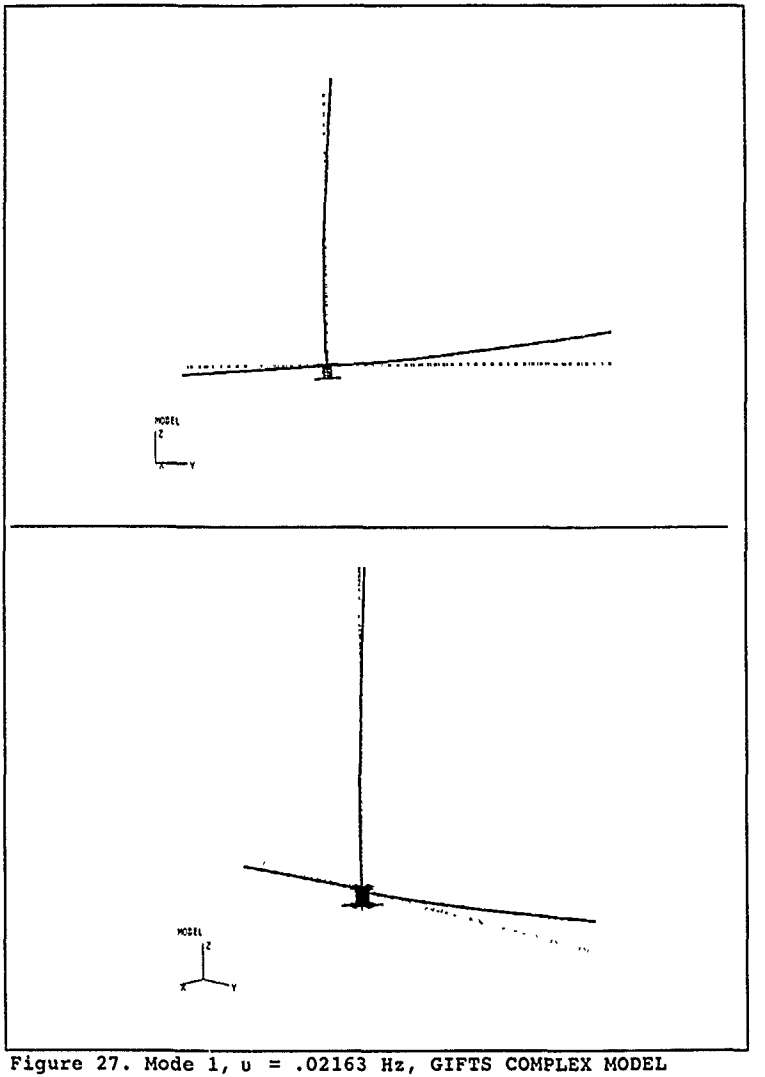

Figure 27. Mode 1, υ = .02163 Hz, GIFTS COMPLEX MODEL

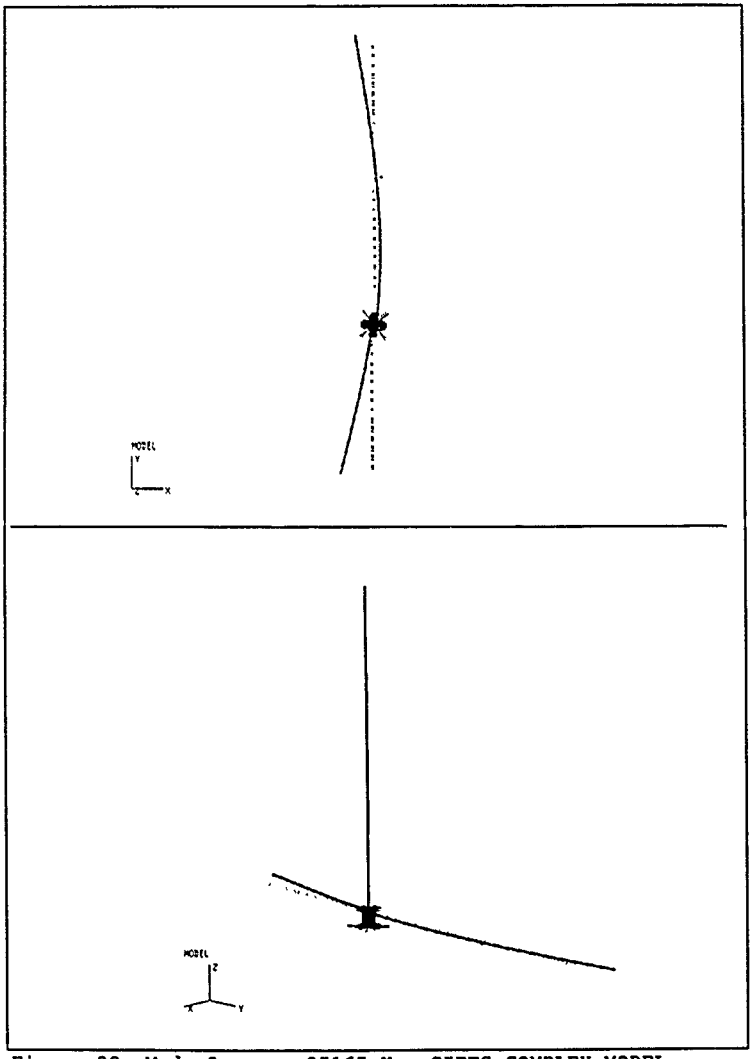

Figure 28. Mode 2, υ = .05165 Hz, GIFTS COMPLEX MODEL

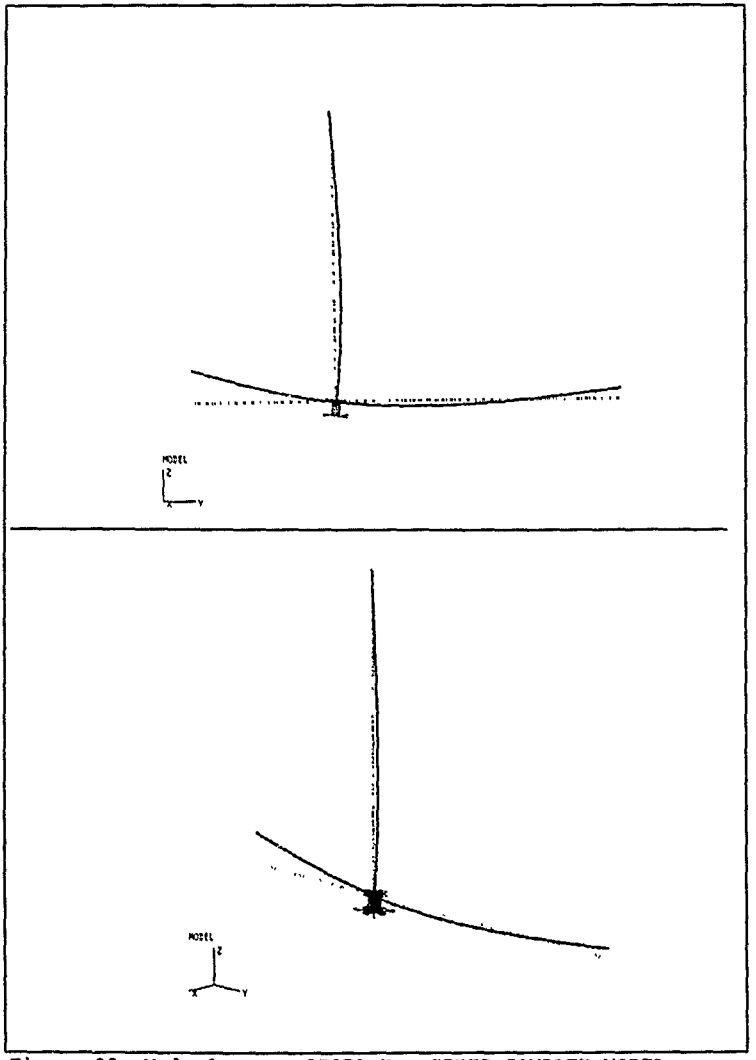

Figure 29. Mode 3, υ = .05879 Hz, GIFTS COMPLEX MODEL

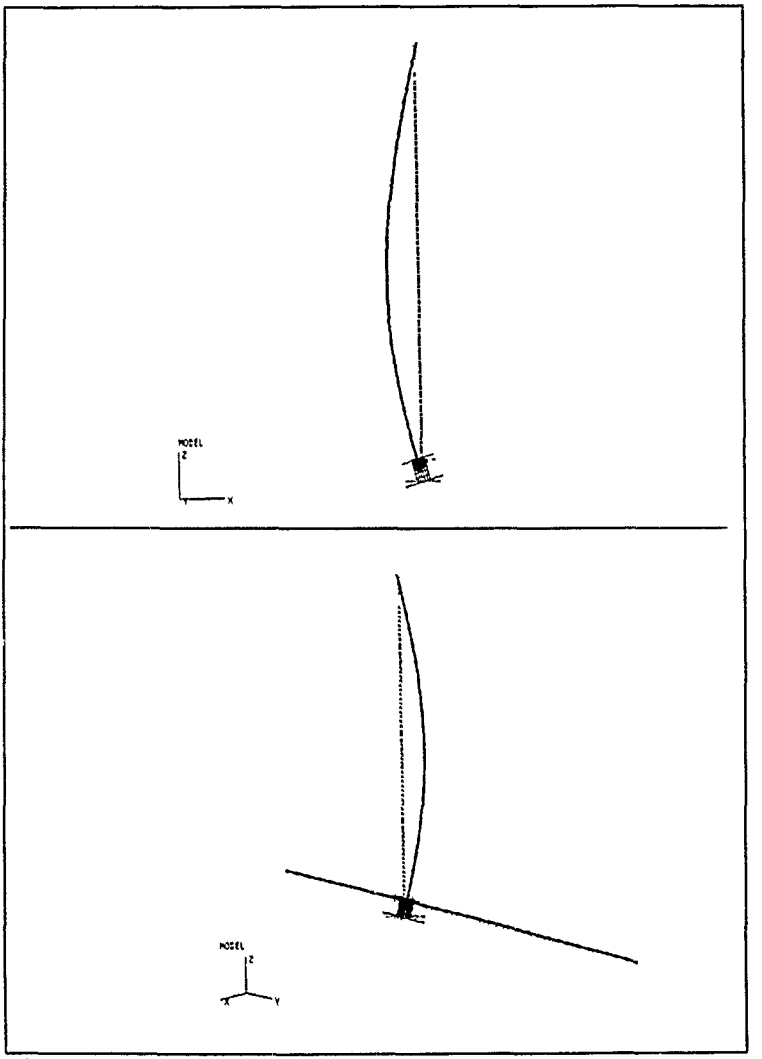

Figure 30. Mode 4, υ = .1253 Hz, GIFTS COMPLEX MODEL

V. THERMOELASTIC EFFECTS

A change in temperature along a bar will change its dimensions. When an isotropic bar is heated uniformly and is free to expand, the sides will increase in length. The material undergoes a uniform thermal strain e_t given by:

$$e_t = \alpha(\Delta T) \tag{44}$$

where α is the coefficient of thermal expansion and ΔT is an increase in temperature. The length of the bar will increase by an amount

$$\delta_t = \alpha(\Delta T)L$$

where L is the length of the bar.

The ABLE booms [Ref. 10] used on LACE are designed so that they undergo minimum thermal bending or twisting in the solar radiation environment. Pretwist is used to prevent thermal twisting or thermal bending that would occur if one longeron is shadowed by another.

This chapter presents analysis for deformations that could result in a worst case scenario. Two possible scenarios considered are when the boom may bend due to unequal heating of the diagonals and unequal heating of the longerons. Unequal heating of the diagonals is more likely to occur than unequal heating of longerons. [Ref. 13]. The following analysis

considers only the unequal heating of the diagonals and assumes no shadowing effects.

Sources of heat include spacecraft components, solar flux, albedo flux and thermal radiation of the earth. The solar flux is defined as the flux existing at a distance of one astronomical unit (AU) from the sun. Albedo flux is the fraction of total incident solar radiation on the earth which is reflected into space as a result of scattering in the atmosphere and reflection from the clouds and earth surfaces. Thermal radiation from the earth is the portion of incident solar radiation absorbed by earth and its atmosphere and re-emitted as thermal radiation according to Stefan-Boltzman law [Ref. 11]. For the computation of LACE thermal deformations, the following data is used [Ref. 13]:

Solar flux: 442 Btu/sq ft hr

Thermal Earth Radiation: 70 Btu/sq ft hr

Albedo flux: 160 Btu/sq ft hr

$\epsilon/\alpha = .8$

where ϵ is the emissivity and α is the absorptivity.

The worst case of unequal diagonal heating occurs when the sun rays are parallel with one set of diagonals and almost perpendicular to the other set. The set of diagonals perpendicular to the sun will receive maximum solar flux. The parallel set will receive no solar flux, but will receive earth's albedo and thermal radiation flux. A simple approach is taken where the hottest and coldest temperatures of the

diagonals are calculated. This results in a maximum temperature of 192°F and a minimum of -5°F. Following the discussion in Ref. 12, calculations are carried out and presented in Appendix G.

It is assumed that the battens and longerons receive equal heating of 80°F. Using a 3-D model of the truss, the temperatures above, and a coefficient of thermal expansion of $1.75 \times 10^{-6}/°R$, the maximum deflection is calculated. Figure 31a shows that the deformed shape is similar to the first bending mode. Figure 31b shows a closeup of the deformation. A maximum deflection of 1.88 inches is calculated using GIFTS. This is a 1.2% deformation for the 150 foot truss and should have negligible effect on the system dynamics.

However, thermal flutter could occur if the period of the thermal loading coincides with the natural frequencies of the spacecraft.

The first bending mode has a natural frequency of .02163 Hz. The thermal loading from the sun occurs over a long period and is on the order of 10^{-4}. The thermal loading is two orders of magnitude lower than the fundamental frequency and as a result should not interact with any natural frequencies.

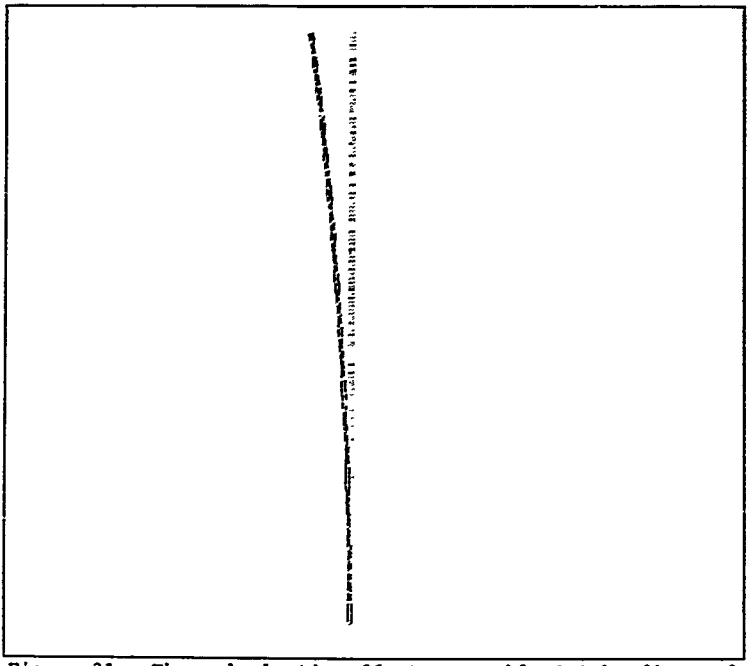

Figure 31a. Thermal elastic effects resemble 1st bending mode shape.

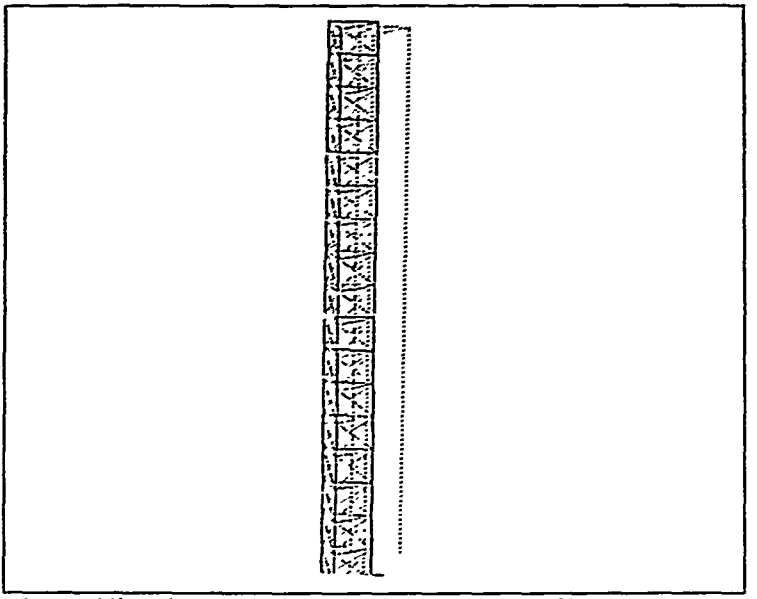

Figure 31b. Close-up view of thermoelastic effects

VI. MULTI-BODY DYNAMICS

A. COMPONENT MODE SYNTHESIS

In the previous chapter, finite element techniques were used to formulate a model of the LACE spacecraft for use in structural dynamics analysis. This section discusses a class of reduction methods known as component mode synthesis, or substructure coupling for dynamic analysis. These methods are useful for analysis of large structural dynamics problems.

The basic idea of component mode synthesis is to treat the complex structure as an assemblage of substructures. Each substructure is analyzed independently and then their dynamic characteristics (mode shapes and natural frequencies) are synthesized to analyze the complete structure. There are many variations of the method of component mode synthesis and extensive literature is available [Ref. 14, 15, 16, 17].

Hurty [Ref. 14] developed a procedure for analysis of structural systems using a displacement method which used three types of generalized coordinates, namely: 1) rigid body coordinates, 2) constraint coordinates, and 3) normal mode coordinates. Hurty used Rayleigh-Ritz approach in his formulation. The Craig-Bampton method [Ref. 15] is similar to the treatment due to Hurty, except that it simplifies the treatment of rigid-body modes of substructures by eliminating

the separation of boundary forces into statically determinate and statically indeterminate reactions [Ref. 15]. MacNeal [Ref. 16] introduced residual flexibility modes to retain the static contribution of a higher frequency truncated modes. Rubin [Ref. 17] developed a new method which adds residual inertial and dissipative results to the method introduced by MacNeal [Ref. 17].

This section will present the basics of component mode synthesis.

Craig [Ref. 18] provides a good overview of component mode synthesis methods. His notation and examples will be used extensively in this discussion.

A substructure is generally connected to one or more adjacent components and is composed of interior degrees of freedom and boundary degrees of freedom. Figure 32 illustrates a substructure connected to other components and shows boundary and interior coordinates.

The equation of motion for a component is given by

$$M\ddot{X} + C\dot{X} + KX = f \qquad (45)$$

where M is the mass matrix, C is the damping matrix and K is the stiffness matrix.

The total set of physical coordinates of the component is defined as P, while interior and boundary points will be defined as I and B respectively. Boundary coordinates are further subdivided into statically determinate (rigid body)

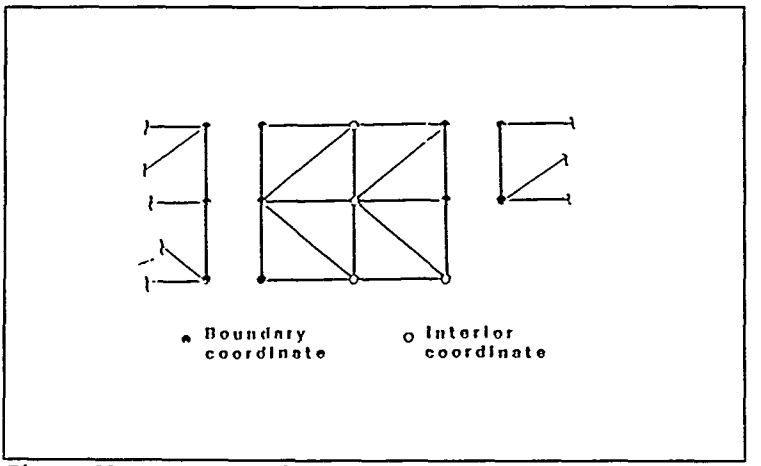

Figure 32. Unrestrained truss component

support of the component and its complement, redundant (excess) boundary coordinates designated as R and E respectively. These designations are used throughout this analysis.

Figure 33 shows a beam divided into several components and will be used to to illustrate mode sets in the following discussion.

The two fundamental steps of component mode synthesis are to: 1) define component modes, and 2) to define coupling of components to form a system.

The physical coordinates, x, can be represented by component generalized coordinates, P by the transformation

$$X = \psi P \qquad (46)$$

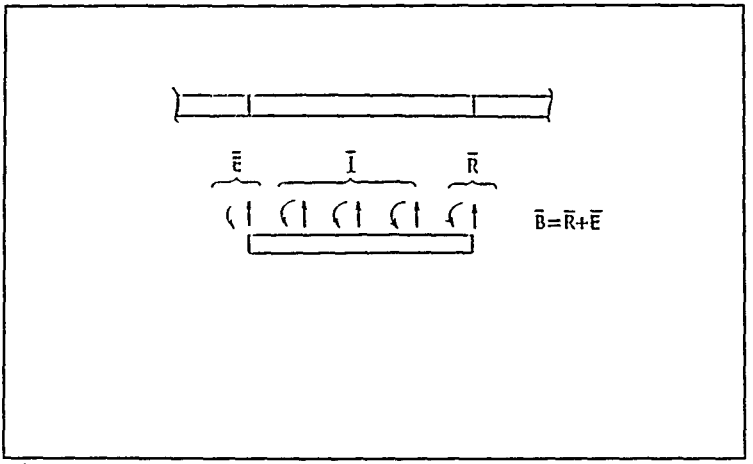

Figure 33. Beam model divided into components

where ψ consists of component modes of specified type [Ref. 14]. These include:

normal modes of free vibration

attachment modes

constraint modes

rigid body modes

inertia relief modes

These modes are defined as follows. [Ref. 17]

1. Normal Modes

Normal modes are classified as fixed interface normal modes, free-interface normal modes or hybrid-interface normal modes depending on how the interface coordinates are restrained when the component normal modes are obtained using

$$(K - W_p^2 m)\phi p = 0 \qquad (47)$$

The modes are normalized with respect to the mass matrix m.

$$\phi_n^T m \phi_n = I_{nn} \qquad \phi_n^T K \phi_n = \Lambda_{nn} = diag(Wp)^2$$

where ϕ_n is component normal modes. The notation ϕ will be used for normal modes, while ψ will be used for assumed modes.

2. Constraint Modes

A constraint mode is defined by statically imposing a unit displacement on one coordinate of a C set of physical coordinates. Let C=E and define a constraint mode by placing a unit displacement on one coordinate of the C set and zero displacement on the remaining C set. The matrix of constraint nodes, ψ_c is defined by the equation:

$$\begin{bmatrix} K_{ii} & K_{ic} & K_{ir} \\ K_{ci} & K_{cc} & K_{cr} \\ K_{ri} & K_{rc} & K_{rr} \end{bmatrix} \begin{bmatrix} \psi_{ic} \\ I_{cc} \\ O \end{bmatrix} = \begin{bmatrix} O \\ R_{cc} \\ R_{rc} \end{bmatrix} \qquad (48)$$

This equation may be simplified to yield

$$\psi_c = \begin{bmatrix} \psi_{ic} \\ I_{cc} \\ O \end{bmatrix} = \begin{bmatrix} -1 \\ -K_{ii}\ K_{ic} \\ I_{cc} \\ O \end{bmatrix} \qquad (49)$$

3. Attachment Modes

Attachment mode is defined by applying a unit force of the coordinates of an A set [Ref. 15]. In this case, attachment modes will be defined for A = E. The matrix of attachment modes ψ_a is shown by the equation

$$\begin{bmatrix} K_{ii} & K_{ia} & K_{ir} \\ K_{ai} & K_{aa} & K_{ar} \\ K_{ri} & K_{ra} & K_{rr} \end{bmatrix} \begin{bmatrix} \psi_{ia} \\ \psi_{ca} \\ O \end{bmatrix} = \begin{bmatrix} O \\ I_{aa} \\ R_{ra} \end{bmatrix} \tag{50}$$

Using the first two rows of equation (50), ψ_a may be represented by

$$\psi_a = \begin{bmatrix} \psi_{ia} \\ \psi_{aa} \\ O \end{bmatrix} = \begin{bmatrix} g_{ia} \\ g_{aa} \\ O \end{bmatrix} \tag{51}$$

where $g = K^{-1}$ is the flexibility matrix.

4. Rigid Body Modes

The boundary conditions are depicted in Figure 45, where the R set will restrain the component from rigid body motion and the E set contains redundant boundary conditions. By defining the rigid body modes relative to the R set, the equation is given by

$$\begin{bmatrix} K_{ii} & K_{ie} & K_{ir} \\ K_{ei} & K_{ee} & K_{er} \\ K_{ri} & K_{re} & K_{rr} \end{bmatrix} \begin{bmatrix} \psi_{ir} \\ \psi_{er} \\ I_{rr} \end{bmatrix} = \begin{bmatrix} O \\ O \\ O \end{bmatrix} \tag{52}$$

which simplifies to

$$\begin{bmatrix} K_{ii} & K_{ie} \\ K_{ei} & K_{ee} \end{bmatrix} \begin{bmatrix} \psi_{ir} \\ \psi_{er} \end{bmatrix} = -\begin{bmatrix} K_{ir} \\ K_{er} \end{bmatrix} \tag{53}$$

The ψ_r matrix is given by

$$\psi_r = \begin{bmatrix} \psi_{ir} \\ \psi_{er} \\ I_{rr} \end{bmatrix} = \begin{bmatrix} -\begin{bmatrix} g_{ii} & g_{ie} \\ g_{ei} & g_{ee} \end{bmatrix} \begin{bmatrix} K_{ir} \\ K_{er} \end{bmatrix} \\ I_{rr} \end{bmatrix} \tag{54}$$

5. Inertia-Relief Modes

This method defines attachment modes for a component with rigid body freedoms. This method was presented by Rubin [Ref. 16] and MacNeal [Ref. 17]. By letting D'Alembert force vectors associated with rigid-body modes be applied statically to a component which is fully constrained on the boundary, ψ_m can be defined as follows.

$$\begin{bmatrix} K_{ii} & K_{ie} & K_{ir} \\ K_{ei} & K_{ee} & K_{er} \\ K_{ri} & K_{re} & K_{rr} \end{bmatrix} \begin{bmatrix} \psi_{im} \\ O \\ O \end{bmatrix} = \begin{bmatrix} M_{ii} & M_{ie} & M_{ir} \\ M_{ei} & M_{ee} & M_{er} \\ M_{ri} & M_{re} & M_{rr} \end{bmatrix} \begin{bmatrix} \psi_{ir} \\ \psi_{er} \\ I_{rr} \end{bmatrix} + \begin{bmatrix} O \\ r_{er} \\ R_{rr} \end{bmatrix} \tag{55}$$

$$\psi_n = \begin{bmatrix} \psi_{im} \\ O \\ O \end{bmatrix} = \begin{bmatrix} K^{-1}(M_{ii}\psi_{ir} = M_{ie}\psi_{er} = M_{ir}) \\ O \\ O \end{bmatrix} \tag{56}$$

6. Coupling of Components

This section describes generalized substructure coupling as applied to free vibration analysis. [Ref. 18]

Assuming two components α and β having a common boundary interface, compatibility of interface displacement requires

$$x_b^\alpha = x_b^\beta \tag{57}$$

The interface forces are related by

$$f_b^\alpha = f_b^\beta = 0 \tag{58}$$

By representing the physical coordinates x, by generalized coordinates p, the following equations are derived

$$x^\alpha = \psi^\alpha p^\alpha \quad , \quad x^\beta = \psi^\beta p^\beta \tag{59}$$

where ψ^α and ψ^β contain assumed static and dynamic modes.

The constraint equations can be written in generalized form to form a single constraint equation

$$CP = O \tag{60}$$

where

$$P = \begin{Bmatrix} P^\alpha \\ P^\beta \end{Bmatrix} \tag{61}$$

Let P be rearranged and partitioned into dependent P_D and independent, P_I, coordinates. Then,

$$[C_{DD} C_{DI}] \begin{Bmatrix} P_D \\ P_I \end{Bmatrix} = O \tag{62}$$

where C_{dd} is nonsingular square matrix and equation

$$P = \begin{Bmatrix} P_D \\ P_I \end{Bmatrix} = \begin{bmatrix} -C_{DD}^{-1} C_{DI} \\ I_{II} \end{bmatrix} P_I = Sg \tag{63}$$

defines S and g, where

$$S = \begin{bmatrix} -C_{DD}^{-1} C_{DI} \\ I_{II} \end{bmatrix} \tag{64}$$

The μ and x corresponding to P are given by

$$\mu = \begin{bmatrix} \mu^{\alpha} & O \\ O & \mu^{\beta} \end{bmatrix}, \quad \varkappa = \begin{bmatrix} \varkappa^{\alpha} & O \\ O & \varkappa^{\beta} \end{bmatrix} \tag{65}$$

The coupled system of equations for an undamped system is given by

$$M\ddot{g} + Kg = 0 \tag{66}$$

where

$$M = S^{T}\mu S \ , \quad K = S^{T}\varkappa S \tag{67}$$

B. DYNAMICS OF FLEXIBLE BODIES IN TREE TOPOLOGY

1. Overview of Multibody Systems

Spacecraft and large spacecraft structures are typical multibody systems. Large strides have been made in the last 20 years in the efficient formulation and solution of multibody systems. Particular interest in multibody dynamics has risen in spacecraft dynamics. Initially, space vehicles were idealized as rigid bodies or elastic beams. In the mid-1980s equations of motion were published for a point-connected set of interconnected rigid bodies in a topological tree. A model containing rigid bodies and elastic appendages was eveloped in the 1970s. The next major step was the incorporation of body flexibility in the topological tree model. [Ref. 19]

2. Multibody Computer Program - TREETOPS

TREETOPS is a computer program developed to deal with multibody structures in an open-tree topology. It is a time

history simulation of a complex multibody flexible structure with active control elements. Some of the features include: 1) any or all bodies can be rigid or deformable, 2) hinges can have zero to six degrees of freedom, 3) the dimension of the problem equals the number of degrees of freedom, 4) individual body deformation can be described by any set of modal vectors, 5) an interactive program, and 6) extensive control simulation capability. [Ref. 18]

The computer simulation consists of three parts: defining a tree topology of flexible structures, define a controller and a set of sensors and actuators.

The structure of the TREETOPS model consists of bodies and hinges with sensors and actuators included for interfacing with the control system. Figure 34 shows a typical structure.

a. Body Types

The program simulates a set of bodies in a tree topology. Each body is defined independently. Sensors, actuators and hinges are connected to specific points called node points. Each body may be defined as rigid or flexible.

Each body is to be defined with an ID number, mass properties, center of mass and all its pertinent node points. [Ref. 20]

b. Hinges

Hinges interconnect two adjacent bodies. One body is called the inboard body and the other is called the outboard body. The inboard body is the one on the side closest

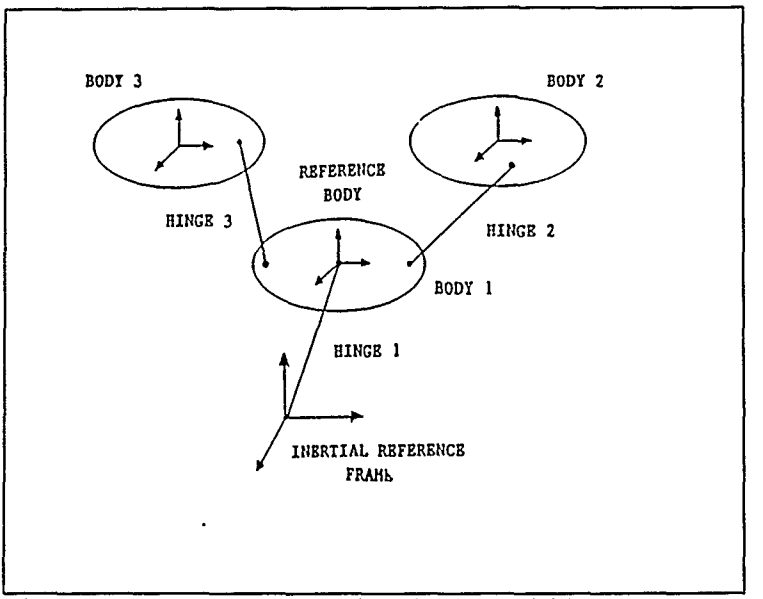

Figure 34. Structure composed of bodies and hinges

to the inertial reference frame. Figure 35 shows a hinge representation.

The functions of the TREETOP hinges are to [Ref.20]:

1. define topology of the structure
2. define kinematic variables of the multibody system
3. define relative orientation between adjacent bodies.

c. Sensors and Actuators

A set of 16 sensors have been built into the simulation. They include rate gyros, resolvers,

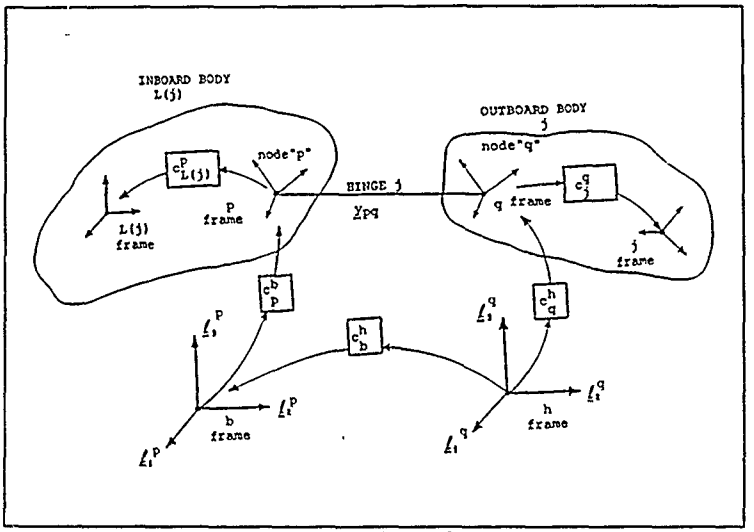

Figure 35. General representation of jth hinge

accelerometers, position and velocity sensors, tachometer, sun and star sensors, etc. The actuators serve as a way to apply force and torque inputs. Inputs may be control or disturbance inputs. Disturbance inputs can be applied with function generators to the actuators. Actuator types include reaction jets, hydraulic cylinder, moment actuator and torque motor.

d. Orbit Environment

TREETOPS has the capability to model the orbit environment of a spacecraft to include gravity gradient and aerodynamic drag. A magnetic field model is included which produces a force through interaction with magnetic actuators. In computing the atmospheric drag, TREETOPS uses atmospheric

density computed from the JACCHIA 1970 atmospheric model. The spacecraft orbit is determined by entering the six orbital parameters.

VII. CHAOTIC VIBRATIONS

A. HOW TO IDENTIFY CHAOTIC VIBRATIONS

Chaos is defined as a motion that is sensitive to initial conditions [Ref. 21]. Chaos can occur only in nonlinear systems, but all nonlinear systems do not exhibit chaos. Chaos can be observed in many physical systems. A partial list is shown:

1. Vibrations of buckled elastic structures
2. Mechanical systems with play
3. Large, three-dimensional vibrations of structures
4. Aereoelastic problems
5. Systems with sliding friction
6. Feedback control devices

In order to identify chaotic motions, several procedures are suggested [Ref. 21], such as

1. Identify nonlinear elements in the system
2. Check for sources of random input in the system
3. Observe time history of the measured signal
4. Observe phase plane history
5. Examine Fourier spectrum of the signal
6. Determine Poincaré map of the signal
7. Vary system parameters

Quantitative characteristics of chaotic vibrations and the diagnostic tools used are summarized as follows:

1. Sensitivity to changes in initial conditions (Lyapunov exponent and fractal basin boundaries)
2. Broad band spectrum of Fourier transform when motion is generated by a single frequency
3. Fractal properties of the motion in phase space which indicate a strange attractor (Poincaré maps, fractal dimension)
4. Increasing complexity of regular motions as experimental parameters are changed
5. Transient or intermittent chaotic motions; nonperiodic bursts of irregular motion or initially random-like motion that settles into regular motion.

1. Nonlinear System Elements

A linear system does not exhibit chaotic vibrations. Typical nonlinear effects from mechanical systems include nonlinear stiffness, material nonlinearity, nonlinear damping, free-play, and nonlinear boundary conditions. Nonlinear elastic effects can be due to large deformation. A good example of material nonlinearity is the stress-strain relations of materials modeling rubber or elastomers.

2. Random Inputs

There are no assumed random inputs in chaotic vibrations. Applied forces and excitations are assumed to be deterministic. By definition, chaotic vibrations arise from deterministic physical systems. A large output signal to input noise ratio is required if nonperiodic response is to be attributed to a deterministic system behavior. [Ref. 21]

3. Observation of Time History

The first indication of chaos may be indicated in the time history. The motion observed shows no visible pattern or periodicity and may be chaotic or random.

This method is not conclusive, since motion could have a long-period behavior that is not detected or quasiperiodic motion where two or more periodic signals are present.

4. Fourier Spectrum

The presence of a broad band Fourier spectrum in the output is another clue that may be used to suspect chaotic vibrations. A precursor to chaos is the presence of w_o/n subharmonics. However, multiharmonic outputs do not always imply chaotic vibrations as hidden degrees of freedom may be present.

5. Phase Plane History

In the phase plane, complete information about a dynamical system is represented by a point. At the next point in time when the system dynamics change, the point is displaced.

This moving point gives the history of the dynamical system. The coordinates chosen for the study of dynamics, typically, are the amplitude and velocity of motion. Figure 36 shows the phase plane of a simple pendulum. The circle on the phase plane represents the motion over one cycle and is called the trajectory. It should be noted that a periodic motion is a closed orbit in the phase plane and is called a limit cycle.

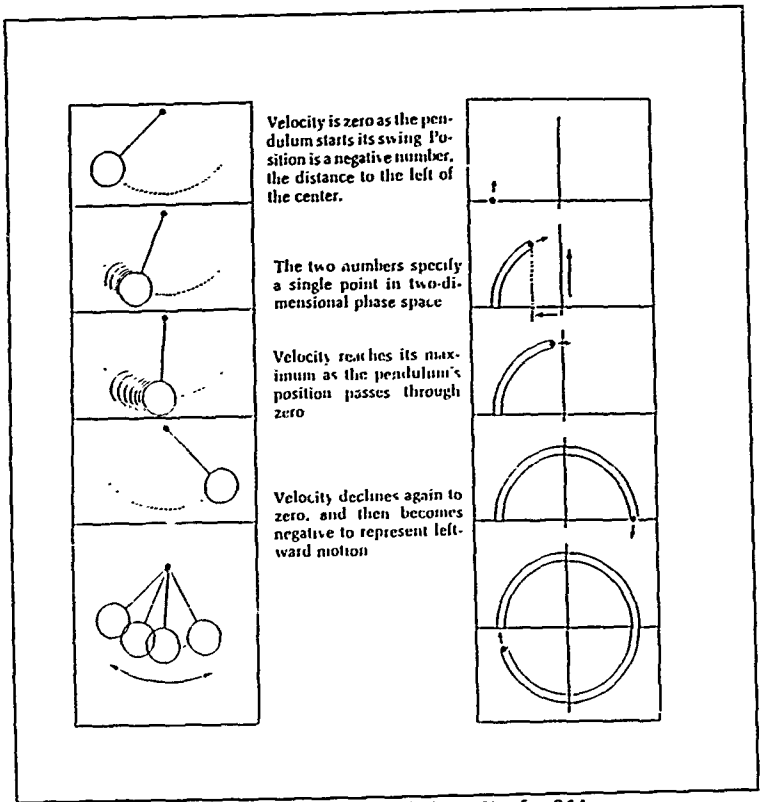

Figure 36. Phase plane of a pendulum [Ref. 21]

Chaotic motions have orbits that never close or repeat. As a result, the trajectory of the orbits will tend to fill up the phase plane.

6. Pseudo-Phase-Space Method

This method is used when only one variable is available, as in typical flight tests where measurements are from a strain-gage or accelerometer. In order to do the 2-D phase plot from strain-gage measurements, the signal must be differentiated. In the case of accelerometer data, the signal has to be integrated twice.

However, by integrating or differentiating, the signal is filtered [Ref. 22]. Differentiating the signal will amplify high frequencies and attentuate low frequencies. Integration will have an opposite effect. As a result, phase plane plots obtained from experimental data will be inaccurate. This resulted in the development of the pseudo-phase-space method or embedding space method. For a one degree system with a measurement x(t), the signal is plotted against itself but delayed or advanced by a fixed time constant: [x(t), x(t+T)]. This plot yields properties similar to the classical phase plane. The closed trajectory in the classical phase plot will be closed in the pseudo-phase method and chaotic motion appear chaotic in both phase planes.

When the state variables are greater than three (position, velocity, time), higher dimension pseudo-phase-space may be constructed using multiple time delays, i.e., (x(t), x(t+T), x(t+2T)).

The advantage of the pseudo-phase plane method is that a single observable variable can be used to construct the

pseudo phase picture and portray the system dynamics without distorting the response through integration or differentiation.

7. Poincaré Section

The Poincaré section can be constructed by placing a two-dimensional surface in a three-dimensional phase space and noting where the points of the trajectory penetrate this surface. This slice will reveal the internal structure of this location.

If the Poincaré section does not consist of a finite set of points or a closed orbit, the motion may be chaotic. For some lightly damped systems, the Poincaré section of chaotic motion appears as a set of unorganized points. This motion is called stochastic and is shown in Figure 37a. In damped systems, the Poincaré section appears more organized with parallel lines as shown in Figures 37b and 37c. The Poincaré sections can be enlarged to observe further structure (Figure 38). After several enlargements, if the structured sets continue to exist, the motion is defined as a strange attractor. This embedding of structure within the structure indicates fractal nature of the behavior, which is a strong indicator of chaotic motions.

B. QUANTITATIVE TESTS FOR CHAOS

The previous section summarized qualitative methods that require experience to evaluate chaotic systems. There are some

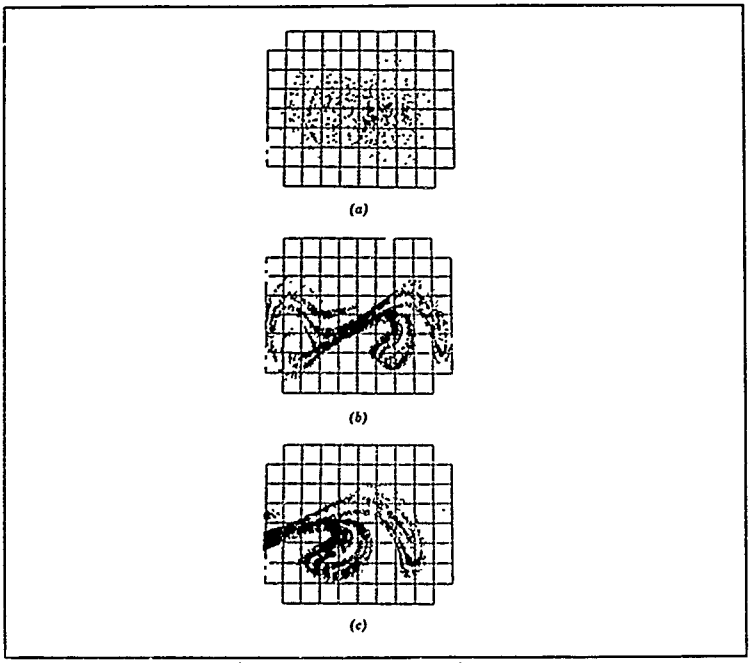

Figure 37. Poincaré maps chaotic motion

quantitative measures to study chaotic motions. Two well-known methods are the Lyapunov exponent and fractal dimension [Refs. 22, 25]. These methods are described below. The Lyapunov exponent will not be used in this analysis and will be discussed summarily.

1. Lyapunov Exponent

The Lyapunov exponent measures how sensitive the system is to changes in initial conditions. It measures the exponential attraction or separation, of two adjacent

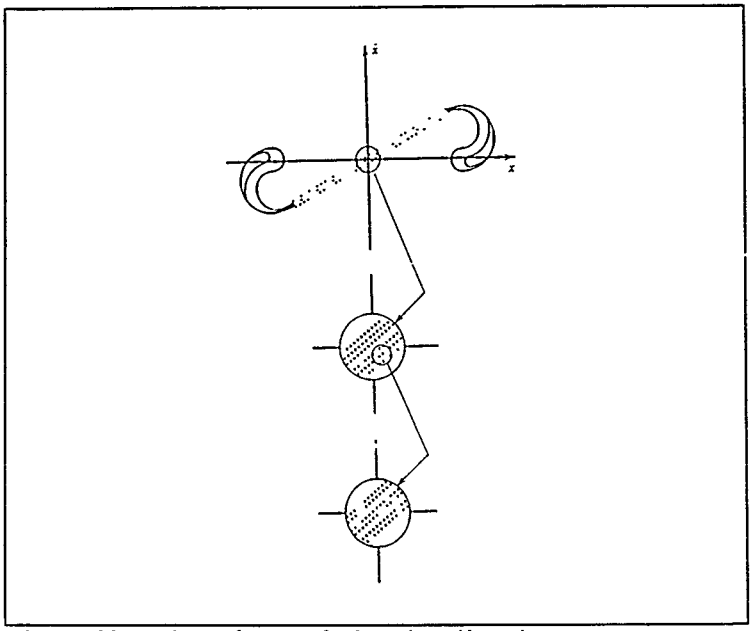

Figure 38. Poincaré map of chaotic vibration

trajectories in phase space with different initial conditions. It is defined as

$$d(t) = d^{2LT} \tag{68}$$

or

$$L = \log_2 \left(\frac{d(t)}{d} \right) \tag{69}$$

where d is the initial distance between two trajectories.

d(t) is the distance at a later time.

L is the Lyapunov exponent.

A positive exponent implies d(t), the later distance will be larger than the initial distance and indicates chaotic dynamics.

2. Fractal Dimension

The fractal dimension is another quantitative test for chaos and gives a lower bound on the number of essential variables needed to model the dynamics of the system. Non-integer values for a fractal dimension indicates presence of a strange attractor. [Refs. 22,25]

There are six ways to classify fractal dimensions. The dimension that will be discussed in this analysis is the correlation fractal dimension.

The correlation fractal dimension is defined as

$$C(r) = r^{d} \tag{70}$$

where: C(r) is the probability of the attractor within a circle, sphere or hypersphere of radius r, and d is the fractal dimension.

By taking the natural logarithm of both sides of equation (70) and solving for d, following equation results:

$$d = \lim_{r \to 0} \left(\frac{\ln C(r)}{\ln r} \right) \tag{71}$$

The procedure adapted in Sarigul-Klijn [Ref. 22] is described below:

1. Start with a point on the attractor and calculate the number of points inside a circle of radius r.

2. Calculate probability C(r) by dividing this number of points by total number of points in the attractor.

3. Repeat this for several points along the attractor.

4. Compute C(r) for several values of r.

5. The slope of log (C(r)) versus log (r) gives d, the correlation fractal dimension.

To obtain the correlation dimension of the attractor of a given system, the procedure must be applied in the pseudo phase space for several embedded dimensions. The asymptotic value of the correlation dimension is the fractal dimension of the attractor and is given by

$$C(r) = \lim_{N\to\infty} \frac{1}{N^2} \sum_{i}^{N} \sum_{j}^{N} H(r - |x_i - x_j|) \qquad (72)$$

where: H(s) = 1 if s>0 and H(s) = 0 if s<0.

$|x_i - x_j|$ is the Euclidean distance between the points.

N is total number of points.

If the fractal dimension is approximately equal to the phase space used for the calculation, the attractor lies in a higher dimensional phase space. If the fractal dimension is non-integer and is independent of the dimension of phase space, the signal is characterized as chaotic. [Ref. 22]

C. LACE SPACECRAFT BOOM AS A NONLINEAR SYSTEM

The booms for the LACE spacecraft have a constant EI distribution [Ref. 10] and the response would appear to be linear. However, at each bay, battens are joined to the

longerons by joints. Freeplay introduced at the joints tend to introduce nonlinearities. In this section, the spacecraft boom alone is modeled and a parametric study to simulate the influence of nonlinearities introduced by the freeplay at the joints on the system response is presented. The resulting behavior of the motion is studied using the methods of chaos [Ref. 21].

The LACE spacecraft boom is modeled as a nonlinear single-degree of freedom system. The equation of motion for such a system is described by

$$m\ddot{u}+f(u,\dot{u},t) = A_0 \cos wt \qquad (73)$$

where f(u,u̇,t) contains nonlinear damping and stiffness terms. The stiffness of the boom is modeled as

$$f_{si} = A, u^3 + B, u^2 + C, u + d_1$$

and the damping as

$$f_{Di} = A_2\dot{u}^2 + B_2\dot{u} + C_2$$

For the present analysis, the damping is assumed to be linear and contains only the linear term corresponding to equivalent viscous damping. The nonlinear stiffness contribution due to the joints is modeled by the cubic term, A_1u^3. The linear term representing the boom stiffness distribution is determined from the experimental stiffness properties of the beam using the relation

$$K = \frac{12EI}{L^3} \tag{74}$$

The coefficient for the cubic term is treated as a parameter and as part of the parametric study, is varied as a function of the linear term as follows

$$A_1 = C_1 + nC_1 \tag{75}$$

where n varies from ±.1 to ±.5. The equation of motion reduces to Duffing's equation in the following form:

$$m\ddot{u} + B_2\dot{u} + A_1u^3 + C_1u = A_0\cos wt \tag{76}$$

The response of this nonlinear system to a forcing function is determined by approximating the derivatives as shown in the equation of motion. A solution based on step-by-step integration is used to generate the time response. A FORTRAN program was developed based on the "linear acceleration method" and is presented in Appendix I. The recursion formulas used for the numerical integration is derived in the following analysis.

In the linear acceleration method adopted here, the acceleration is approximated for a given step by the following relation:

$$\ddot{u}(\tau) = \ddot{u}_i + \frac{\Delta\ddot{u}_i}{\Delta t}\tau \tag{77}$$

Integration of equation (77) yields

$$\dot{u}_{i+1} = \dot{u}_i + \ddot{u}_i\tau + \frac{(\Delta \ddot{u}_i)}{\Delta t}\frac{\tau^2}{2} \tag{78}$$

and

$$u_{i+1} = u_i + \dot{u}_i\tau + \ddot{u}_i\frac{\tau^2}{2} + \frac{\Delta \ddot{u}_i}{\Delta t}\frac{\tau^3}{6} \tag{79}$$

By using incremental quantities, Δp_i, Δu_i, $\Delta \dot{u}_i$, and $\Delta \ddot{u}_i$, the computational algorithm is set up. Equation (79) may be solved for $\ddot{u}_i$ and equations (78) and (79) are be combined to give $\Delta \dot{u}_i$ as follows:

$$\Delta \ddot{u}_i = \frac{6}{\Delta t^2}\Delta u_i - \frac{6}{\Delta t}\dot{u}_i - 3\ddot{u}_i \tag{80}$$

$$\Delta \dot{u}_i = \frac{3}{\Delta t}\Delta u_i - 3\dot{u}_i - \ddot{u}_i\frac{\Delta t}{2} \tag{81}$$

Since equation (73) is satisfied at both t_i and t_{i+1}, it may be written as

$$m\Delta \ddot{u}_i + C_i\Delta \dot{u}_i + k_i\Delta u_i = \Delta p_i \tag{82}$$

Combining equations (80), (81), and (82) yields the incremental equation of motion

$$K_i^*\Delta u_i = \Delta p_i^* \tag{83}$$

where

$$K_i^* = K_i - \left(\frac{3C_i}{\Delta t_i}\right) + \frac{6m}{\Delta t_i^2} \tag{84}$$

and

$$\Delta p_i^* = \Delta p_i + \left[\frac{6m}{\Delta t} + 3C_i\right]\dot{u}_i + \left[3m + \frac{C_i \Delta t}{2}\right]\ddot{u}_i \tag{85}$$

Once Δu_i is determined from equation (83), $\Delta \dot{u}_i$ is obtained from equation (81) and $\Delta \ddot{u}_i$ from equation (80). The updated values of u, $\dot{u}$, and $\ddot{u}$ at step (i+1) is computed from

$$\begin{aligned} u_{i+1} &= u_i + \Delta u_i \\ \dot{u}_{i+1} &= \dot{u}_i + \Delta \dot{u}_i \\ \ddot{u}_{i+1} &= \ddot{u}_i + \Delta \ddot{u}_i \end{aligned} \tag{86}$$

This step by step procedure described determines the response of the LACE spacecraft boom modeled as a nonlinear system. The numerical integration provides a time history of the response, namely deflection, u, velocity, v, and acceleration, a.

Since experimental data for a 23-foot LACE-model boom is available from AEC-ABLE Engineering, the length of the boom analyzed is taken to be 23 feet. In the parametric study, the parameters varied are the excitation amplitude, frequency and the coefficient of the cubic stiffness term. The excitation amplitudes used gives deflections of 2.5%, 5%, 10%, 20%, and 25% of the length of the spacecraft boom. The frequencies used

are $1/3w_n$ and $3w_n$. These frequencies are chosen based on the cubic term of the stiffness that generates subharmonic and superharmonic response at one-third and three times the excitation frequency, respectively. The coefficient of the cubic stiffness term is varied from ±.1 to ±.5 of the linear stiffness term.

The constant terms used in the equation of motion are as follows:

K = 3.02 lbs/in

m = .1475 slugs

c = .177 slugs/sec

w_n = 4.6 rad/sec

where $c = 2\sqrt{km}\zeta$. The damping factor ζ was obtained from AEC-ABLE Engineering using the Logarithmic Decrement method. A 23 foot boom mounted in its deployment cannister rigidly attached to a wall yields ζ=.039 and a 23-foot boom rigidly mounted to a wall yields ζ=.001. The first case approximates the LACE spacecraft configuration. Both damping cases are considered in the present simulation.

D. CHAOTIC VIBRATION ANALYSIS

A comprehensive FORTRAN program called CHAOS was developed by Sarigul-Klijn [Ref. 22] to analyze chaotic vibrations. The time history data from the numerical simulation program is used by the CHAOS program for the chaotic vibration analysis. The program CHAOS currently has 12 analysis options. They are

1. Plot the time history
2. Plot onto toroidal phase space
3. Take Poincaré section of toroidal phase space
4. Plot onto 2-D phase space
5. Plot onto 2-D Van der Pol plane
6. Plot onto 3-D phase space
7. Take Poincaré section of 3-D phase space
8. 3-D Poincaré section of a 4-D hyperspace
9. Compute fourier power spectrum
10. Compute statistics
11. Compute Lyapunov exponent
12. Compute fractal correlation dimension

As discussed earlier, the stiffness term is modeled as a combination of linear and cubic terms. The coefficient of the cubic term is varied as a percentage of the linear term from 10% to 50%, and is seen to yield no significant changes in the response. Therefore, an average value of 30% is used in all subsequent numerical simulation.

In order to focus the present study within the scope of this research, the study is divided into four specific groups. Each group is identified by excitation frequency and damping. In each group, the excitation amplitudes are 20.8 lbs, 41.7 lbs, 83.4 lbs, 166.7 lbs, and 208.4 lbs respectively. This yields a deflection of 2.5%, 5%, 10%, 20%, and 25% of the length of the beam, respectively. Table VI contains the group identification.

Table VI GROUP IDENTIFICATION

GROUP	Ω	C
A	1.53	.77
B	13.8	.177
C	1.53	.0454
D	13.8	.0454

The initial analysis consists of studying four qualitative indicators of chaos. They are time history, fourier power spectrum, pseudo-phase plane and Poincare section respectively. Then, quantitative measures of the motion are computed.

Figures 39-43 and 44-48 present the qualitative indicators for cases A and B respectively. The time history is initially transient and then becomes periodic in both cases. The fourier power spectrum indicates a broad-band frequency spectrum, with the number of spikes increasing with an increase in amplitude. The pseudo-phase plane plot indicates that the motion settles to a single limit cycle for case A and a double limit cycle for case B. The Poincaré section is very sparse and indicates a periodic system. The periodic time history also indicates a non-chaotic response.

Figures 49-53 and 54-58 present the qualitative indicators of chaos for groups C and D. In all cases, the time history is seen to be non-periodic and the Fourier power spectrum is observed to be broad-band. In both cases, there appears to be two limit cycles in the pseudo-phase plot. The Poincaré

sections appear more dense than the previous groups and has the appearance of a strange attractor. These systems appear to be chaotic.

To ascertain the quantitative nature of the response, the fractal correlation dimension is computed for each group and is shown in Table VII. Figures 59 and 60 show the fractal dimension for increasing phase space dimension for two cases of damping with F=20.8 and Ω=1.53 respectively. The plots for the other cases are given in Appendix J.

A non-integer fractal dimension is indicative of the presence of chaos in a system [Refs. 22,23,24,25]. This is consistent with the qualitative indicators of groups C and D. The inconsistency with groups A and B indicate that the fractal dimension by itself does not confirm the strangeness of the strange attractor as believed in the reported literature and must be used in conjunction with other indicators of chaos. Additional results pertaining to this parametric study are reported elsewhere [Ref. 26].

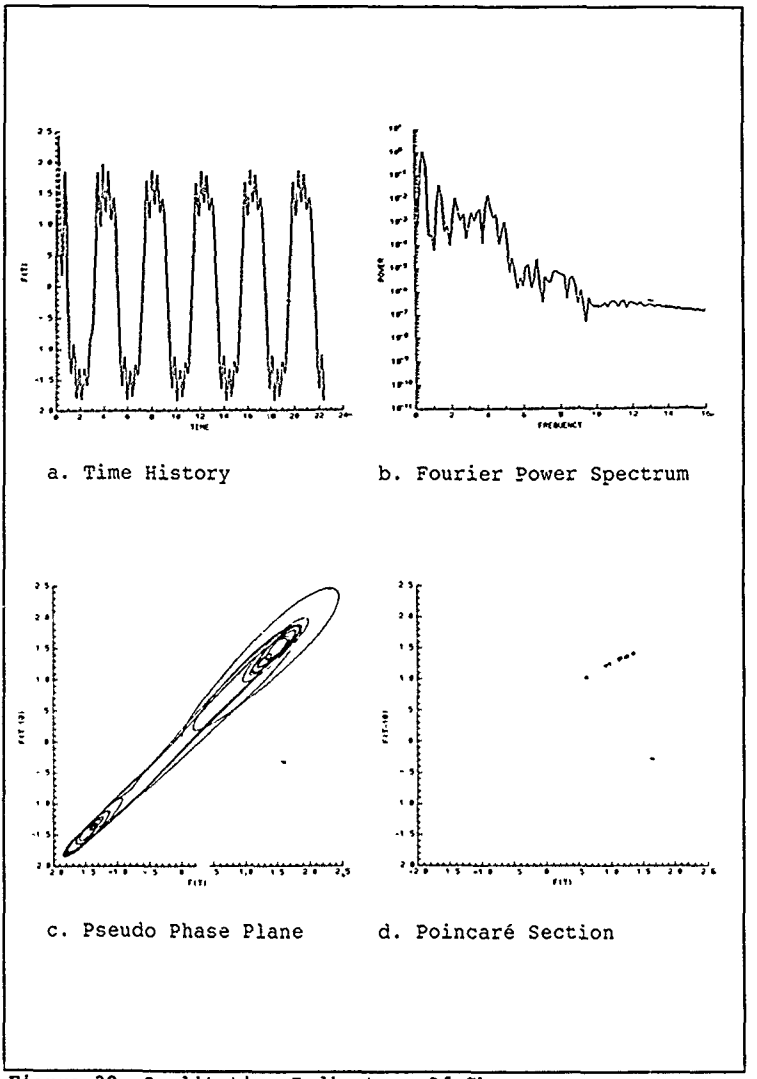

Figure 39. Qualitative Indicators Of Chaos.
F=20.8 lbs, Ω=1.53 Hz, C=.177.

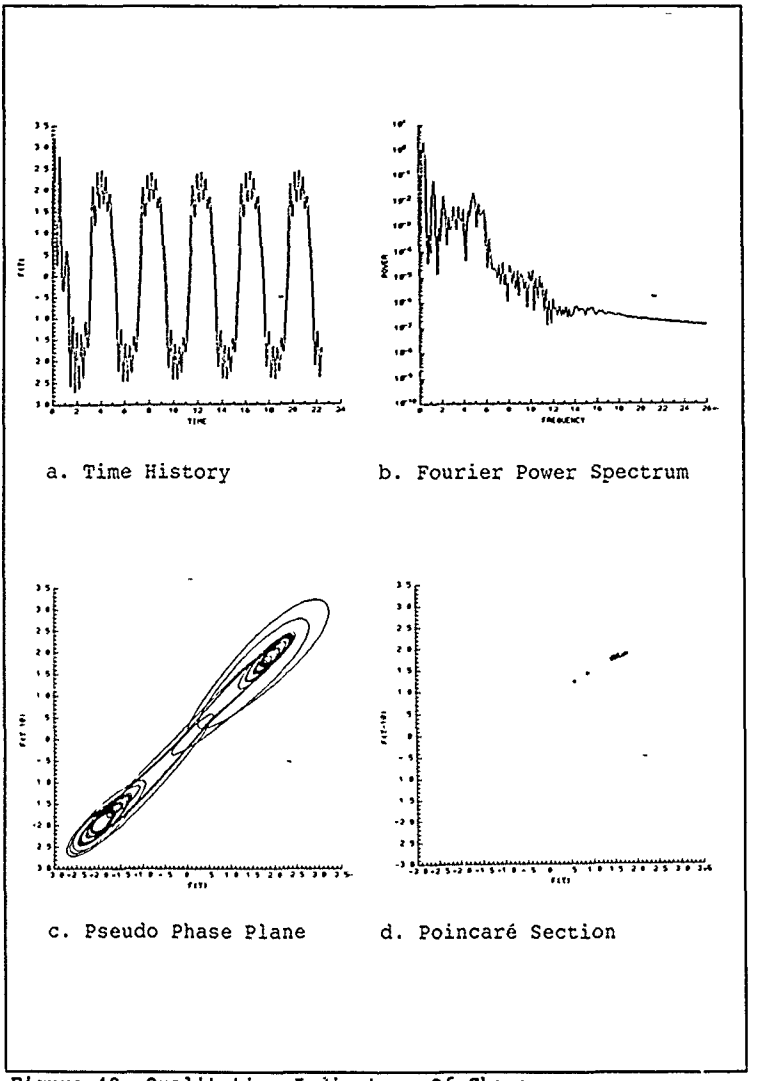

a. Time History

b. Fourier Power Spectrum

c. Pseudo Phase Plane

d. Poincaré Section

Figure 40. Qualitative Indicators Of Chaos.
F=41.68 lbs, Ω=1.53 Hz, C=.177

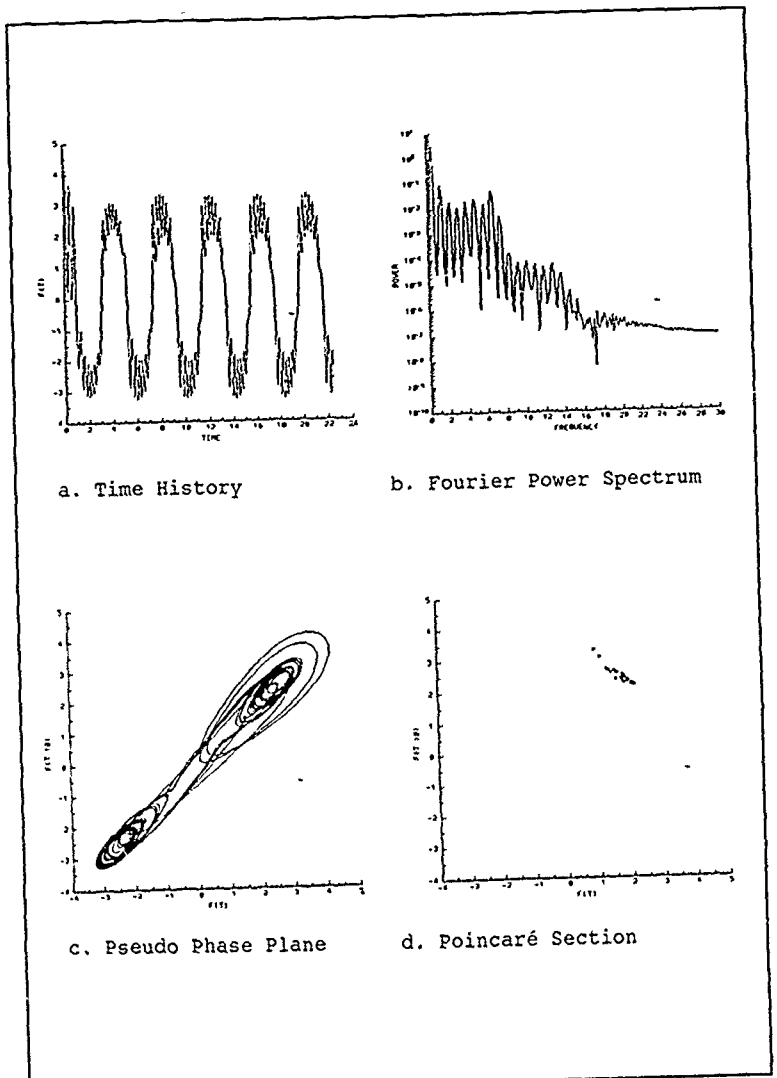

a. Time History

b. Fourier Power Spectrum

c. Pseudo Phase Plane

d. Poincaré Section

Figure 41. Qualitative Indicators Of Chaos.
F=83.352 lbs, Ω=1.53 Hz, C=.177

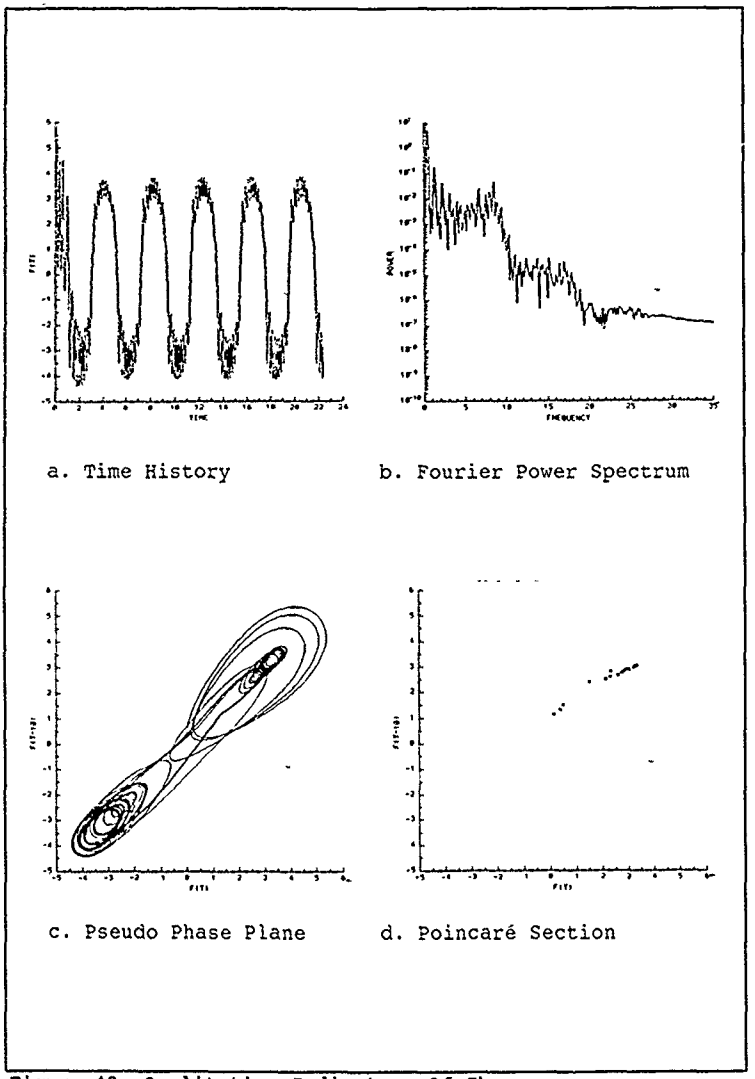

a. Time History

b. Fourier Power Spectrum

c. Pseudo Phase Plane

d. Poincaré Section

Figure 42. Qualitative Indicators Of Chaos.
F=166.7 lbs, Ω=1.53 Hz, C=.177

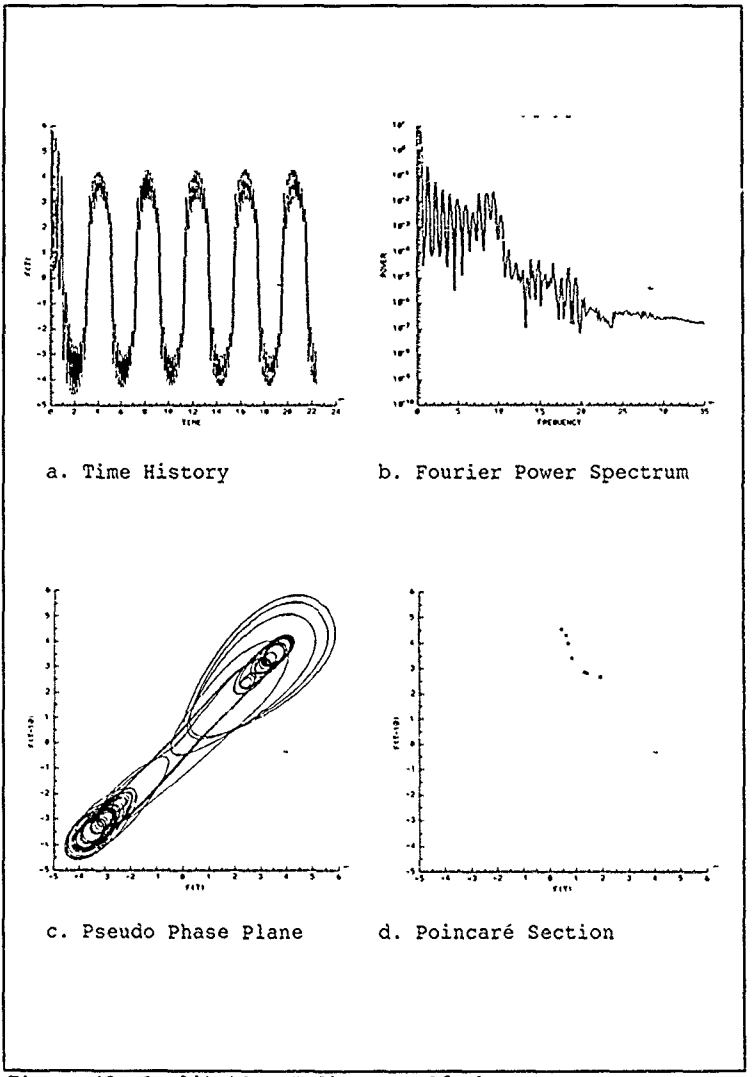

a. Time History

b. Fourier Power Spectrum

c. Pseudo Phase Plane

d. Poincaré Section

Figure 43. Qualitative Indicators Of Chaos.
F=208.38 lbs, Ω=1.53 Hz, C=.177

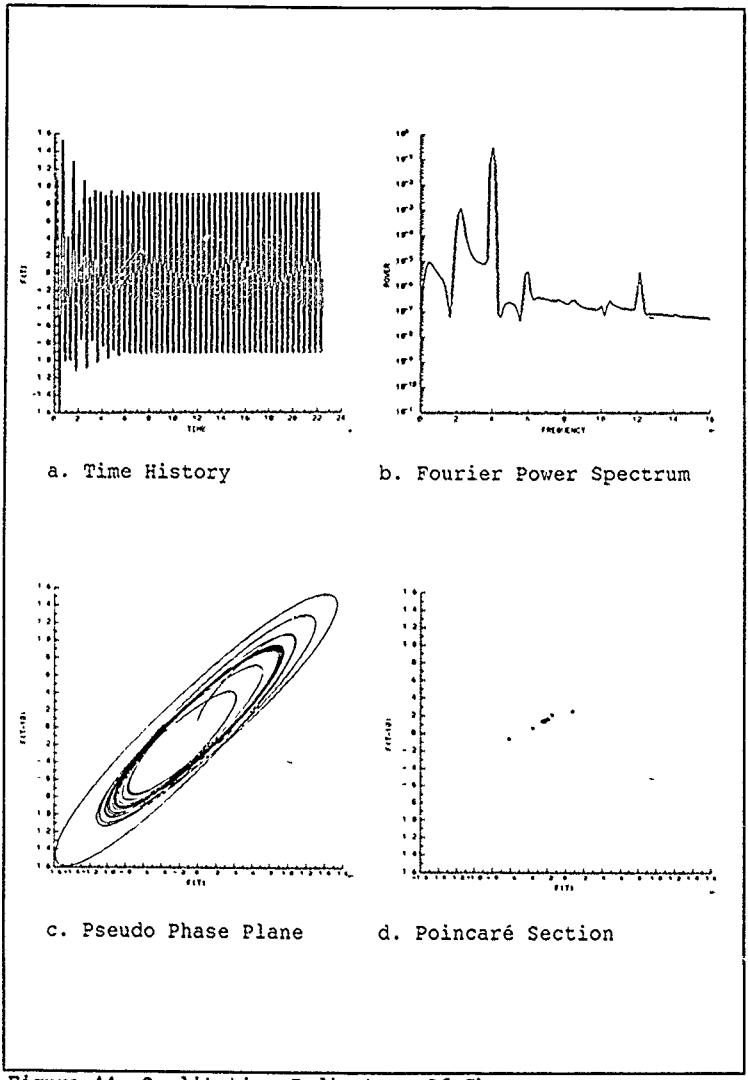

a. Time History

b. Fourier Power Spectrum

c. Pseudo Phase Plane

d. Poincaré Section

Figure 44. Qualitative Indicators Of Chaos.
F=20.8 lbs, Ω=13.8 Hz, C=.177

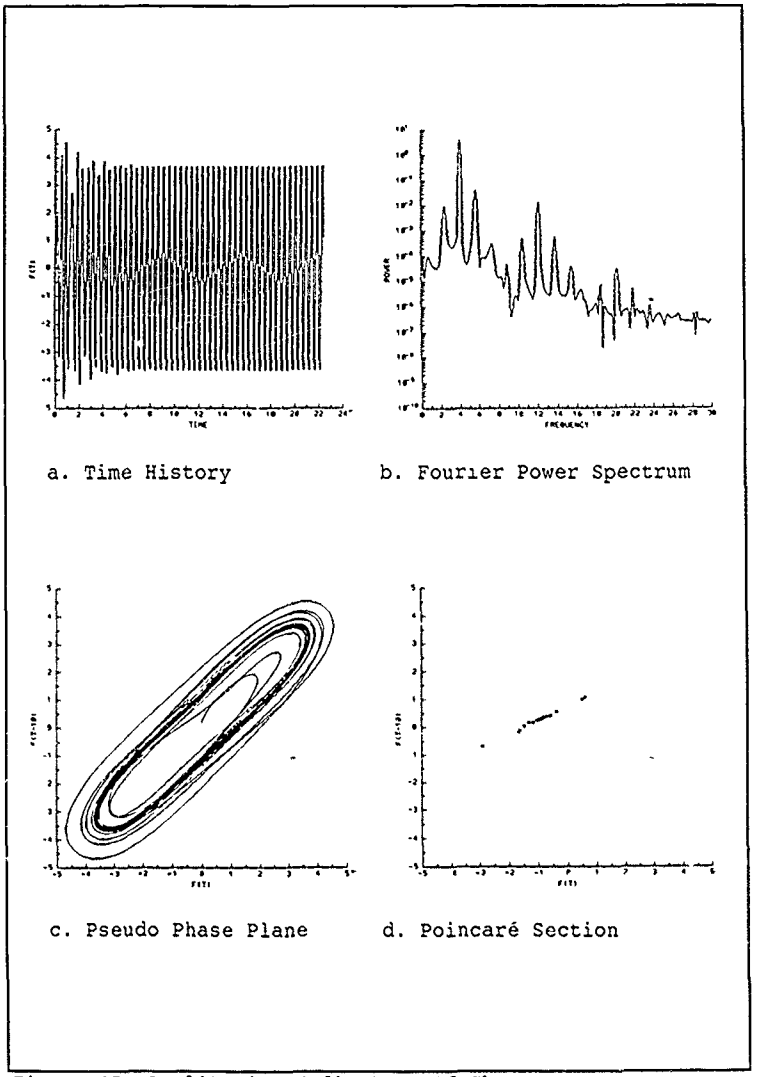

a. Time History

b. Fourier Power Spectrum

c. Pseudo Phase Plane

d. Poincaré Section

Figure 45. Qualitative Indicators Of Chaos.
F=41.68 lbs, Ω=13.8 Hz, C=.177

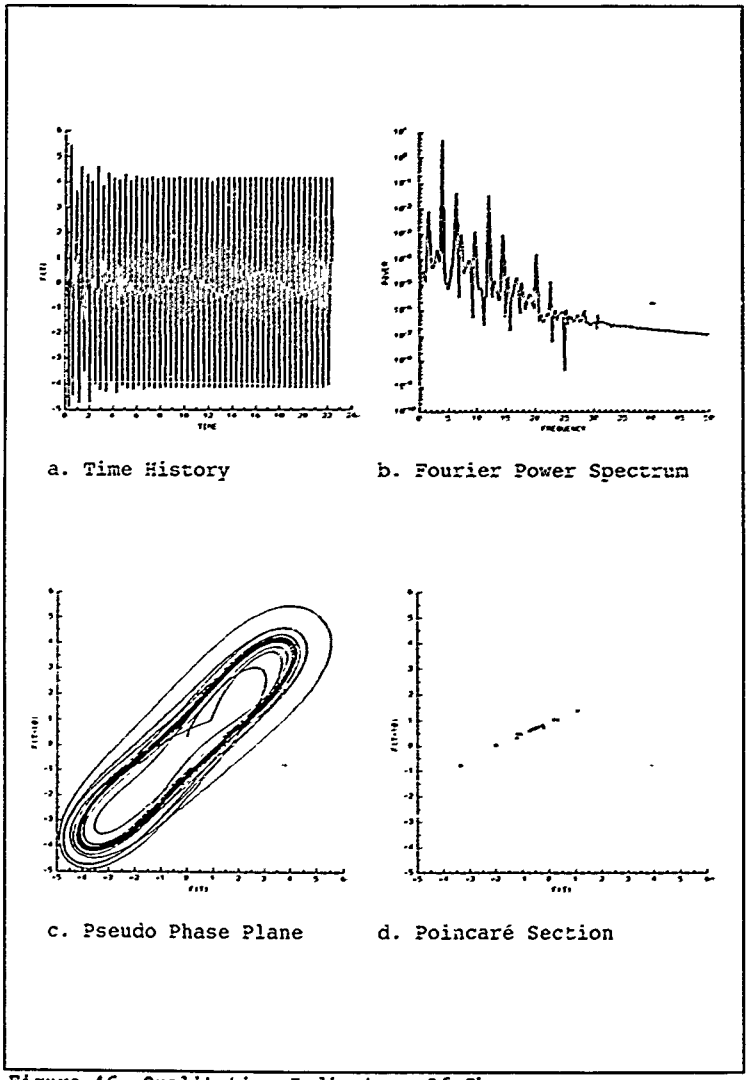

a. Time History

b. Fourier Power Spectrum

c. Pseudo Phase Plane

d. Poincaré Section

Figure 46. Qualitative Indicators Of Chaos.
F=83.352 lbs, Ω=13.8 Hz, C=.177

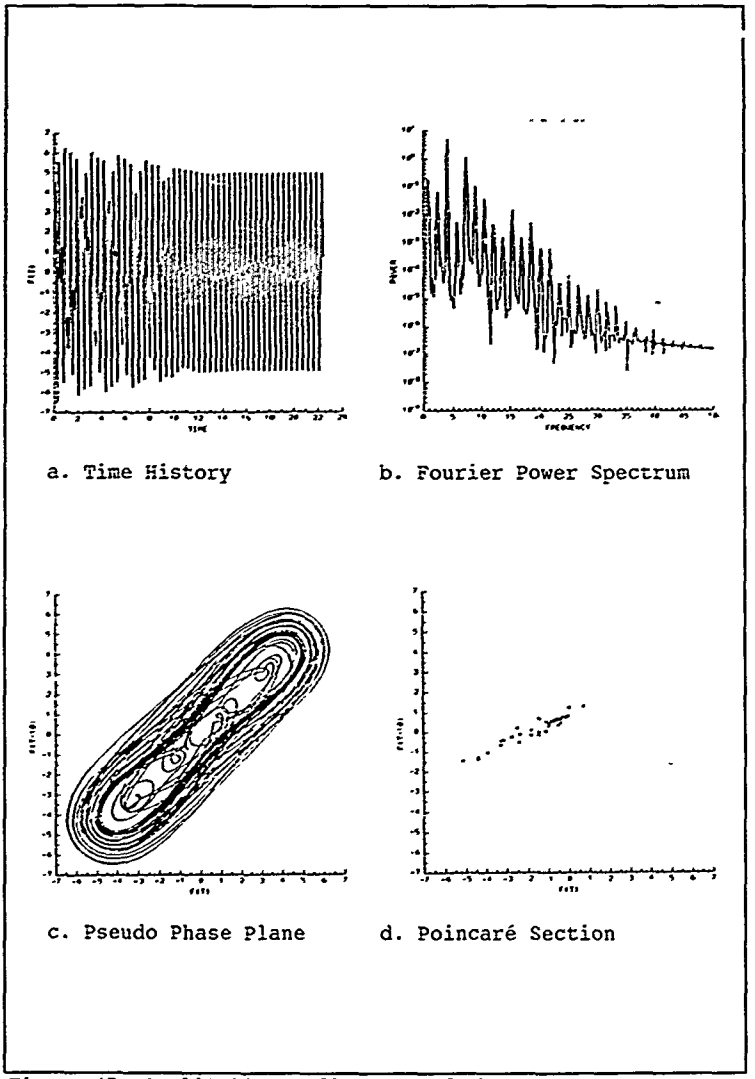

a. Time History

b. Fourier Power Spectrum

c. Pseudo Phase Plane

d. Poincaré Section

Figure 47. Qualitative Indicators Of Chaos.
F=166.7 lbs, Ω=13.8 Hz, C=.177

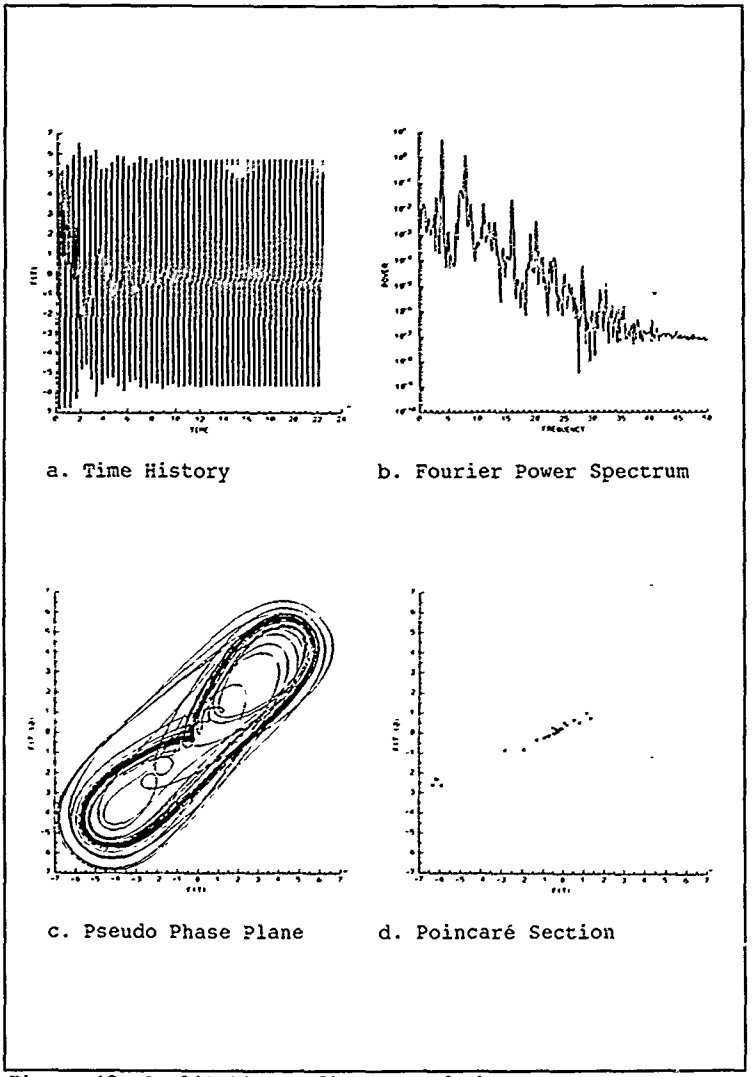

Figure 48. Qualitative Indicators Of Chaos.
F=208.38 lbs, Ω=13.8 Hz, C=.177

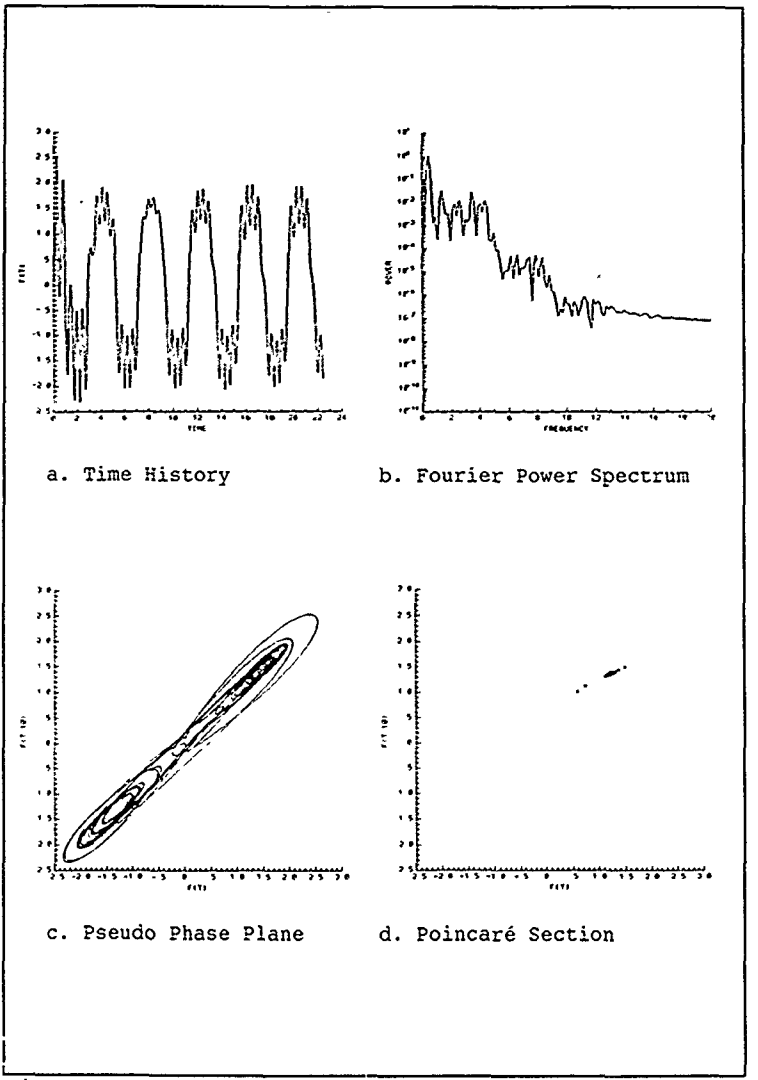

a. Time History

b. Fourier Power Spectrum

c. Pseudo Phase Plane

d. Poincaré Section

Figure 49. Qualitative Indicators Of Chaos.
F=20.8 lbs, Ω=1.53 Hz, C=.0454

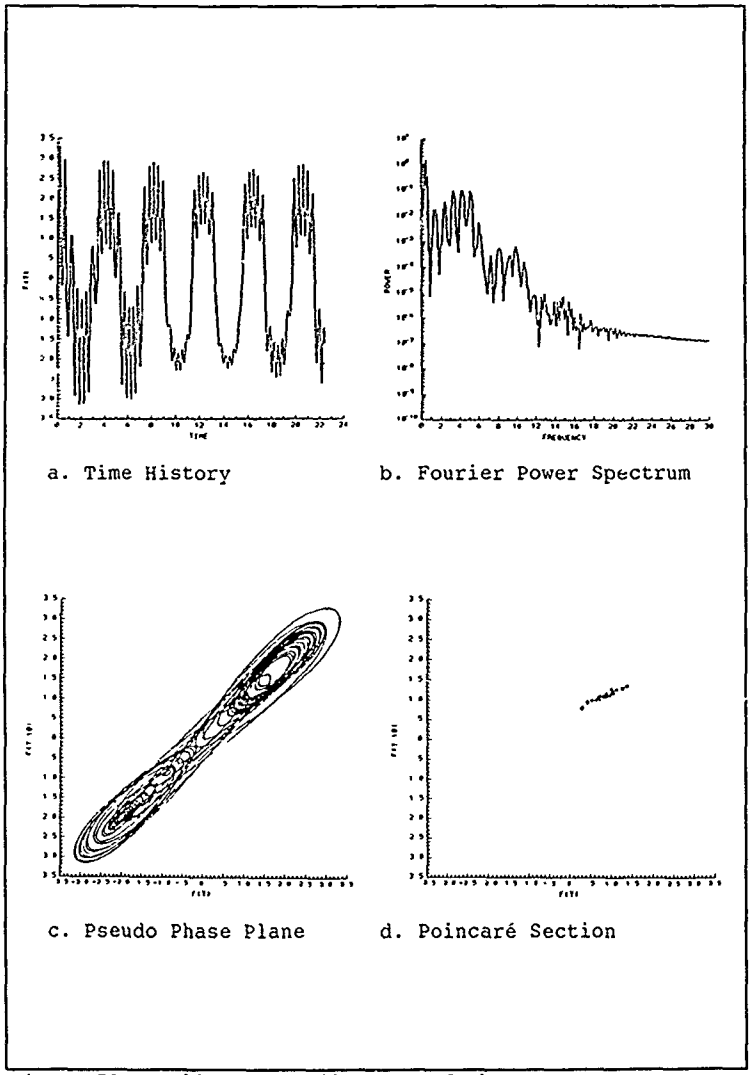

a. Time History

b. Fourier Power Spectrum

c. Pseudo Phase Plane

d. Poincaré Section

Figure 50. Qualitative Indicators Of Chaos.
F=41.68 lbs, Ω=1.53 Hz, C=.0454

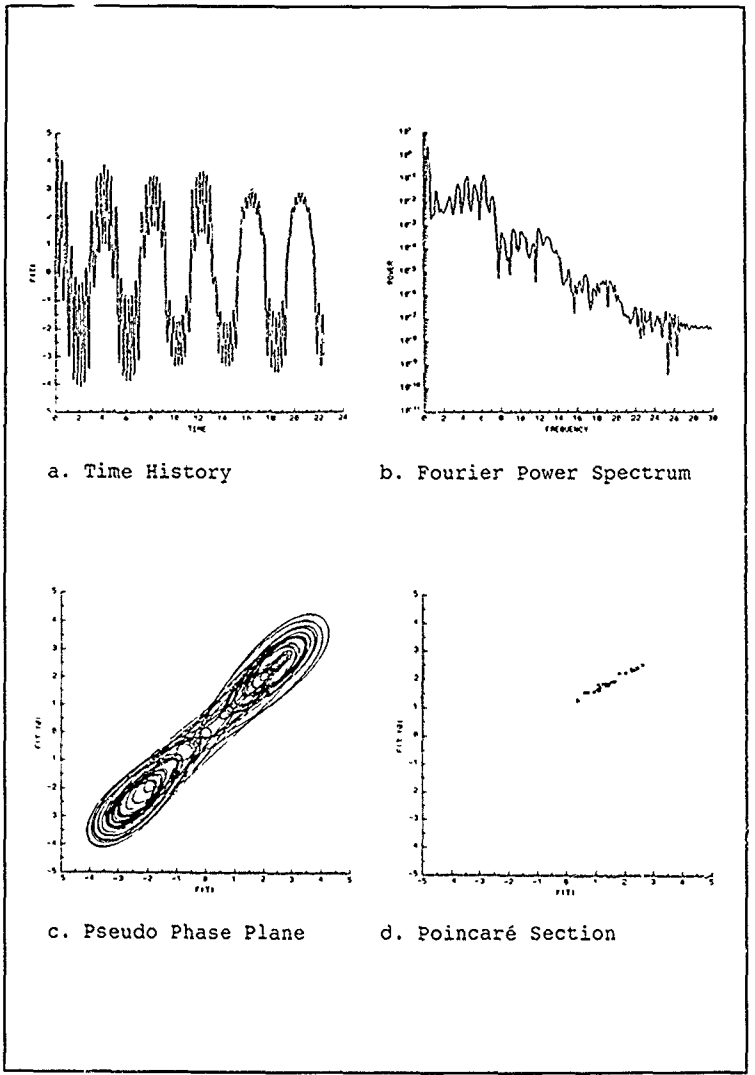

a. Time History

b. Fourier Power Spectrum

c. Pseudo Phase Plane

d. Poincaré Section

Figure 51. Qualitative Indicators Of Chaos.
F=83.352 lbs, Ω=1.53 Hz, C=.0454

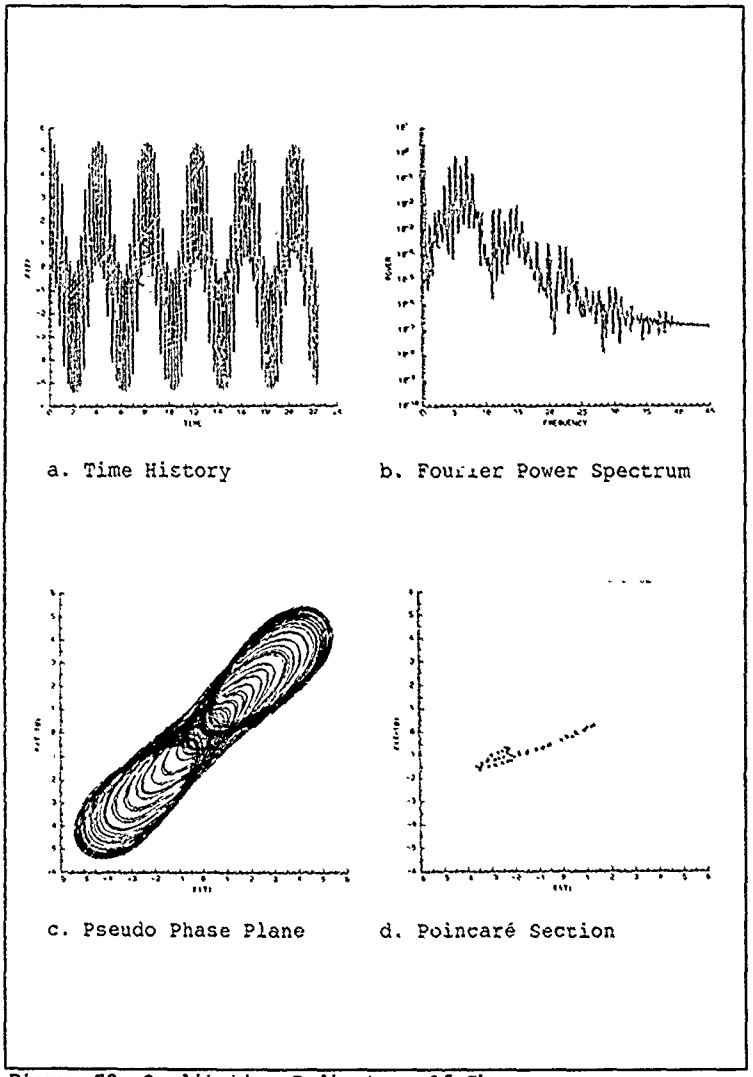

Figure 52. Qualitative Indicators Of Chaos.
F=166.7 lbs, Ω=1.53 Hz, C=.0454

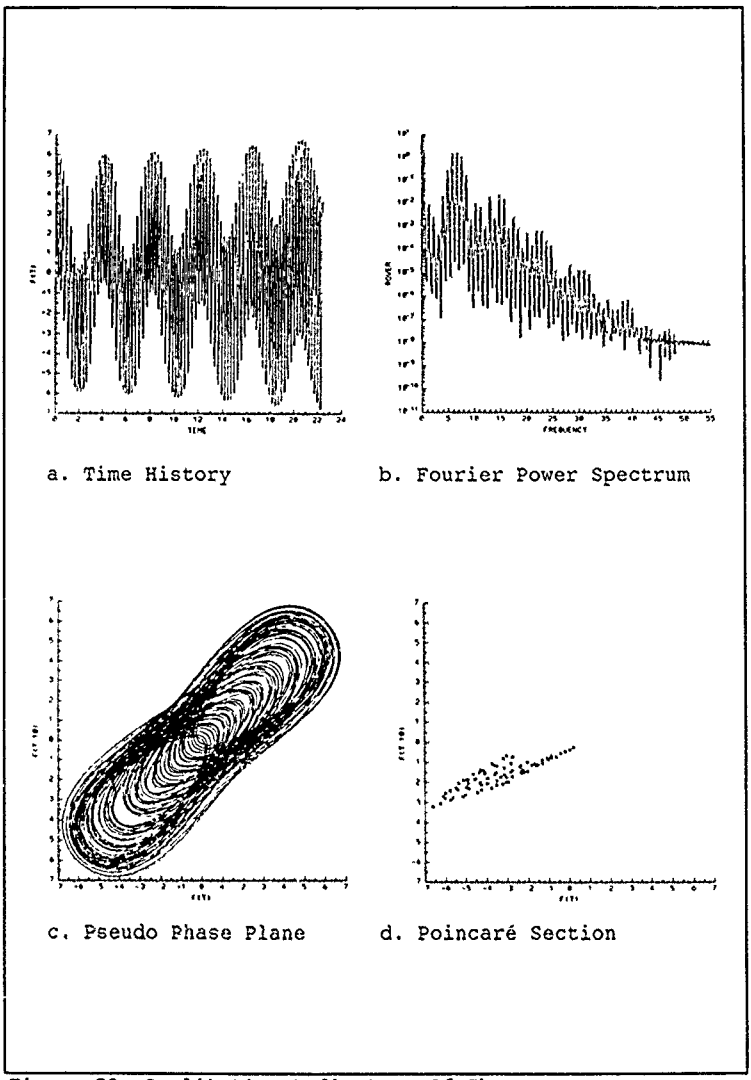

a. Time History

b. Fourier Power Spectrum

c. Pseudo Phase Plane

d. Poincaré Section

Figure 53. Qualitative Indicators Of Chaos.
F=208.38 lbs, Ω=1.53 Hz, C=.0454

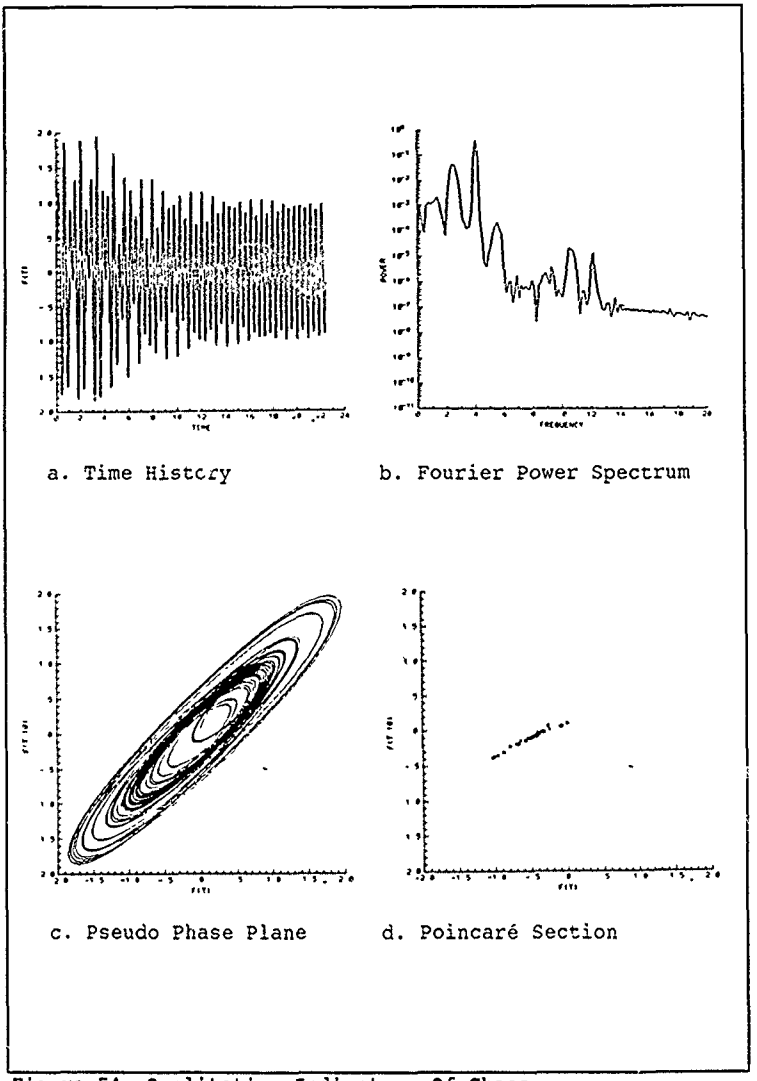

a. Time History

b. Fourier Power Spectrum

c. Pseudo Phase Plane

d. Poincaré Section

Figure 54. Qualitative Indicators Of Chaos. F=20.8 lbs, Ω=13.8 Hz, C=.0454

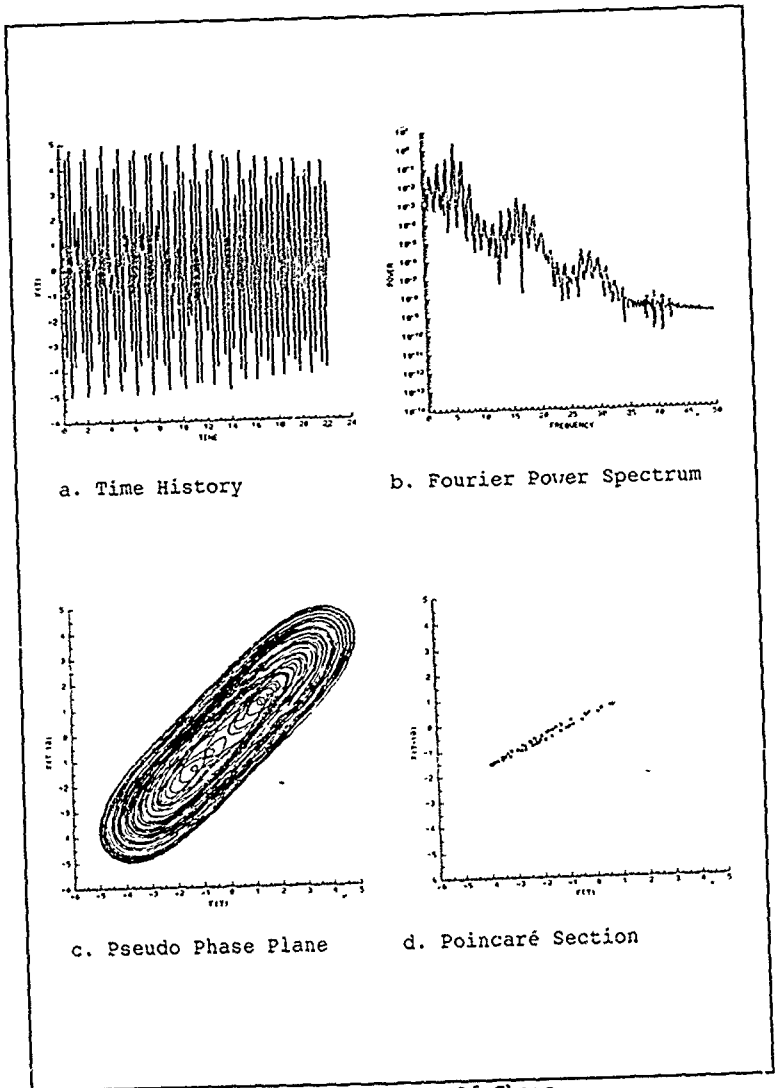

Figure 55. Qualitative Indicators Of Chaos.
F=41.68 lbs, Ω=13.8 Hz, C=.0454

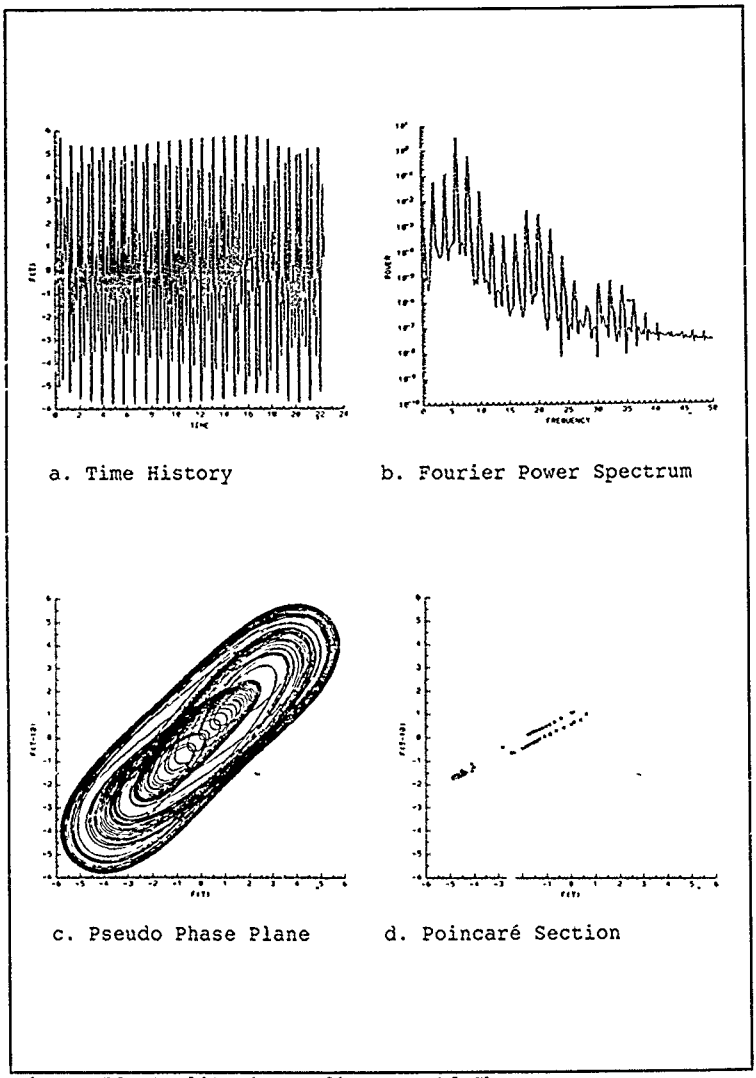

Figure 56. Qualitative Indicators Of Chaos.
F=83.352 lbs, Ω=13.8 Hz, C=.0454

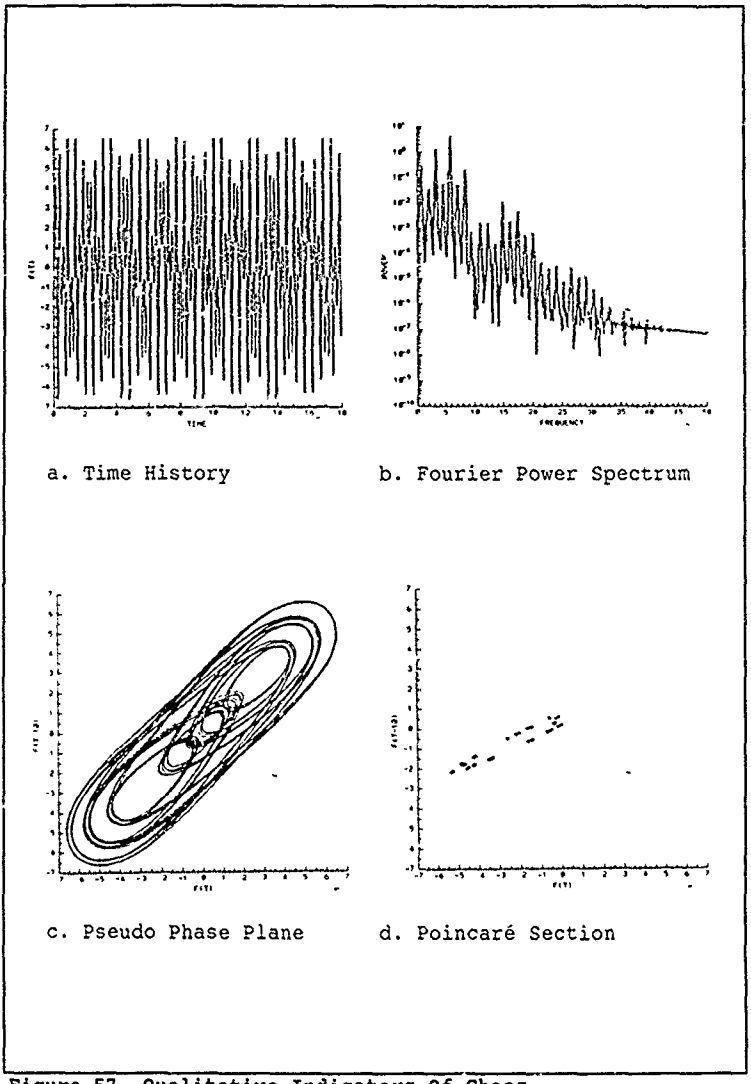

a. Time History

b. Fourier Power Spectrum

c. Pseudo Phase Plane

d. Poincaré Section

Figure 57. Qualitative Indicators Of Chaos.
F=166.7 lbs, Ω=13.8 Hz, C=.0454

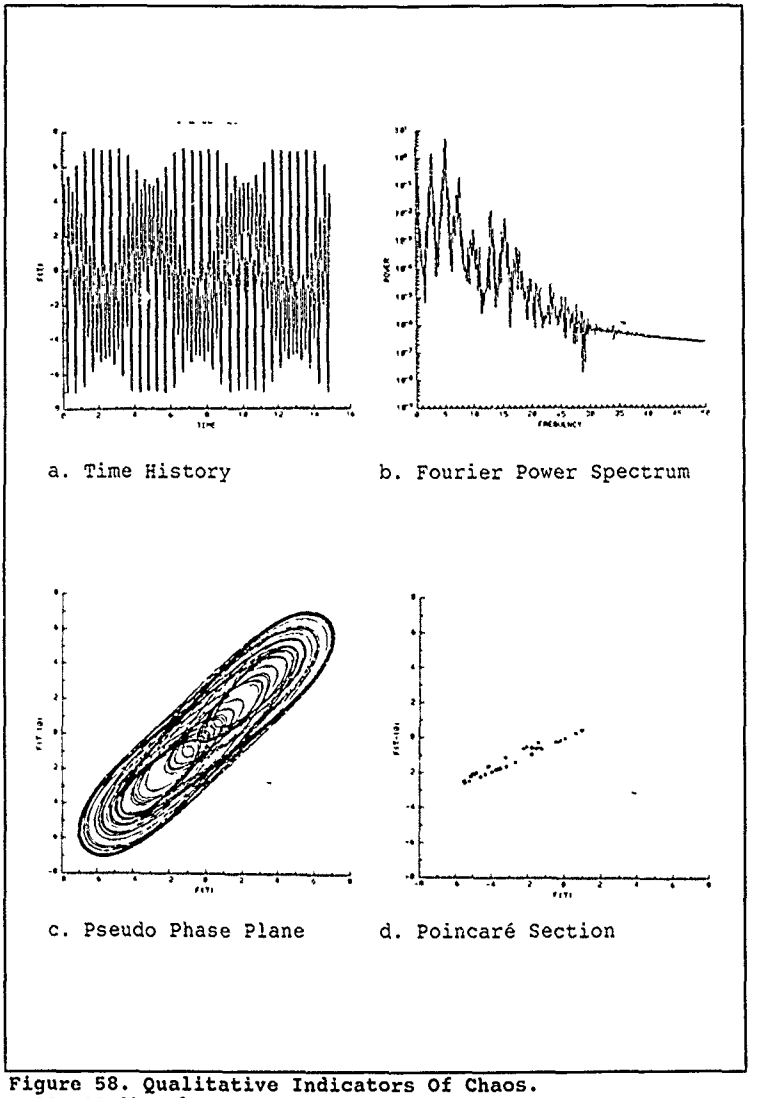

a. Time History

b. Fourier Power Spectrum

c. Pseudo Phase Plane

d. Poincaré Section

Figure 58. Qualitative Indicators Of Chaos.
F=208.38 lbs, Ω=13.8 Hz, C=.0454

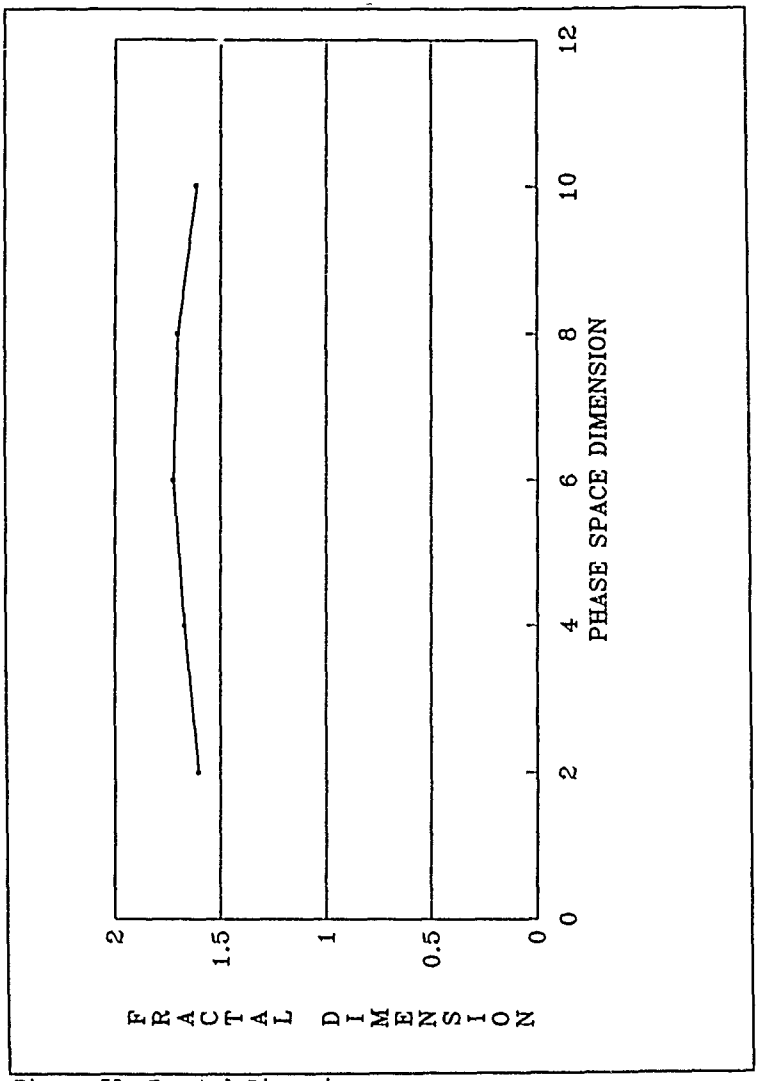

Figure 59. Fractal Dimension
F=20.8, Ω=1.53, C=.177

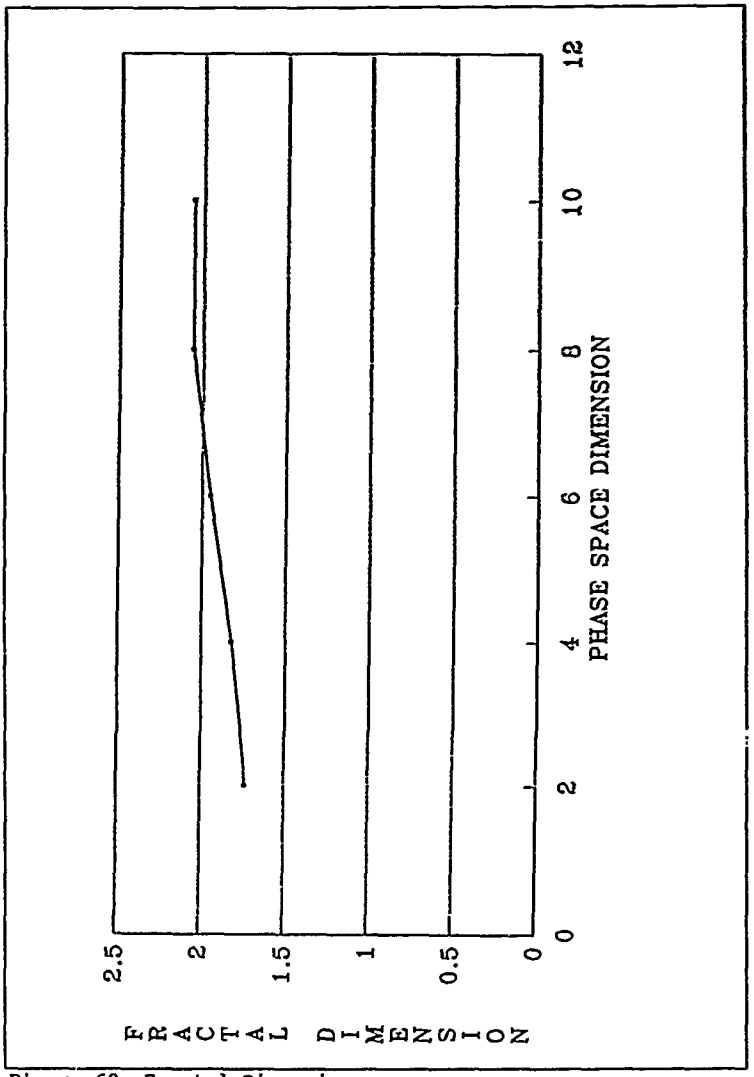

Figure 60. Fractal Dimension.
F=20.8, Ω=1.53, C=.0454

Table VII. FRACTAL DIMENSION

	F	Ω	C	FRACTAL DIMENSION
a)	20.8	1.53	.177	1.7
	41.7	1.53	.177	1.6
	83.4	1.53	.177	1.7
	166.7	1.53	.177	1.7
	208.4	1.53	.177	1.7
b)	20.8	13.8	.177	1.2
	41.7	13.8	.177	1.2
	83.4	13.8	.177	1.3
	166.7	13.8	.177	1.6
	208.4	13.8	.177	1.4
c)	20.8	1.53	.0454	2.05
	41.7	1.53	.0454	2.4
	83.4	1.53	.0454	2.05
	166.7	1.53	.0454	2.1
	201.4	1.53	.0454	2.6
d)	20.8	13.8	.0454	2.1
	41.7	13.8	.0454	2.4
	13.4	13.8	.0454	1.95
	166.7	13.8	.0454	2.1
	208.4	13.8	.0454	

VIII. CONCLUSIONS AND SCOPE FOR FURTHER RESEARCH

A. CONCLUSIONS

A detailed finite-element model of the LACE spacecraft has been developed using the finite element program GIFTS. A dynamic analysis was performed on the model to determine the natural frequencies and mode shapes. This model will provide a basis for comparison when actual orbital test data is available.

Thermoelastic effects of the LACE spacecraft boom were investigated for a worst case temperature scenario. The results indicated that the deflections induced would have negligible effect on the systems dynamics and would not affect the on-orbit systems identification or induced thermal flutter.

A preliminary study was conducted on a 23-foot section of the LACE spacecraft boom to investigate the possibility of chaotic vibrations occuring by varying the excitation amplitude and frequency. The system was modeled as a single-degree-of-freedom system with arbitrary nonlinear stiffness, and nonlinear damping excited by a sinusoidal function. A numerical integration program was developed to determine the system response using various excitation amplitudes and frequencies. Four qualitative methods, time history, fourier

power spectrum, pseudo-plane, and Poincaré section methods were used to evaluate chaotic vibrations. In addition, quantitative analysis included computation of correlation fractal dimension. It was evidenced that a combination of all appoaches was needed to determine the nature of vibrations. Chaotic vibrations were present for the low-damped system while periodic response was indicated for highly damped systems.

A non-integer correlation fractal dimension, which is believed to be a quantitative indication of chaos in a system, was evidenced for both periodic and non-periodic responses of the system. This important result, which is further being confirmed from analysis of flight test data [Ref. 21] shows that the fractal dimension by itself is not enough to characterize the attractors found in nonlinear dynamical systems. Modeling the "looseness" of joints for triangular space trusses by Moon & Li [Ref. 27], who report interesting chaotic behavior, was brought to the attention of the author during the write-up of this report, which reveal the importance of understanding the nonlinear dynamic behavior of large flexible structures.

B. SCOPE FOR FUTURE RESEARCH

Future research may be beneficial in two main areas.

The first is the development of a multi-body dynamics model of the LACE spacecraft. A structural model using GIFTS has

already been developed. The results generated may be used to model the flexibility effects, while other effects introduced due to on-orbit, such as gravity gradients effects, atmospheric drag, etc., may be evaluated. These models may be used as baselines for comparison when the orbital test data from LACE becomes available. This comparison will provide an opportunity for improvements and adequacy of these computer models.

The availability of the orbital test data will provide information needed to conduct a more detailed study of chaotic vibrations on the fully deployed LACE spacecraft boom and assess the sensitivity of the highly flexible boom structure to accidental or intentional excitation. Assessing the exact nature of the response of large flexible space structures is important for missions that require accurate pointing accuracies and in suppression and control of vibrations.

APPENDIX A

```
$ ! COM FILE TO GENERATE SIMPLE MODEL OF LACE SPACECRAFT AND
$ ! DERIVE THE NATURAL FREQUENCIES.

$ ! FILENAME IS LACE.COM

DEL LACE.*;*

$ BEAMCS
LACE
OLB/LACECS
QUIT
$ BULKM
LACE
OLB/LACEBM
QUIT
$ LOADBC
LACE
OLB/LACEBC
QUIT
$ BULKF
LACE
$ OPTIM
LACE
1///
$ ADSTIF
LACE
$ ELSTFF
LACE
$ STASS
LACE
$ SUBS
LACE

$ GENERATES SOLID CIRCULAR BEAM USING PROCESSOR BEAMCS

$ FILENAME IS LACECS.SRC

CIRCS/1/.9585/

END

$  SIMPLE FINITE ELEMENT MODEL OF THE  LACE SPACECRAFT USING
BULKM
```

```
$  FILENAME IS LACEBM.SRC

$  ESTABLISH THE KEYPOINTS OF THE MODEL

KPOINT/1/0,0,0/2/0,1800,0/3/0,-900,0/
KPOINT/4/0,0,1800/5/50,0,0/

$  DEFINE MATERIAL PROPERTIES

ELMAT,4/1/3.E3,8.E6,.29,.000014752/

$  DEFINE BEAM CHARACTERISTICS

LETY
BEAM2
1,1

$  GENERATE THE BEAMS

SLINE,10/112/1,2,31/5/113/1,3,16/5/114/1,4,31/5/

END


$ GENERATES POINT MASSES FOR THE SPACECRAFT

$ FILENAME IS LACEBC.SRC

MASS/MASSP/1/6.4078E/2/.0906/3/.0906/4/.517/

END
```

APPENDIX B

The following calculations model structural honeycomb panels as aluminum panels with equivalent thickness and weight. The stiffness for a honeycomb panel is given as

$$D = \frac{E t h^2}{2(1-\nu)}$$

and the equation for an aluminum plate is

$$D = \frac{E t^3}{12(1-\nu^2)}$$

where

$E = 9.9 \times 10^6$ lbs/in^2
$\upsilon = .33$
h = core thickness of honmeycomb panel
t = face thickness

Throughout this appendix the following notation is used.

ρ = density

V = volume

W = weight

where subscripts h indicates honeycomb core and f refers to aluminum face skins. A panel size of 54" x 90" is assumed.

A. PRIMARY STRUCTURE

h = .9

t = .05

1. **Determine Stiffness of Honeycomb Panel**

$$D = \frac{(9.9x10^6)(.05)(.9)^2}{2(1-.33)^2} = 2.25\,x10^5\ lbs./in$$

2. **Determine Equivalent Aluminum Plate Thicknessu**

$$D = \frac{E t^3}{12(1-\nu^3)} \rightarrow 2.250\,x10^5 = \frac{(9.9\,x10^6)\,t^3}{2(1-.33^2)}$$

$$t = .624\ in$$

3. **Determine Honeycomb Panel Mass**

ρ_h* = 6 lbs/ft^3 = 3.47 x 10^{-3} lbs/in^3

ρ_f* = 9.81 x 10^{-2} lbs/in^3

V_h = .9 x 54 x 96 = 4665.6 in^3

V_f* = .1 x 54 x 96 = 518.4 in^3

W_h = 4665.6 x 3.47 x 10^{-3} = 16.2 lbs

W_f* = 518.4 x 9.81 x 10^{-2} = 50.8 lbs

*asterik items remain constant throughout the calculations

Total weight = 67 lbs

$$Total\ mass = \frac{67\ lbs}{386.4\ in/sec^2} = .1734\ (lbs\text{-}sec^2)/in\ \ (GIFTS\ units)$$

4. **Determine Equivalent Density**

$$Volume\ of\ aluminum\ panel = .624\,x54\,x96 = 3234.8\ in^3$$

$$Equivalent\ density = \frac{.1735\,(lbs\text{-}sec^2)/in}{3234.8\ in^3} = 5.364\,x10^{-5}\ (lbs\text{-}sec^2)/in^4$$

B. SECONDARY STRUCTURE

1. Fixed and Deployable Solar Array Substrate

h = .4

t = .05

$$D = \frac{(9.9 \times 10^6)(.05)(.4)^2}{2(1-.33^2)} = 4.44 \times 10^4 \; lbs\text{-}in$$

a. Determine Equivalent Aluminum Thickness

$$4.44 \times 10^4 \; lbs\text{-}in = \frac{(9.9 \times 10^6)\, t^3}{12(1-.33^2)}$$

$$t = .3634 \text{ in}$$

b. Determine Honeycomb Panel Mass

$V_h = .4 \times 54 \times 96 = 2073.6 \text{ in}^3$

$W_h = 2073.6 \times 3.47 \times 10^{-3} = 7.195 \text{ lbs}$

Total weight = 58 lbs

Total mass = $58/386.4 = .15 \text{ lbs-sec}^2/\text{in}$

c. Determine Equivalent Density

Volume of aluminum panel = 1884 in^3

$$Equivalent\ density = \frac{15}{1884} = 7.96 \times 10^{-5} \; lbs\text{-sec}^2/in^4$$

2. Deployable Sensor Panels

h = .65

t = .05

$$D = \frac{(9.9 \times 10^6)(.05)(.65)^2}{2(1-.33^2)} = 1.173 \times 10^5 \; lbs\text{-}in$$

a. Determine Equivalent Aluminum Thickness

$$1.173 \times 10^5 = \frac{(9.9 \times 10^6)\, t^3}{12(1 - .33^2)}$$

$$t = .502 \text{ in}$$

b. Determine Honeycomb Mass

$V_h = .65 \times 54 \times 96 = 3369.6 \text{ in}^3$

$W_h = 3369.6 \times 3.47 \times 10^3 = 11.7 \text{ lbs}$

Total weight = 62.5 lbs

Total mass = .1617 $\text{lbs-sec}^2/\text{in}$

c. Determine Equivalent Density

Volume of aluminum panel = $.502 \times 54 \times 96 = 2602.4 \text{ in}^3$

$$\textit{Equivalent density} = \frac{.1617}{2602.4} = 6.22 \times 10^{-5} \ (\textit{lbs-sec}^2)/\textit{in}^4$$

APPENDIX C

```
$ ! COM FILE TO GENERATE THE MAIN SPACECRAFT BODY

$ ! FILENAME IS XLACE.COM

DEL LACE.*;*
$  BEAMCS
LACE
OLB/LACECS
QUIT
$  BULKM
LACE
OLB/LACEBM
QUIT
$  EDITM
LACE
OLB/LACEM
QUIT
$  LOADBC
LACE
MASS
OLB/MASS
QUIT


$ GENERATES THE BEAM CROSS SECTIONS FOR THE LACE SPACECRAFT
$ GENERATES THE FILE USING THE PROCESSOR BEAMCS
$ SOURCE FILE NAME IS LACECS.SRC

ANGLE,11/1/2.875,3/.25,.25/0,1.938/90/

TBEAM,10/2/2.75,3/.25,.25/0,1.938/

CHANNEL/3/7.75,3/.125,.125/

CIRCH,1/9/5.605,5.5/0,5.5525/

END


$ GENERATES LACE SPACECRAFT MAIN STRUCTURE

$ GENERATES THE FILE USING THE PROCESSOR BULKM
```

```
$ FILENAME IS LACEBM.SRC

$ ELEMENT MATERIAL DEFINITIONS

$ FRAME ELEMENTS

ELMAT,4/1/1.8E4,9.9E6,.33,2.5382E-4/

$ PRIMARY STRUCTURE

ELMAT,4/2/1.8E4,9.9E6,.33,5.364E-5/

$ SECONDARY STRUCTURE-FIXED AND DEPLOYABLE SOLAR ARRAY
SUBSTRATE

ELMAT,4/3/1.8E4,9.9E6,.33,8.1915E-5/

$ SECONDARY STRUCTURE-DEPLOYABLE SENSOR PANELS

ELMAT,4/4/1.8E4,9.9E6,.33,6.22E-5/

$ SECONDARY STRUCTURE-DEPLOYABLE SENSOR ARMS AND BOTTOM PANEL

ELMAT,4/5/1.8E4,9.9E6,.33,2.5382E-4/

$ DEFINE ELEMENT THICKNESS

$ PRIMARY STRUCTURE PANELS

ETH,1/4/.624/

$ SECONDARY STRUCTURE PANELS- SOLAR ARRAY SUBSTRATE

ETH,1/5/.3634/

$ SECONDARY STRUCTURE PANELS-DEPLOYABLE SENSOR PANELS

ETH,1/6/.502/

$ SECONDARY STRUCTURE PANELS- DEPLOYABLE SENSOR ARMS AND
BOTTOM
$ PANEL

ETH,1/7/.125/

$ ESTABLISH THE KEYPOINTS FOR THE PRIMARY STRUCTURE

KPOINT/1/26,26,0/2/-26,26,0/3/26,-26,0/4/-26,-26,0/
KPOINT/5/26,26,41.75/6/-26,26,41.75/7/26,-26,41.75/8/-26,-26
,41.75/
```

```
KPOINT/9/26,26,68.375/10/-26,26,68.375/11/26,-26,68.375/
KPOINT/ 12/-26,-26,68.375/13/26,26,96/
KPOINT/14/-26,26,96/15/26,-26,96/16/-26,-26,96/

$ ESTABLISH KEYPOINTS FOR THE CIRCULAR ARCS

$ SIDE C+Y

KPOINT/17/13,26,68.375/18/13,26,76.5/19/13,26,87.5/20/13,26,
96/
KPOINT/21/18.5,26,82/22/7.5,26,82/

$ SIDE C-Y

KPOINT/23/-13,-26,68.375/24/-13,-26,76.5/25/-13,-26,87.5/
KPOINT/26/-13,-26,96/27/-7.5,-26,82/28/-18.5,-26,82/

$ SIDE +Z

KPOINT/29/26,0,96/30/5.5,0,96/31/-5.5,0,96/32/-26,0,96/
KPOINT/33/0,-5.5,96/34/0,5.5,96/

$ GENERATE VERTICAL ANGLE BEAM MEMBERS FOR C-SECTION PANELS

LETY/BEAM2/1,1/

SLINE,10/L913/9,13,6/10/L1014/10,14,6/9/L1216/12,16,6/10/
SLINE,10/L1115/11,15,6/9/


$ GENERATE VERTICAL ANGLE BEAM MEMBERS FOR B-SECTION PANELS

SLINE,10/L59/5,9,3/6/L610/6,10,3/5/L812/8,12,3/7/L711/7,11,3
/5/

$ GENERATE VERTICAL ANGLE BEAM MEMBERS FOR A-SECTION PANELS

SLINE,10/L15/1,5,3/2/L26/2,6,3/1/L48/4,8,3/3/L37/3,7,3/1/

$ GENERATE HORIZONTAL ANGLE BEAMS FOR TOP AND BOTTOM MEMBERS

$ BOTTOM MEMBERS

SLINE/L12/1,2,6/L34/3,4,6/L13/1,3,5/L24/2,4,5/

$ TOP MEMBERS

SLINE/L1320/13,20,2/L1420/14,20,5/L1432/14,32,3/L1632/16,32,3/
SLINE/L1626/16,26,2/L1526/15,26,5/L1329/13,29,3/L1529/15,29,3/

$ GENERATE HORIZONTAL T-SECTION BEAM MEMBERS
```

```
$ B-SECTION PANELS

LETY/BEAM2/1,2/
SLINE,10/L56/5,6,6/7/L78/7,8,6/5/L57/5,7,5/6/L68/6,8,5/5/

$ C-SECTION PANELS
SLINE,10/L917/9,17,2/13/L1017/10,17,5/14/L1012/10,12,5/9/
SLINE,10/L1223/12,23,2/10/L1123/11,23,5/9/L911/9,11,5/10/

$ GENERATE LINES ASSOCIATED WITH CIRCULAR ARCS

SLINE/L1718/17,18,2/L1920/19,20,2/L2324/23,24,2/L2526/25,26,2/
SLINE/L2930/29,30,2/L3132/31,32,2/

$ GENERATE CIRCULAR ARCS

$ C+Y SIDE PANEL

CARC/C1819/18,22,19,4/C1918/19,21,18,4/

$ C-Y SIDE PANEL

CARC/C1819/18,22,19,4/C1918/19,21,18,4/

$ C-Y SIDE PANEL

CARC/C2425/24,28,25,4/C2524/25,27,24,4/

$ TOP PANEL +Z

CARC/C3031/30,33,31,4/C3130/31,34,30,4/

$ GENERATE COMPLINES

COMPLINE/L1314/L1320,L1420/L1416/L1432,L1632/L1315/L1329,L15
29/
COMPLINE/L1516/L1526,L1626/L1720/L1718,C1819,L1920/
COMPLINE/L2017/L1920,C1918,L1718/L2326/L2324,C2425,L2526/
COMPLINE/L2326/L2324,C2425,L2526/L2623/L2526,C2524,L2324/
COMPLINE/L910/L917,L1017/L1112/L1123,L1223/
COMPLINE/L2932/L2930,C3031,L3132/L3229/L3132,C3130,L2930/

$ GENERATE GRID ELEMENTS

GETY/QB4/2,4/

$ A-PANELS

GRID4/A+Y/L12,L56,L15,L26/A-X/L24,L68,L26,L48/
GRID4/A-Y/L34,L78,L48,L37/A+X/L13,L57,L15,L37/
```

```
$ B-PANELS

GRID4/B+Y/L56,L910,L59,L610/B-X/L68,L1012,L610,L812/
GRID4/B-Y/L78,L1112,L812,L711/B+X/L57,L911,L59,L711/

$ GENERATE C-PANELS

GRID4/C+YL/L917,L2017,L1320,L913/C+YR/L1017,L1014,L1420,L1720/
GRID4/C-YL/L1223,L2326,L1626,L1216/C-YR/L1123,L1115,L1526,L2
623/
GRID4/C+X/L913,L1315,L1115,L911/C-X/L1014,L1416,L1216,L1012/

$ GENERATE TOP PANEL

GRID4/ZL/L1529,L1516,L1632,L2932/ZR/L1329,L3229,L1432,L1314/

$ GENERATE RF PANEL

GRID4/RF/L56,L68,L78,L57/

$ GENERATE BOTTOM PANEL

GETY/QB4/5,7/
GRID4/BOTTOM/L12,L24,L34,L13/

$ GENERATE KEYPOINTS FOR SENSOR PANELS AND SENSOR ARMS

KPOINT/35/19,26,0/36/19,75.25,0/37/-19,26,0/38/-19,75.25,0/
KPOINT/39/-26,19,0/40/-75.25,19,0/41/-26,-19,0/42/-75.25,-19
,0/
KPOINT/43/-19,-26,0/44/-19,-75.25,0/45/19,-26,0/46/19,-75.25
,0/
KPOINT/47/26,-19,0/48/75.25,-19,0/49/26,19,0/50/75.25,19,0/
KPOINT/51/79.03,79.03,0/52/-79.03,79.03,0/53/-79.03,-79.03,0/
KPOINT/54/79.03,-79.03,0/

$ GENERATE LINES FOR SENSOR PANELS

SLINE/L3536/35,36,5/L3738/37,38,5/L3537/35,37,4/L3638/36,38,4/
SLINE/L4344/43,44,5/L4546/45,46,5/L4345/43,45,4/L4446/44,46,4/
SLINE/L4748/47,48,5/L4950/49,50,5/L4749/47,49,4/L4850/48,50,4/

$ GENERATE GRID ELEMENTS

GETY/QB4/4,6/

GRID4/+Y/L3536,L3738,L3537,L3638/-X/L3940,L4142,L3941,L4042/
GRID4/-Y/L4344,L4546,L4345,L4446/+X/L4748,L4950,L4749,L4850/

$ GENERATE CHANNEL BEAM ELEMENTS FOR SENSOR ARMS
```

```
LETY/BEAM2/3,1/
SLIN2,10/L151/1,51,6/52/L252/2,52,6/51/L453/4,53,6/54/
SLINE,10/L354/3,54,6/53/

$ GENERATE KEYPOINTS FOR SOLAR PANEL FOLDOUTS

KPOINT/55/24,26,96/56/24,68.5,96/57/-24,26,96/58/-24,68.5,96/
KPOINT/59/-26,24,96/60/-68.5,24,96/61/-26,-24,96/62/-68.5,-2
4,96/
KPOINT/63/-24,-26,96/64/-24,-68.5,96/65/24,-26,96/66/24,-68.
5,96/
KPOINT/67/26,-24,96/68/68.5,-24,96/69/26,24,96/70/68.5,24,96/

$ GENERATE LINES FOR SOLAR PANEL FOLDOUTS

SLINE/L5556/55,56,3/L5758/57,58,3/L5557/55,57,3/L5658/56,58,3/
SLINE/L5960/59,60,3/L6162/61,62,3/L5961/59,61,3/L6062/60,62,3/
SLINE/L6364/63,64,3/L6566/65,66,3/L6365/63,65,3/L6466/64,66,3/
SLINE/L6768/67,68,3/L6970/69,70,3/L6769/67,69,3/L6870/68,70,3/

$ GENERATE GRID ELEMENTS

GETY/QB4/3,5/

GRID4/D+Y/L5556,L5758,L5557,L5658/D-X/L5960,L6162,L5961,L6062/
GRID4/D-Y/L6364,L6566,L6365,L6466/D+X/L6768,L6970,L6769,L6870/

$ GENERATE KEYPOINTS FOR SOLAR FIXED PANELS

$ A+Y PANELS

KPOINT/71/-26,26,20/72/-26,26,46/73/-14,26,46/74/-14,26,60/
KPOINT/75/14,26,60/76/14,26,46/77/26,26,46/78/26,26,20/

$ A-Y

KPOINT/79/26,-26,20/80/26,-26,46/81/14,-26,46/82/14,-26,60/
KPOINT/83/-14,-26,60/84/-14,-26,46/85/-26,-26,46/86/-26,-26,
20/

$ C+X

KPOINT/87/26,26,30/88/26,26,45/89/26,14,45/90/26,14,56.01/
KPOINT/91/26,26,56.01/92/26,26,88.5/93/26,-26,88.5/94/26,-26
,56.01/
KPOINT/95/26,-14,56.01/96/26,-14,45/97/26,-26,45/98/26,-26,30/

$ C-X

KPOINT/99/-26,26,30/100/-26,26,45/101/-26,14,45/102/-26,14,5
6.01/
```

```
KPOINT/103/-26,26,56.01/104/-26,26,88.5/105/-26,-26,88.5/
KPOINT/106/-26,-26,56.01/107/-26,-14,56.01/108/-26,-14,45/
KPOINT/109/-26,-26,45/110/-26,-26,30/


END


$ EDIT THE MODEL-GENERATE VERTICAL ANGLE BEAM ELEMENTS

$ GENERATES THE FILE USING THE PROCESSOR EDITM

$ FILE NAME IS LACEM.SRC

PTRM/1/PTRTH/1

$ GENERATE TOP ANGLE MEMBERS

BEAM2/13,55,29/20,55,29/20,57,32/14,57,32/
BEAM2/14,59,20/32,59,31/32,61,31/16,61,26/
BEAM2/16,63,32/26,63,32/26,65,32/15,65,29/
BEAM2/15,67,26/29,67,26/29,69,30/13,69,20/

$ GENERATE BOTTOM ANGLE MEMBERS

BEAM2/1,35,3/35,37,3/2,37,4/
BEAM2/2,39,1/39,41,1/4,41,3/
BEAM2/4,43,2/43,45,2/3,45,1/
BEAM2/3,47,4/47,49,4/1,49,2/
BEAM2/419,422,1/411,414,1/135,139,1/138,142,1/

$ GENERATE HOLLOW CIRCULAR BEAM CROSS SECTION FOR CYLINDRICAL
$ CANNISTERS

PTRTH/9/

BEAM2/19,364,9/25,352,9/31,405,9/

END


$  GENERATES POINT AND GRID MASSES FOR THE LACE SPACECRAFT

$  GENERATES THE FILE USING THE PROCESSOR LOADBC

$  SOURCE FILE NAME IS MASS.SRC

$  GENERATE MASS DISTRIBUTIONS FOR A-PANELS

$  MASS LOADING FOR A-Y PANEL
```

```
MASSP/8/6.31E-3/166/1.54E-2/165/1.65E-2/
MASSP/164/1.65E-2/163/1.19E-2/7/2.87E-3/
MASSP/133/9.76E-3/325/2.48E-2/324/2.25E-2/
MASSP/323/2.25E-2/322/1.65E-2/134/7.4E-3/
MASSP/4/6.31E-3/142/1.23E-2/141/8.88E-3/
MASSP/140/8.88E-3/139/7.4E-3/3/7.4E-3/

$  MASS LOADING FOR A+Y PANEL

MASSP/5/2.87E-3/159/1.37E-2/160/2.03E-2/
MASSP/161/1.61E-2/162/9.47E-3/6/2.87E-3/
MASSP/131/5.27E-3/315/1.61E-2/316/2.69E-2/
MASSP/317/2.93E-2/318/1.61E-2/132/2.87E-3/
MASSP/1/5.27E-3/135/5.27E-3/136/9.47E-3/
MASSP/137/1.61E-2/138/9.47E-3/2/2.87E-3/

$  MASS LOADING FOR A-X PANEL

MASSP/6/7.01E-3/170/1.86E-2/171/3.07E-2/
MASSP/172/2.36E-2/8/7.97E-3/
MASSP/132/2.55E-2/319/5.57E-2/320/7.22E-2/
MASSP/321/4.66E-2/133/7.97E-3/
MASSP/2/2.2E-2/146/4.05E-2/147/4.48E-2/
MASSP/148/2.64E-2/4/3.44E-3/

$  MASS LOADING FOR A+X PANEL

MASSP/7/3.44E-3/169/1.88E-2/168/2.3E-2/
MASSP/167/7.66E-3/5/3.44E-3/
MASSP/134/1.32E-2/328/4.7E-2/
MASSP/327/6.0E-2/326/3.89E-2/131/1.62E-2/
MASSP/3/1.32E-2/145/3.16E-2/144/4.03E-2/
MASSP/143/3.46E-2/1/1.62E-2/

$ GENERATES MASS DISTRIBUTIONS FOR B-PANELS

$ MASS LOADING FOR B+Y PANEL

MASSP/5/8.4E-3/127/8.4E-3/329/8.4E-3/159/8.4E-3/
MASSP/160/1.92E-3/330/1.92E-3/161/3.4E-2/
MASSP/331/3.4E-2/162/1.59E-2/332/1.59E-2/


$ MASS LOADING FOR B-X PANEL

MASSP/170/7.47E-3/171/7.47E-3/172/7.47E-3/
MASSP/333/7.47E-3/335/7.47E-3/
MASSP/334/8.9E-3/177/2.16E-3/

$ MASS LOADING FOR B+X PANEL
```

```
MASSP/11/4.27E-3/184/8.83E-3/183/9.81E-3/
MASSP/182/1.7E-2/9/1.24E-2/130/4.27E-3/
MASSP/342/1.31E-2/341/1.89E-2/340/3.48E-2/
MASSP/127/2.57E-2/7/6.91E-4/169/5.25E-3/
MASSP/168/9.81E-3/167/1.79E-2/5/1.39E-2/

$ GENERATES MASS DISTRIBUTIONS FOR C-PANELS

$ MASS LOADING FOR C+Y PANEL

MASSP/344/3.96E-3/345/3.96E-3/347/3.96E-3/
MASSP/348/3.96E-3/174/3.96E-3/175/3.96E-3/

$ MASS LOADING FOR C-Y PANEL

MASSP/181/4.84E-3/357/4.84E-3/360/9.68E-3/
MASSP/363/4.84E-3/366/4.84E-3/
MASSP/180/4.84E-3/356/4.84E-3/359/9.68E-3/
MASSP/362/4.84E-3/365/4.84E-3/

$ MASS LOADING FOR C-X PANEL

MASSP/379/8.67E-3/380/8.67E-3/383/8.67E-3/
MASSP/384/8.67E-3/387/8.67E-3/388/8.67E-3/

$ MASS LOADING FOR C+X PANEL

MASSP/158/3.35E-3/378/3.35E-3/368/3.08E-3/
MASSP/369/3.08E-3/372/3.08E-3/373/3.08E-3/
MASSP/371/3.81E-3/

$ GENERATES MASS DISTRIBUTIONS FOR THE TOP PANEL

MASSP/16/5.29E-3/153/4.21E-3/32/3.56E-3/
MASSP/152/9.7E-4/14/2.06E-3/15/2.06E-3/
MASSP/158/9.7E-4/29/9.7E-4/157/9.7E-4/
MASSP/13/2.06E-3/26/5.71E-3/156/3.77E-3/
MASSP/155/3.77E-3/154/2.47E-3/149/2.47E-3/
MASSP/150/3.44E-3/151/3.44E-3/20/2.47E-3/
MASSP/394/4.21E-3/393/2.26E-3/392/2.26E-3/
MASSP/391/9.7E-4/30/9.7E-4/193/9.7E-4/
MASSP/194/9.7E-4/31/9.7E-4/195/9.7E-4/
MASSP/196/9.7E-4/398/9.7E-4/397/1.94E-3/
MASSP/396/1.94E-3/395/9.7E-4/


$ GENERATE MASS DISTRIBUTIONS FOR THE RF PANEL

MASSP/8/2.16E-3/172/2.16E-3/171/2.52E-3/
MASSP/170/2.16E-3/6/2.16E-3/166/5.49E-3/
MASSP/410/1.29E-2/406/8.34E-3/402/2.16E-3/
```

```
MASSP/162/2.16E-3/165/6.0E-3/409/1.18E-2/
MASSP/405/1.66E-2/401/1.07E-2/161/1.07E-2/
MASSP/164/6.0E-3/408/9.88E-3/404/2.32E-2/
MASSP/400/1.93E-2/160/1.93E-2/163/5.49E-3/
MASSP/407/9.37E-3/403/1.46E-2/399/1.07E-2/
MASSP/159/1.07E-2/7/2.56E-3/169/6.03E-3/
MASSP/168/6.32E-3/167/2.16E-3/5/2.16E-3/


$ GENERATES MASS DISTRIBUTION ON THE BOTTOM PANEL

MASSP/4/5.85E-3/148/9.65E-3/147/1.06E-2/
MASSP/146/8.36E-3/2/5.85E-3/142/3.19E-2/
MASSP/422/3.77E-2/418/1.73E-2/414/2.23E-2/
MASSP/138/1.28E-2/141/2.83E-2/421/5.5E-2/
MASSP/417/6.07E-2/413/4.34E-2/137/1.15E-2/
MASSP/140/2.57E-2/420/5.8E-2/416/6.21E-2/
MASSP/412/3.39E-2/136/5.91E-3/139/2.94E-2/
MASSP/419/3.78E-2/415/1.9E-2/411/1.56E-2/
MASSP/135/7.14E-3/3/5.85E-3/145/7.14E-3/
MASSP/144/8.62E-3/143/1.1E-2/1/5.85E-3/

$ GENERATES MASS DISTRIBUTIONS ON THE SENSOR PANELS AND SENSOR
ARMS

$ GENERATE MASS LOADINGS FOR THE SENSOR ARMS

MASSP/1/8.16E-3/283/7.89E-3/284/1.12E-2/
MASSP/285/7.89E-3/286/8.16E-3/51/7.89E-3/
MASSP/2/8.16E-3/287/7.89E-3/288/1.12E-2/
MASSP/289/7.89E-3/290/8.16E-3/52/7.89E-3/
MASSP/3/8.16E-3/295/7.89E-3/296/1.12E-2/
MASSP/297/7.89E-3/298/8.16E-3/54/7.89E-3/
MASSP/4/8.16E-3/291/7.89E-3/292/1.12E-2/
MASSP/293/7.89E-3/294/8.16E-3/53/7.89E-3/

$ GENERATE MASS LOADINGS FOR THE SENSOR PANELS

$ GENERATE MASS LOADINGS FOR +Y PANEL

MASSP/37/7.83E-3/246/6.47E-3/247/5.56E-3/
MASSP/248/5.63E-3/38/6.02E-3/
MASSP/250/4.66E-3/426/1.22E-2/
MASSP/427/1.22E-2/428/7.18E-3/252/4.66E-3/
MASSP/249/4.66E-3/423/1.22E-2/424/1.22E-2/
MASSP/425/7.18E-3/251/4.66E-3/
MASSP/35/6.02E-3/243/6.47E-3/
MASSP/244/5.56E-3/245/5.63E-3/36/6.02E-3/

$ GENERATE MASS LOADINGS FOR -X PANEL
```

```
MASSP/41/3.49E-3/256/4.66E-3/257/3.49E-3/
MASSP/258/4.14E-3/42/5.43E-3/
MASSP/260/1.87E-2/431/1.93E-2/
MASSP/432/6.66E-3/433/6.28E-3/262/4.08E-3/
MASSP/259/1.87E-2/429/2.11E-2/430/6.66E-3/
MASSP/431/6.28E-3/261/4.08E-3/39/5.3E-3/253/2.85E-3/
MASSP/253/2.85E-3/254/3.49E-3/255/4.14E-3/40/5.43E-3/

$ GENERATE MASS LOADINGS FOR -Y PANEL

MASSP/44/6.3E-3/265/5.91E-3/264/5.85E-3/
MASSP/263/6.75E-3/43/8.11E-3/271/4.94E-3/
MASSP/437/7.47E-3/436/1.25E-2/435/1.25E-2/
MASSP/269/4.94E-3/272/4.94E-3/440/7.47E-3/
MASSP/439/1.25E-2/438/1.25E-2/270/4.94E-3/
MASSP/46/6.3E-3/268/5.91E-3/267/5.85E-3/
MASSP/266/8.57E-3/45/6.3E-3/

$ GENERATE MASS LOADINGS FOR +X PANEL

MASSP/48/5.14E-3/275/4.79E-3/274/3.45E-3/
MASSP/273/2.55E-3/47/4.79E-3/281/3.78E-3/
MASSP/443/5.98E-3/442/8.18E-3/441/3.78E-3/
MASSP/279/4.79E-3/282/3.78E-3/446/5.07E-3/
MASSP/445/8.18E-3/444/3.71E-3/280/3.78E-3/
MASSP/50/5.14E-3/278/4.79E-3/277/3.84E-3/
MASSP/276/2.48E-3/49/3.78E-3/

$ GENERATES GRID MASS FOR SOLAR PANELS

$ SURFACE MOUNT SOLAR PANELS

MASSG/A+Y/1.531815E-5,1.531815E-5,1.531815E-5,1.531815E-5/
MASSG/A-Y/1.531815E-5,1.531815E-5,1.531815E-5,1.531815E-5/
MASSG/B+Y/2.402E-5,2.402E-5,2.402E-5,2.402E-5/
MASSG/B-Y/2.402E-5,2.402E-5,2.402E-5,2.402E-5/
MASSG/A+X/1.196E-5,1.196E-5,1.196E-5,1.196E-5/
MASSG/A-X/1.196E-5,1.196E-5,1.196E-5,1.196E-5/
MASSG/B+X/1.8755E-5,1.8755E-5,1.8755E-5,1.8755E-5/
MASSG/B-X/1.8755E-5,1.8755E-5,1.8755E-5,1.8755E-5/
MASSG/C+X/1.8076E-5,1.8076E-5,1.8076E-5,1.8076E-5/
MASSG/C-X/1.8076E-5,1.8076E-5,1.8076E-5,1.8076E-5/

$ DEPLOYED SOLAR PANELS

MASSG/D+X/6.343E-6,6.343E-6,6.343E-6,6.343E-6/
MASSG/D-X/6.343E-6,6.343E-6,6.343E-6,6.343E-6/
MASSG/D+Y/6.343E-6,6.343E-6,6.343E-6,6.343E-6/
MASSG/D-Y/6.343E-6,6.343E-6,6.343E-6,6.343E-6/

$ DETERMINES MISCELLANEOUS UNACCOUNTED MASS
```

```
$ DISTRIBUTED OVER SPACECRAFT PANELS

$ A-PANELS

MASSG/A+X/1.4691E-5,1.4691E-5,1.4691E-5,1.4691E-5/
MASSG/A-X/1.4691E-5,1.4691E-5,1.4691E-5,1.4691E-5/
MASSG/A+Y/1.4691E-5,1.4691E-5,1.4691E-5,1.4691E-5/
MASSG/A+Y/1.4691E-5,1.4691E-5,1.4691E-5,1.4691E-5/

$ B-PANELS

MASSG/B+X/2.303662E-5,2.303662E-5,2.303662E-5,2.303662E-5/
MASSG/B-X/2.303662E-5,2.303662E-5,2.303662E-5,2.303662E-5/
MASSG/B+Y/2.303662E-5,2.303662E-5,2.303662E-5,2.303662E-5/
MASSG/B-X/2.303662E-5,2.303662E-5,2.303662E-5,2.303662E-5/

$ C-PANELS

MASSG/C+X/2.220272E-5,2.220272E-5,2.220272E-5,2.220272E-5/
MASSG/C-X/2.220272E-5,2.220272E-5,2.220272E-5,2.220272E-5/

$ TOP PANEL

MASSG/ZL/5.897597E-6,5.897597E-6,5.897597E-6,5.897597E-6/
MASSG/ZR/5.897597E-6,5.897597E-6,5.897597E-6,5.897597E-6/

$ RF PANEL

MASSG/RF/1.226228E-5,1.226228E-5,1.226228E-5,1.226228E-5/

$ BOTTOM PANEL

MASSG/BOTTOM/1.179519E-5,1.179519E-5,1.179519E-5,1.179519E-5/


 END
```

COMPONENT PLACEMENT

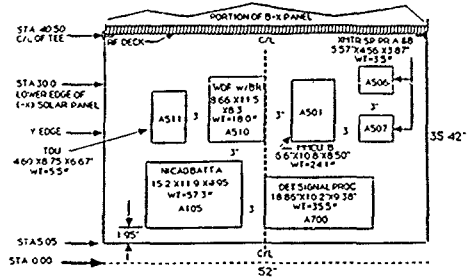

PANEL (A-X)

WEIGHT

NICADBATT B	57.3#
PFCU B	24#
WDF	18.0
TDU	55
XMTR SP PROC A	35
XMTR SP PROC B	35
PANEL SUBSTRATE	275
HARNESS (ESTIMATE)?	290
OSP	355
TOTAL	1949#

GRID DESCRIPTION

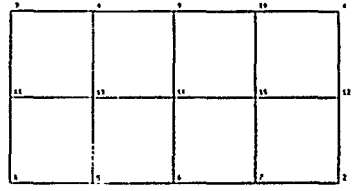

Weight Distribution by Point (lbs)

Pt.	Wt.	Pt.	Wt.	Pt.	Wt.	Pt.	Wt.	Pt.	Wt.
3	2.71	8	7.21	9	11.86	10	9.11	4	3.08
11	.987	13	21.51	14	27.9	15	18	12	3.08
1	8.49	5	15.63	6	17.31	7	10.21	2	1.33

COMPONENT PLACEMENT

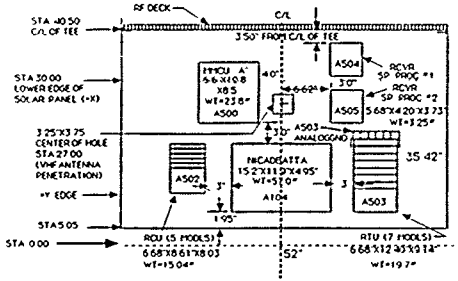

PANEL (A+X)

NICADBATTA	570
PPICU A	238
RTU	197
RCU	1504
RCVR SP PROC A	325
RCVR SP PROC B	325
PANELSUBSTRATE	202
HARNESS (ESTIMATE)	2200
TOTAL	16624

GRID DESCRIPTION

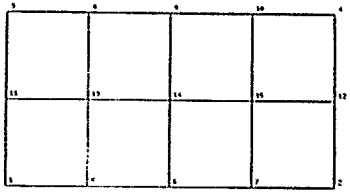

A PANEL (A+X)

Weight Distribution by Point (lbs)

Pt.	Wt.	Pt.	Wt.	Pt.	Wt.	Pt.	Wt.	Pt.	Wt.
3	1.33	8	7.28	9	8.91	10	2.96	4	1 33
11	5.09	13	18.17	14	23.16	15	15.02	12	6.26
1	5.09	5	12.22	6	15.58	7	13.39	2	6.26

COMPONENT PLACEMENT

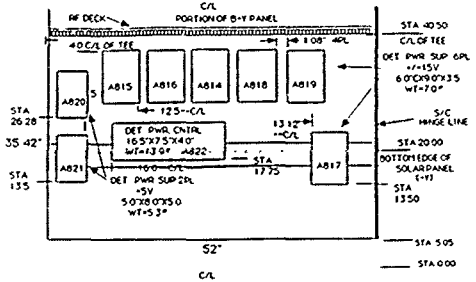

PANEL (A-Y)

WEIGHT

DET PWR SUP 5V(2)	10.6#
DET PWR SUP +/-15V (6)	42.0
POWER CONTROL UNIT	13.9
PANEL SUBSTRATE	27.5
HARNESS (ESTIMATE)?	20.0
TOTAL	114.0#

GRID DESCRIPTION

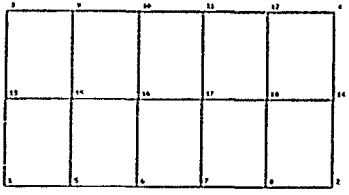

A PANEL (A-Y)

Weight Distribution by Point (lbs)

Pt.	Wt.	Pt.	Wt.	Pt.	Wt.	Pt.	Wt.	Pt.	Wt.	Pt.	Wt.
3	2.44	9	5.94	10	6.36	11	6.36	12	4.61	4	1.11
13	3.77	15	9.59	16	8.68	17	8.68	18	6.36	14	2.86
1	2.44	5	4.76	6	3.43	7	3.43	8	2.86	2	2.86

COMPONENT PLACEMENT

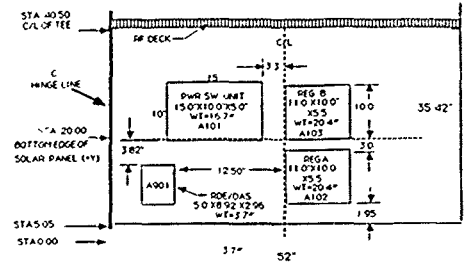

PANEL (A+Y)

WEIGHT

REG UNIT A&B	40.8#
PWR SW UNIT	16.7#
RDE/DAS ACQSYS	3.7#
PANEL SUBSTRATE	27.2#
HARNESS (ESTIMATE)?	20.0#
TOTAL	108.4#

GRID DESCRIPTION

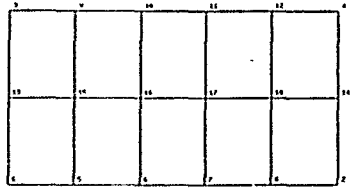

A PANEL (A+Y)

Weight Distribution by Point (lbs)

Pt.	Wt.	Pt.	Wt.	Pt.	Wt.	Pt.	Wt.	Pt.	Wt.	Pt.	Wt.
3	1.11	9	5.28	10	7.84	11	6.21	12	3.66	4	1.11
13	2.04	15	6.21	16	10.4	17	11.31	18	6.21	14	1.11
1	2.04	5	2.04	6	3.66	7	6.21	8	3.66	2	1.11

COMPONENT PLACEMENT

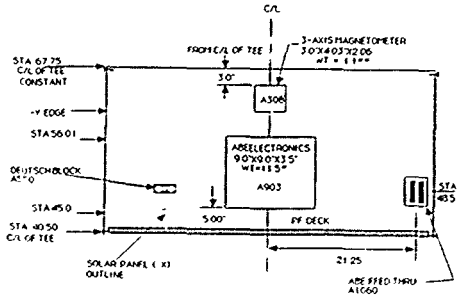

PANEL (B-X)

WEIGHT

MAGNETOMETER	11*
ABE ELECTRONICS	156*
PANEL SUBSTRATE	210*
HARNESS (ESTIMATE)?	20
TOTAL	397*

GRID DESCRIPTION

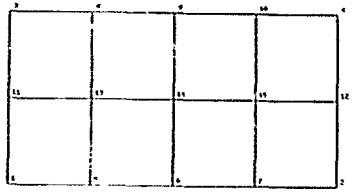

B PANEL (B-X)

Weight Distribution by Point (lbs)

Pt.	Wt.	Pt.	Wt.	Pt.	Wt.	Pt.	Wt.	Pt.	Wt.
3	-	8	-	9	.836	10	-	4	-
11	-	13	2.89	14	3.44	15	2.89	12	-
1	-	5	2.89	6	2.89	7	2.89	2	-

COMPONENT PLACEMENT

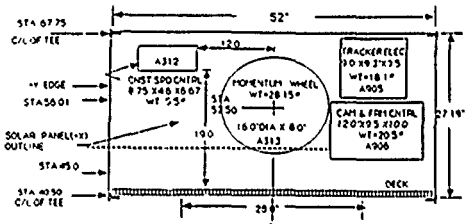

WEIGHT

PWA	28.15#
CONST+SPEEDCONTR	5.5
TRACKER ELEC	18.1
CAM & FRAME CNTRL	20.5
PANEL SUBSTRATE	21.1
HARNESS (ESTIMATE)?	4.0
TOTAL	97.35#

GRID DESCRIPTION

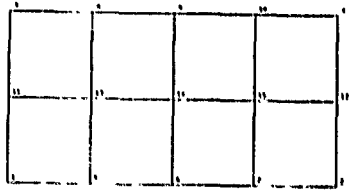

Weight Distribution by Point (lbs)

Pt.	Wt.	Pt.	Wt.	Pt.	Wt.	Pt.	Wt.	Pt.	Wt.
3	1.65	8	3.41	9	3.79	10	6.56	4	4.8
11	1.65	13	5.17	14	7.31	15	13.44	12	9.93
1	.267	5	2.03	6	3.79	7	6.91	2	5.39

PANEL (3+X)

B PANEL (B-Y)

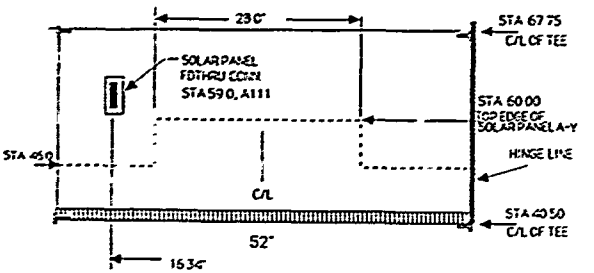

PANEL (B-Y)

WEIGHT	
PANELSUBSTRATE	206
TOTAL	206

COMPONENT PLACEMENT

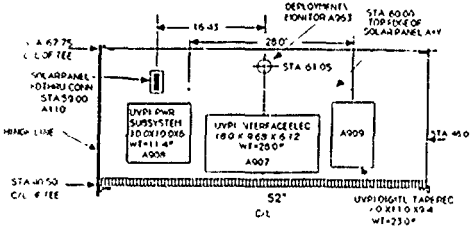

PANEL (B+Y)

WEIGHT

UVPI INTERFACE ELEC	29.0#
UVPI POWER SUB	11.4
UVPI DIGITAL TAPE REC	23.0
PANEL SUBSTRATE	206
HARNESS (est)	40
TOTAL	87.0#

GRID DESCRIPTION

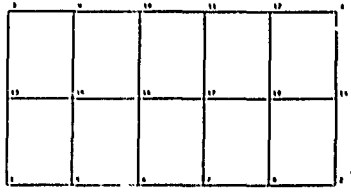

B PANEL (B+Y)

Weight Distribution by Point (lbs)

Pt.	Wt.	Pt.	Wt.	Pt.	Wt.	Pt.	Wt.	Pt.	Wt.	Pt.	Wt.
3	-	9	-	10	-	11	-	12	-	4	-
13	3.25	15	3.25	16	13.15	17	7.0	18	6.15	14	-
1	3.25	5	3.25	6	13.15	7	6.15	8	-	2	

COMPONENT PLACEMENT

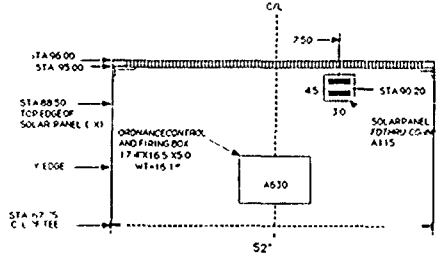

PANEL (C-X)

WEIGHT	
ORDNANCE CONTROL BOX	16.1#
SOLAR PANEL FEED THRU CONNECTOR	
PANEL SUBSTRATE	20.8#
HARNESS (ESTIMATE)	4.0#
TOTAL	40.9#

GRID DESCRIPTION

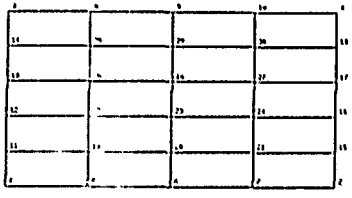

C PANEL (C-X)

Weight Distribution by Point (lbs)

Pt.	Wt.	Pt.	Wt.	Pt.	Wt.
22	3.35	23	3.35	24	3.35
19	3.35	20	3.35	21	3.35

All other points are zero

COMPONENT PLACEMENT

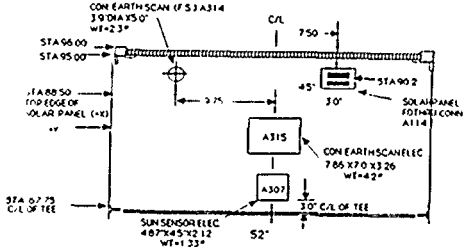

PANEL (C+X)

WEIGHT	
SUN SENSOR ELECTRONICS	1 33
CON EARTH SCANNER	2 3#
CON EARTH SCAN ELEC	42#
PANEL SUBSTRATE	20 7
HARNESS (est)	1 0
TOTAL	29.53#

GRID DESCRIPTION

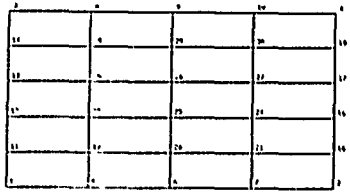

C PANEL (C+X)

Weight Distribution by Point (lbs)

Pt.	Wt.	Pt.	Wt.	Pt.	Wt.
8	1.29	9	-	10	-
28	1.29	29	-	30	-
25	-	26	1.19	27	1.19
22	-	23	1.19	24	1.19
19	-	20	1.47	21	-

All other points are zero

COMPONENT PLACEMENT

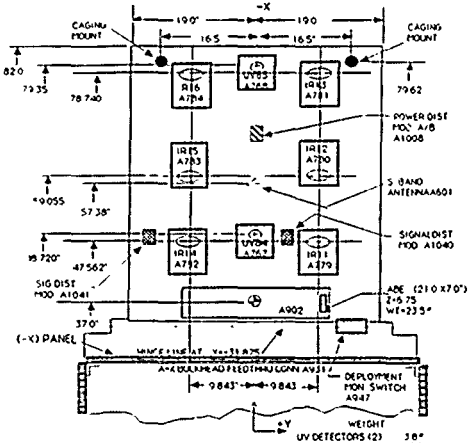

SENSOR PANEL (-X)

UV DETECTORS (2)	38
IR DETECTORS (6)	120
S-BAND ANTENNA (1)	15
POWER DIST MODULES (2)	14
SIG-ALDIST MODULES (2)	14
ABE	235
PANEL SUBSTRATE	2254
CAGING MOUNTS AND HINGES	40
HARNESS	120
TOTAL	8214

GRID DESCRIPTION

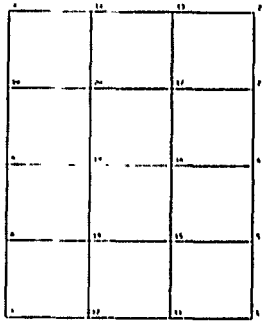

Weight Distribution by Point (lbs)

Pt.	Wt.	Pt.	Wt.	Pt.	Wt.	Pt.	Wt.
4	2.1	14	1.58	13	1.58	2	2.1
10	1.6	20	2.42	17	2.42	7	1.6
9	1.35	19	2.58	16	2.58	6	1.35
8	1.8	18	7.45	15	8.15	5	1.1
3	1.35	12	7.22	11	7.22	1	2.05

COMPONENT PLACEMENT

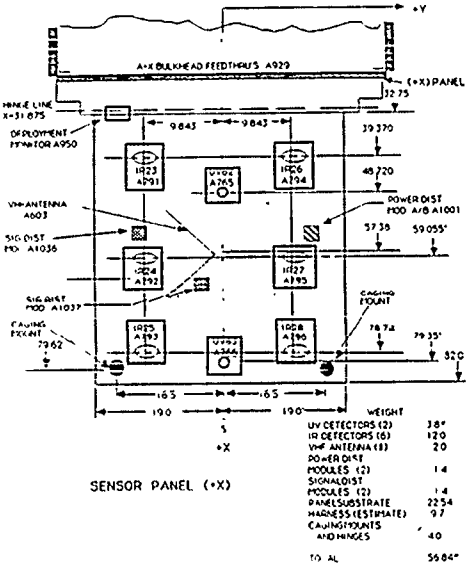

SENSOR PANEL (+X)

GRID DESCRIPTION

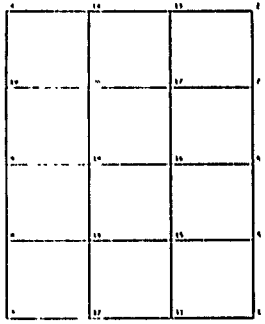

SENSOR PANEL (+X)

Weight Distribution by Point (lbs)

Pt.	Wt.	Pt.	Wt.	Pt.	Wt.	Pt.	Wt.
4	1.48	14	1.48	13	1.46	2	1.46
10	.98	20	1.46	17	1.44	7	.96
9	1.34	19	3.16	16	3.16	6	1.68
8	1.48	18	2.31	15	1.96	5	1.48
3	1.98	12	1.46	11	1.46	1	1.98

COMPONENT PLACEMENT

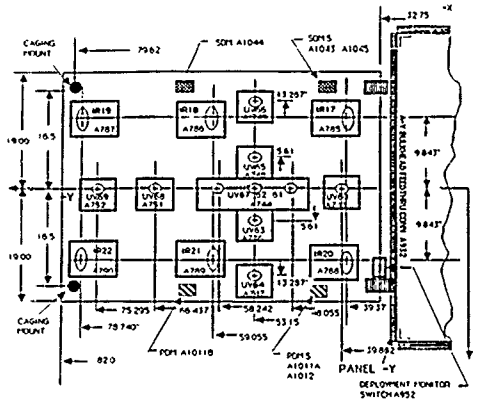

SENSOR PANEL (-Y)

■ = POWER DIST MODULE (PDM)

▨ = SIGNAL DIST MODULE (SDM)

WEIGHT	
UV PHOTODETECTORS (7)	13.30
U-SPACE (13)	9.0
IR DETECTORS (16)	12.0
POWER DIST MODULES (3)	2.1
SIGNAL DISTRIBUTION UNIT (3)	2.1
PANEL SUBSTRATE	22.54
CASING AND HINGES	6.2
HARNESS (ESTIMATE)	19.7
TOTAL	80.74#

GRID DESCRIPTION

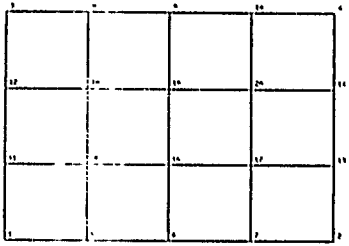

Weight Distribution by Point (lbs)

Pt.	Wt.	Pt.	Wt.	Pt.	Wt.	Pt.	Wt.	Pt.	Wt.
3	2.44	8	2.28	9	2.26	10	2.61	4	3.14
12	1.91	18	2.88	19	4.84	20	4.84	14	1.91
11	1.91	15	2.88	16	4.84	17	4.14	13	1.91
1	2.44	5	2.28	6	2.26	7	3.31	2	2.44

COMPONENT PLACEMENT

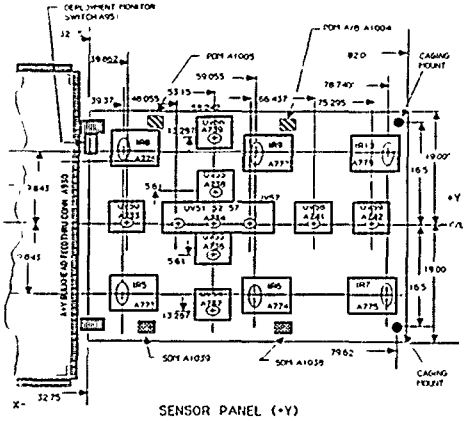

WEIGHT	
UV DETECTORS (7)	1530
UV 3 PAC (3)	60
IR DETECTORS (6)	120
POWER DIST MODULES (1)	21
SIGNAL DIST MODULES (2)	14
PANEL SUBSTRATE	2254
CASING AND HINGES	40
HARNESS	165
TOTAL	7784*

GRID DESCRIPTION

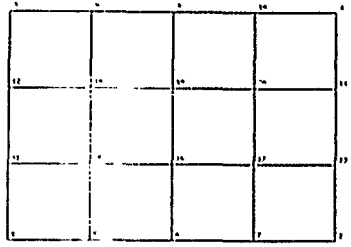

SENSOR PANEL (-Y)

Weight Distribution by Point (lbs)

Pt.	Wt.	Pt.	Wt.	Pt.	Wt.	Pt.	Wt.	Pt.	Wt.
3	2.44	8	2.28	9	2.26	10	2.61	4	3.14
12	1.91	18	2.88	19	4.84	20	4.84	14	1.91
11	1.91	15	2.88	16	4.84	17	4.84	13	1.91
1	2.44	5	2.28	6	2.26	7	3.31	2	2.44

COMPONENT PLACEMENT

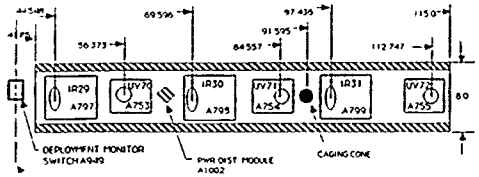

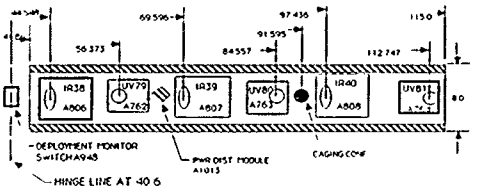

WEIGHT (FOR EACH ARM)

UV-REMOTE DETECTORS (3)	5.7*
IR REMOTE DETECTORS (3)	6.0
POWER DIST MODULES (1)	7
SENSOR ARM	10.0
HARNESS	6.9
TOTAL	29.3*

POINT DESIGNATION

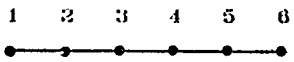

Weight Distribution by Point (lbs)

Pt.	Wt.
1	3.15
2	3.09
3	4.33
4	3.09
5	3.15
6	3.09

COMPONENT PLACEMENT

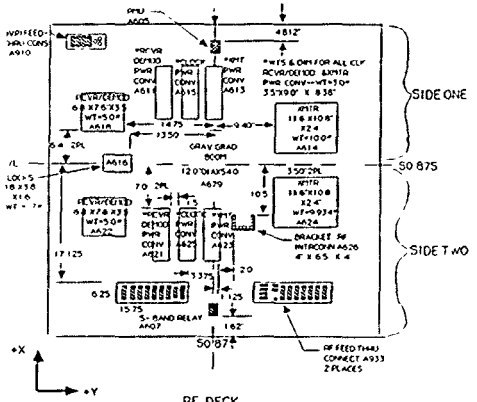

RF DECK

WEIGHT

XMTRS (2)	19934*
XMTR P.S. S (2)	60
RCVR/DEFROOS (2)	10306
RCVR P.S.S (2)	60
STABLE CLOCK (1)	781
CLOCK P.S.S (2)	60
DMS	28
PFU	11
PANEL SUBSTRATE	32035
HARNESS (ESTIMATE)??	250
TOTAL	105 445

GRID DESCRIPTION

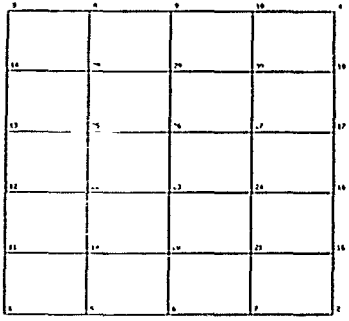

RF DECK

Weight Distribution by Point (lbs)

Pt.	Wt	Pt.	Wt.	Pt.	Wt.	Pt.	Wt.	Pt.	Wt.
3	.833	8	.833	9	.97	10	.833	4	.833
14	2.12	28	4.98	29	3.22	30	.833	18	.833
13	2.32	25	4.56	26	6.41	27	4.13	17	4.13
12	2.32	22	3.82	23	8.96	24	7.46	16	7.46
11	2.12	19	3.62	20	5.64	21	4.13	15	4.13
1	.833	5	2.33	6	2.44	7	.835	2	.835

EARTH END PANEL

COMPONENT PLACEMENT

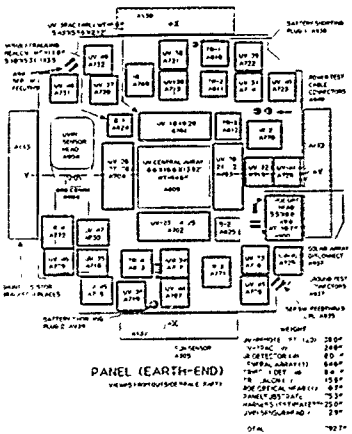

PANEL (EARTH-END)

GRID DESCRIPTION

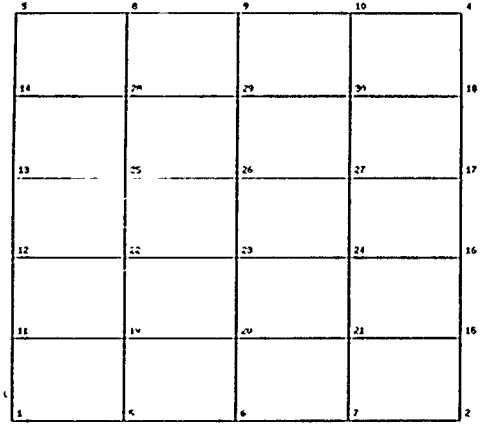

Weight Distribution by Point (lbs)

Pt.	Wt.	Pt.	Wt.	Pt.	Wt.	Pt.	Wt.	Pt.	Wt.
3	2.26	8	3.73	9	4.12	10	3.23	4	2.26
14	12.34	28	14.57	29	6.76	30	8.63	18	4.93
13	10.92	25	21.24	26	23.46	27	16.76	17	4.46
12	9.94	22	22.24	23	23.98	24	13.13	16	2.28
11	11.36	19	14.59	20	7.33	21	6.03	15	2.76
1	2.26	5	2.76	6	3.33	7	4.26	2	2.27

COMPONENT PLACEMENT

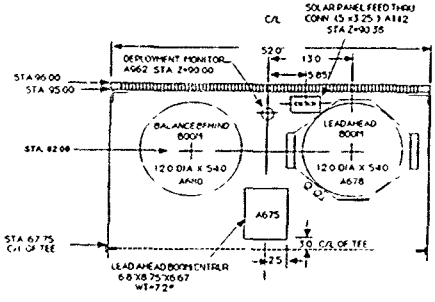

PANEL (C+Y)

WEIGHT	
LEADAHEAD BOOM CNTRLR	72#
PANEL SUBSTRATE	196
HARNESS	20
TOTAL	282#

GRID DESCRIPTION

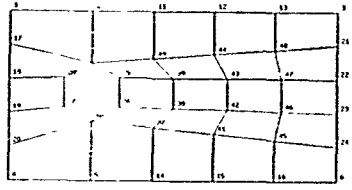

PANEL C (C+Y)

Weight Distribution by Point (lbs)

Pt.	Wt.	Pt.	Wt.
38	1.53	42	1.53
37	1.53	41	1.53
14	4.53	15	1.53

All other points are zero

COMPONENT PLACEMENT

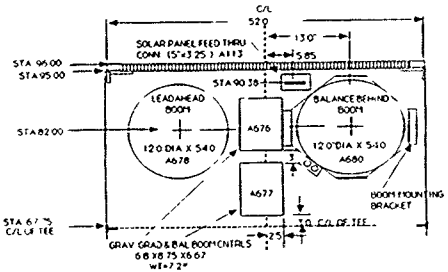

PANEL (C-Y)

WEIGHT

BALANCE BOOM CONTR	72#
GRAVGRAD BOOM CONTR	72#
HARNESS ???	80#
PANEL SUBSTRATE	170#
TOTAL	394#

GRID DESCRIPTION

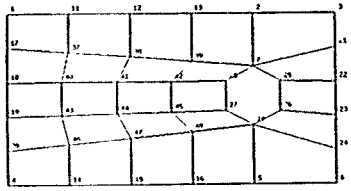

PANEL C (C-Y)

Weight Distribution by Point (lbs)

Pt.	Wt.	Pt.	Wt.
38	1.87	39	1.87
41	1.87	42	1.87
44	3.74	45	3.74
47	1.87	48	1.87
15	1.87	16	1.87

COMPONENT PLACEMENT

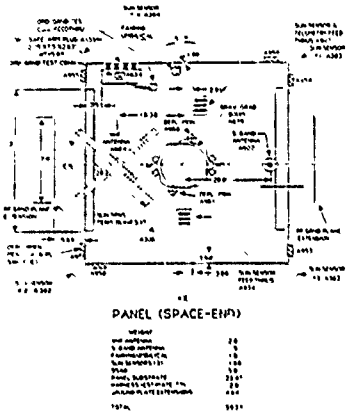

PANEL (SPACE-END)

GRID DESCRIPTION

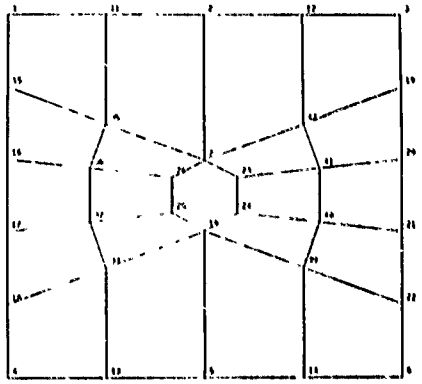

SPACE END PANEL

Weight Distribution by Point (lbs)

Pt.	Wt.	Pt.	Wt.	Pt.	Wt.	Pt.	Wt.	Pt.	Wt.	Pt.	Wt.
1	2.04	11	1.63	2	1.38	-	-	12	.38	3	.80
15	2.2	35	1.63	7	.38	-	-	42	.38	19	.96
16	1.46	36	.9	26	.38	23	.31	41	.38	20	1.33
17	1.46	37	.88	25	.38	24	.38	40	.38	21	1.33
18	.96	38	.38	10	.38	-	-	39	.31	22	.96
4	.8	13	.38	5	.38	-	-	14	.38	6	.80

APPENDIX E

```
! COM FILE TO GENERATE 150' TRUSS AS A SUBSTRUCTURE TO BE
! ATTACHED TO THE MAIN BODY OF THE SPACECRAFT

$ BEAMCS
TRUS150
OLB/TRUSCS
QUIT
$ BULKM
TRUS150
OLB/TRS150BM
QUIT
$ LOADBC
TRUS150
OLB/TRUSBC
OLB/TRSMAS15
QUIT
$ BULKF
TRUS150
1///
$ DEFCS
TRUS150
6
1,2,3,4,5,6
OLB/TRUSDEF
QUIT
$ ADSTIF
TRUS150
$ STASS
TRUS150
$ DECOM
TRUS150
$ REDCS
TRUS150

!  FILENAME IS TRUSCS.SRC

!  GENERATES CROSS SECTION TYPE AND DIMENSION OF BEAM ELEMENTS

CIRCS/8/.075/END

!  BULKM FILE THAT GENERATES 150' TRUSS

!  FILENAME IS TRUS150BM.SRC
```

```
ELMAT,4/6/6.0E4,8.0E6,.29,1.940994E-4/
KPOINT/1/0,0,4.763/2/0,8.25,0/3/0,0,-4.763/4/1800,0,4.763/
KPOINT/5/1800,8.25,0/6/1800,0,-4.763/7/90,0,50/
LSTY/BEAM2/6,8/
SLINE,10/L14/1,4,301/7/L36/3,6,301/7/L25/2,5,301/8/L12/1,2,3
/7/
SLINE,10/L23/2,3,3/7/L13/1,3,3/7/L45/4,5,3/7/L56/5,6,3/7/
SLINE,10/L46/4,6,3/7/
END

! EDITM FILE TO ADD BATTENS AND DIAGONALS TO THE 150' TRUSS

! FILENAME IS TRS150EM.SRC

PTRTH/8/PTRTM/6/

$ VERTICAL MEMBERS

BEAM2/9,307,7,149/157,455,7/158,307,7,149/306,455,7/

$ BOTTOM MEMBERS

BEAM2/9,158,7,149/157,306,7/

$ DIAGONAL MEMBERS

ETH,1/9/.001963/
PTRTH/9/
ROD2/9,159,148/156,306/10,158,148/157,305/9,308,148/156,455/
ROD2/10,307,148/157,454/158,308,148/305,455/159,307,148/306,
454/
ROD2/1,307/2,9/3,9/1,158/3,307/2,158/4,455/5,157/5,306/6,455/
ROD2/6,157/4,306/
END

! GENERATES POINT MASSES FOR THE 150' TRUSS

! FILENAME IS TRSMAS15.SRC

MASSP/1/2.71E-5/2/2.71E-5/3/2.71E-5/
MASSP/4/2.71E-5/5/2.71E-5/6/2.71E-5/
MASSP/9,307,299/2.71E-5,2.71E-5/308,606,299/2.71E-5,2.71E-5/
MASSP/607,905,299/2.71E-5,2.71E-5/
END
```

POINT	MASS X	MASS Y	MASS Z
440	1.234E-02	1.234E-02	1.234E-02
441	8.650E-03	8.650E-03	8.650E-03
442	1.305E-02	1.305E-02	1.305E-02
443	1.085E-02	1.085E-02	1.085E-02
444	8.580E-03	8.580E-03	8.580E-03
445	1.305E-02	-1.987E+00	1.305E-02
446	9.940E-03	4.594E-02	9.940E-03
447	1.842E-02	1.842E-02	-1.583E-03
448	1.842E-02	1.842E-02	1.842E-02
449	-6.583E-03	1.842E-02	1.842E-02
450	1.842E-02	1.842E-02	1.842E-02

APPENDIX F

```
$ ! COM FILE TO GENERATE AND CONNECT SPACECRAFT TRUSSES

$ ! FILENAME IS TRUSS.COM

DEL TRUSS.*;*

$ BEAMCS
LACE
OLB/TRUSCS
QUIT
$BULKM
LACE
OLB/TRUSSBM
QUIT
$ EDITM
LACE
OLB/TRUSSEM
QUIT
$ LOADBC
LACE
OLB/TRUSMASS
QUIT

$ GENERATES THE FILE FOR THE THREE TRUSSES OF THE LACE
$ SPACECRAFT USING THE PROCESSOR BULKM
$ BULKM FILE TO GENERATE 150 FOOT TRUSS IN +Y DIRECTION
$ ELEMENT MATERIAL

ELMAT,4/6/6.0E4,8.0E6,.29,1.94099E-4/

KPOINT/451/8.237,26,79.25/452/8.237,1826,79.25/
KPOINT/453/13,26,87.5/454/13,1826,87.5/
KPOINT/455/17.763,26,79.25/456/17.763,1826,79.25/
KPOINT/457/67.763,926,79.25/

LETY/BEAM2/6,8/

SLINE,10/LTR12/451,452,301/457/LTR34/453,454,301/457/
SLINE,10/LTR56/455,456,301/457/LTR13/451,453,3/457/
SLINE,10/LTR35/453,455,3/457/LTR15/451,455,3/457/
SLINE,10/LTR24/452,454,3/457/LTR46/454,456,3/457/
SLINE,10/LTR26/452,456,3/457/

$ FILE TO GENERATE 150 FOOT TRUSS IN +Z DIRECTION
```

```
$ ELEMENT MATERIAL

ELMAT,4/6/6.0E4,8.0E6,.29,1.94099E-4/

KPOINT/458/2.75,4.763,96/460/-5.5,0,96/
KPOINT/462/2.75,-4.763,96/459/2.75,4.763,1896/
KPOINT/461/-5.5,0,1896/463/2.75,-4.763,1896/
KPOINT/470/52.75,0,996/

LETY/BEAM2/6,8/

SLINE,10/LTR89/458,459,301/470/LTR6263/462,463,301/470/
SLINE,10/LTR01/460,461,301/470/LTR5860/458,460,3/470/
SLINE,10/LTR6062/460,462,3/470/LTR5862/458,462,3/470/
SLINE,10/LTR5961/459,461,3/470/LTR6163/461,463,3/470/
SLINE,10/LTR5963/459,463,3/470/


$ GENERATES A FILE TO CONNECT 75 FOOT  -Y-TRUSS BOOMS TO
$ MAIN SPACECRAFT

KPOINT/464/-17.763,-26,79.25/
KPOINT/466/-13,-26,87.5/
KPOINT/468/-8.237,-26,79.25/
KPOINT/465/-17.763,-926,79.25/
KPOINT/467/-13,-926,87.5/
KPOINT/469/-8.237,-926,79.25/
KPOINT/471/67.763,-463,79.25/

LETY/BEAM2/6,8/

SLINE,10/L46869/468,469,151/471/L46465/464,465,151/471/
SLINE,10/L46667/466,467,151/471/L46567/465,467,3/471/
SLINE,10/L46769/467,469,3/471/L46569/465,469,3/471/
SLINE,10/L46466/464,466,3/471/L46668/466,468,3/471/
SLINE,10/L46468/464,468,3/471/

END


$ GENERATES BATTENS AND DIAGONALS FOR SPACECRAFT TRUSS
$ USING THE PROCESSOR EDITM

$ FILENAME IS TRUSSEM.SRC

$ THIS FILE MERGES THE TRUSSES TO THE SPACECRAFT

MERGEP/546/451/19/453/549/455/
MERGEP/557/548/31/461/553/462/
MERGEP/550/464/25/466/553/468/
```

```
$ GENERATES VERTICAL,BOTTOM,DIAGONAL MEMBERS FOR 150 FT TRUSS
$ IN THE +Y DIRECTION

PTRTH/8
PTRM/6

$ VERTICAL/BOTTOM MEMBERS

BEAM2/974,1273,457,299/1272,1571,457/
BEAM2/675,974,457,299/973,1272,457/
BEAM2/675,1273,457,299/973,1571,457

$ GENERATES BATTENS AND DIAGONALS FOR SPACECRAFT TRUSS
$ USING THE PROCESSOR EDITM

$ FILENAME IS TRUSSEM.SRC

$ THIS FILE MERGES THE TRUSSES TO THE SPACECRAFT

MERGEP/546/451/19/453/549/455/
MERGEP/557/548/31/461/553/462/
MERGEP/550/464/25/466/553/468/

$ GENERATES VERTICAL,BOTTOM,DIAGONAL MEMBERS FOR 150 FT TRUSS
$ IN THE +Y DIRECTION

PTRTH/8
PTRM/6

$ VERTICAL/BOTTOM MEMBERS

BEAM2/974,1273,457,299/1272,1571,457/
BEAM2/675,974,457,299/973,1272,457/
BEAM2/675,1273,457,299/973,1571,457

$ DIAGONAL MEMBERS

ETH,1/10/.001963/

PTRTH/10/

ROD2/455,675/451,1273/455,974/453,1273/453,675/451,974/
ROD2/975,1273,298/1272,1570/974,1274,298/1271,1571/
ROD2/675,975,298/972,1272/676,974,298/973,1271/
ROD2/675,1274,298/972,1571/676,1273,298/973,1570/
ROD2/456,973/452,1571/456,1272/454,1571/452,1272/454,973/

$ GENERATES VERTICAL,BOTTOM,DIAGONAL MEMBERS FOR 150 FT TRUSS
$ IN THE +Z DIRECTION

PTRTH/8
```

```
PTRM/6

$ VERTICAL/BOTTOM MEMBERS

BEAM2/1578,1877,464,299/1876,2175,464/
BEAM2/1578,2176,464,299/1876,2474,464/
BEAM2/1877,2176,464,299/2175,2474,464

$ DIAGONAL MEMBERS

ETH,1/10/.001963/

PTRTH/10/

ROD2/463,1876/459,2175/461,1876/459,2474/461,2175/463,2474/
ROD2/1877,2177,298/2174,2474/1878,2176,298/2175,2473/
ROD2/1579,1877,298/1876,2174/1578,1878,298/1875,2175/
ROD2/1579,2176,298/1876,2473/1578,2177,298/1875,2474/
ROD2/462,2176/462,1578/460,1877/460,1578/458,2176/458,1877/

$ GENERATES VERTICAL,BOTTOM,DIAGONAL MEMBERS FOR 75 FT TRUSS
$ IN THE -Y DIRECTION

PTRTH/8
PTRM/6

$ VERTICAL/BOTTOM MEMBERS

BEAM2/2630,2779,470,149/2778,2927,470/
BEAM2/2481,2779,470,149/2629,2927,470/
BEAM2/2481,2630,470,149/2629,2778,470/

$ DIAGONAL MEMBERS

ETH,1/10/.001963/

PTRTH/10/

ROD2/464,2779/466,2630/464,2481/468,2630/468,2779/466,2481/
ROD2/2630,2780,148/2777,2927/2631,2779,148/2778,2926/
ROD2/2482,2630,148/2629,2777/2481,2631,148/2628,2778/
ROD2/2481,2780,148/2628,2927/2482,2779,148/2629,2926/
ROD2/465,2927/467,2778/465,2629/469,2778/469,2927/467,2629/

END


$ GENERATES MASS FOR THE COMPLETE TRUSS MODEL

$ GENERATES MASS FOR THE 150 FOOT TRUSS IN +Y DIRECTION
```

```
MASSP/451/8.8846E-5/452/8.8846E-5/453/8.8846E-5/
MASSP/454/8.8846E-5/455/8.8846E-5/456/8.8846E-5/
MASSP/1273,1571,299/8.8846E-5,8.8846E-5/
MASSP/675,973,299/8.8846E-5,8.8846E-5/
MASSP/974,1272,299/8.8846E-5,8.8846E-5/

$ GENERATES MASS FOR THE 150 FOOT TRUSS IN +Z DIRECTION

MASSP/464/8.8846E-5/465/8.8846E-5/466/8.8846E-5/
MASSP/467/8.8846E-5/468/8.8846E-5/469/8.8846E-5/
MASSP/2779,2927,149/8.8846E-5,8.8846E-5/
MASSP/2630,2778,149/8.8846E-5,8.8846E-5/
MASSP/2481,2629,149/8.8846E-5,8.8846E-5/

$ GENERATES MASS FOR THE 75 FOOT TRUSS IN -Y DIRECTION

MASSP/458/8.8846E-5/459/8.8846E-5/460/8.8846E-5/
MASSP/461/8.8846E-5/462/8.8846E-5/463/8.8846E-5/
MASSP/1578,1876,299/8.8846E-5,8.8846E-5/
MASSP/1877,2175,299/8.8846E-5,8.8846E-5/
MASSP/2176,2474,299/8.8846E-5,8.8846E-5/

$ GENERATES TIPMASS FOR EACH TRUSS

MASSP/459/1.72533E-1/461/1.72533E-1/463/1.72533E-1/
MASSP/452/3.0193E-2/454/3.0193E-2/456/3.0193E-2/
MASSP/465/3.0193E-2/467/3.0193E-2/469/3.0193E-2/

END
```

APPENDIX G

Before the LACE spacecraft was in its fully deployed state, it underwent three different configurations. Figures G1 to G4 show the natural frequencies and mode shapes of the LACE spacecraft in its initial configuration with the gravity gradient extended to 75 feet. Figures G5 to G8 show LACE with the gravity gradient extended to 150 feet. Figures G9 to G12 show the LACE spacecraft in its final configuration before full deployment with the lead and trail booms extended to 119.5 feet.

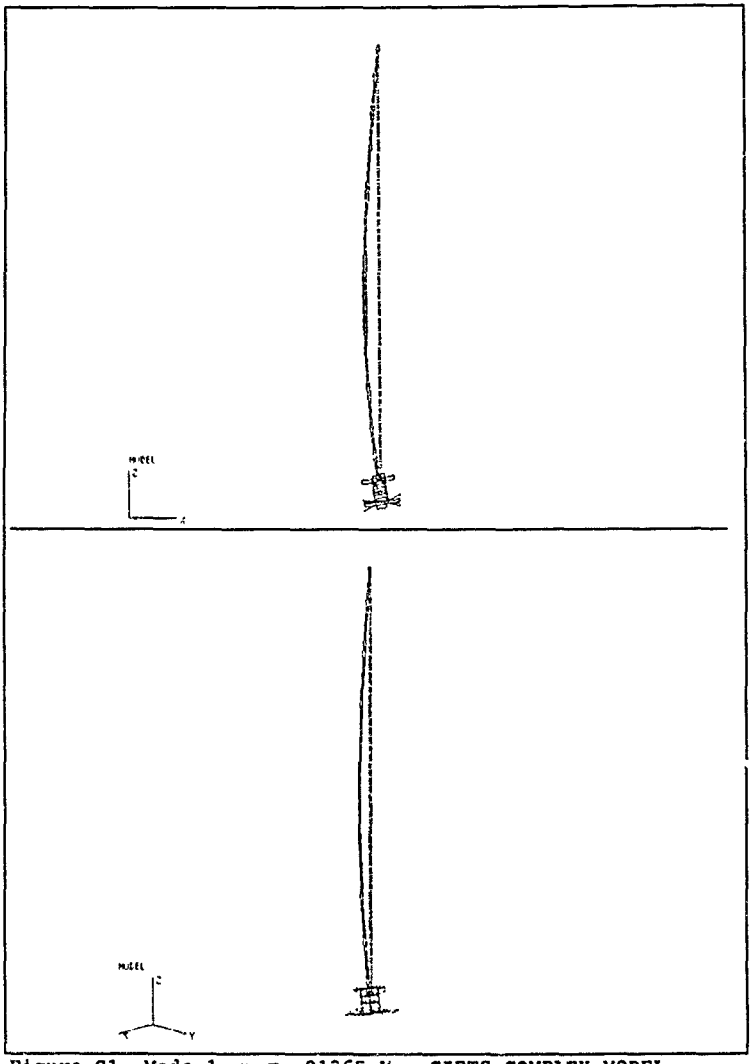

Figure G1. Mode 1, υ = .01365 Hz, GIFTS COMPLEX MODEL

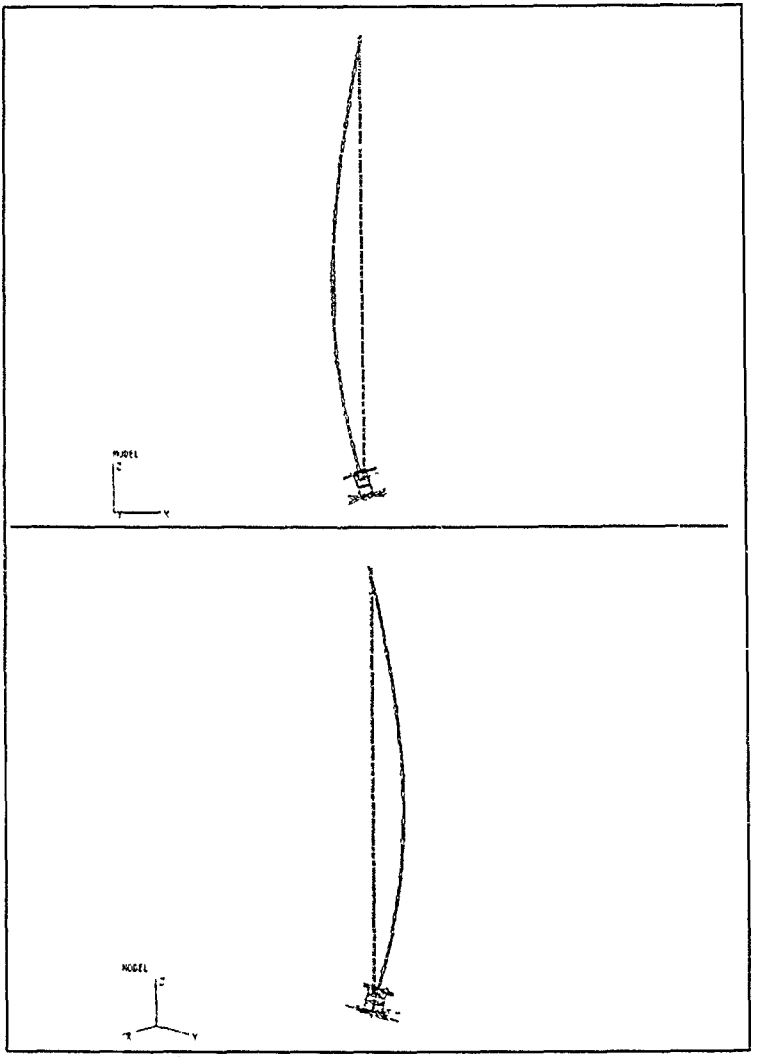

Figure G2. Mode 2, υ = .01379 Hz, GIFTS COMPLEX MODEL

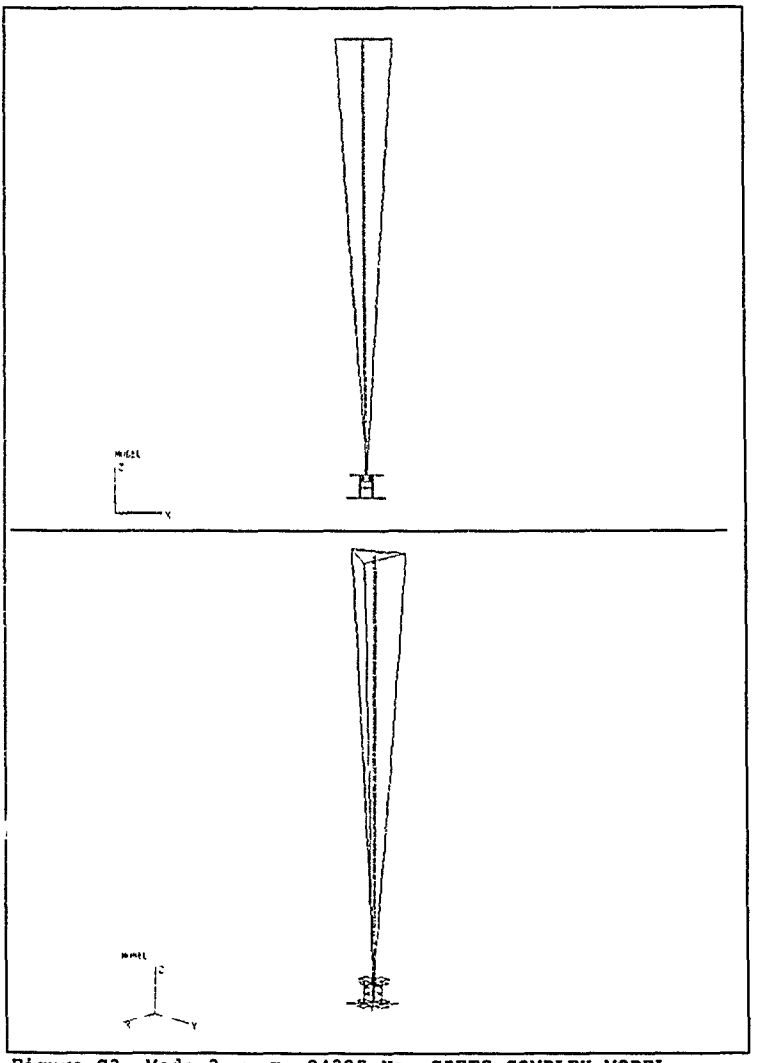

Figure G3. Mode 3, υ = .04325 Hz, GIFTS COMPLEX MODEL

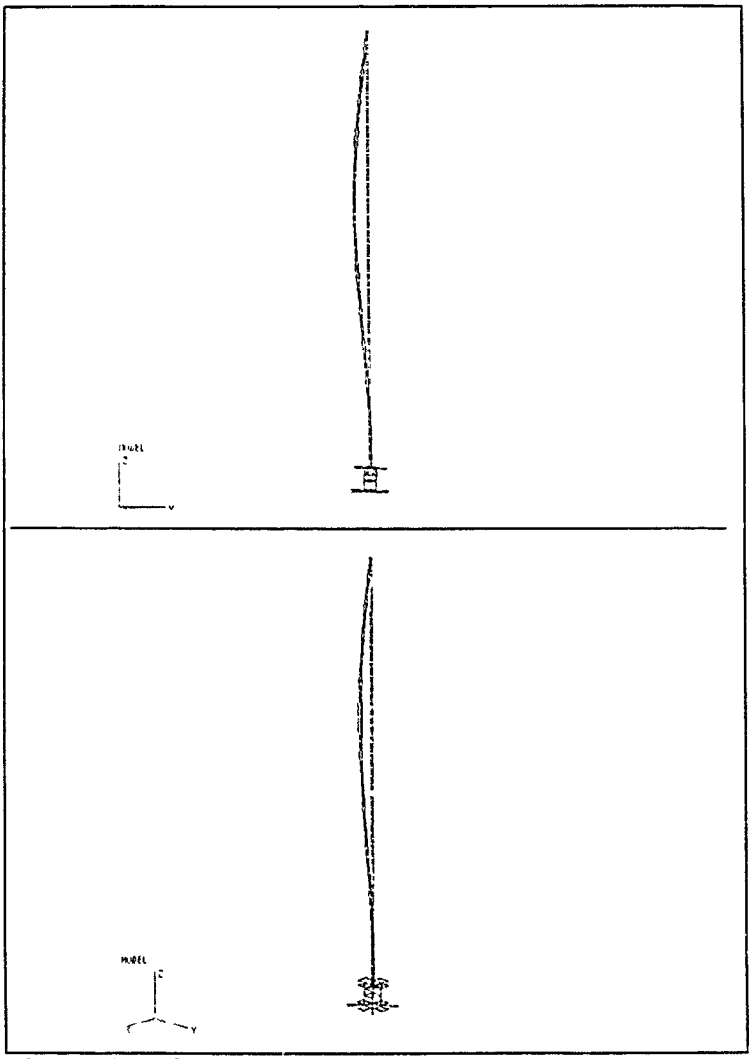

Figure G4. Mode 4, υ = .04579 Hz, GIFTS COMPLEX MODEL

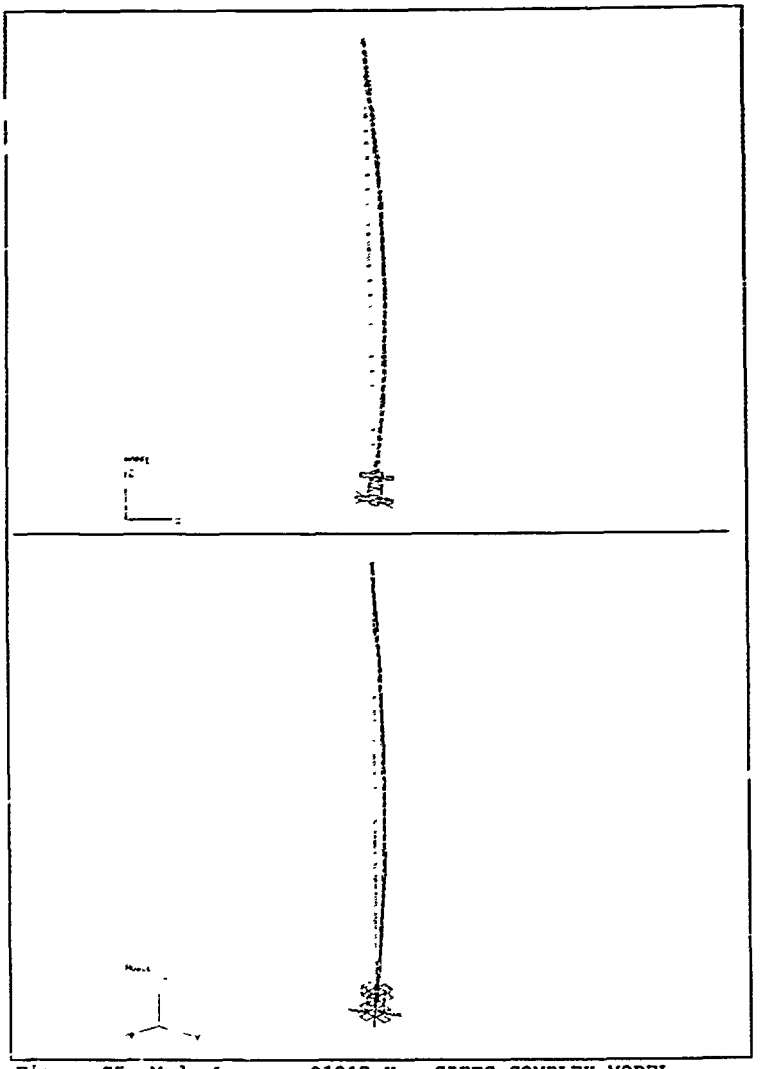

Figure G5. Mode 1, υ = .01217 Hz, GIFTS COMPLEX MODEL

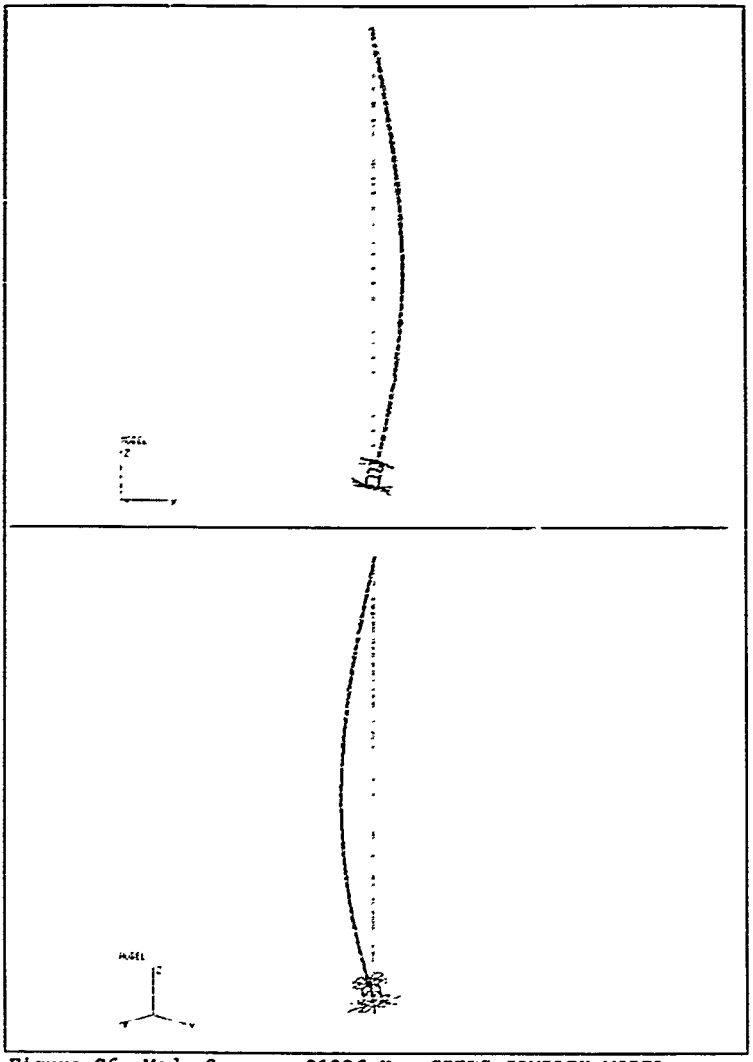

Figure G6. Mode 2, υ = .01226 Hz, GIFTS COMPLEX MODEL

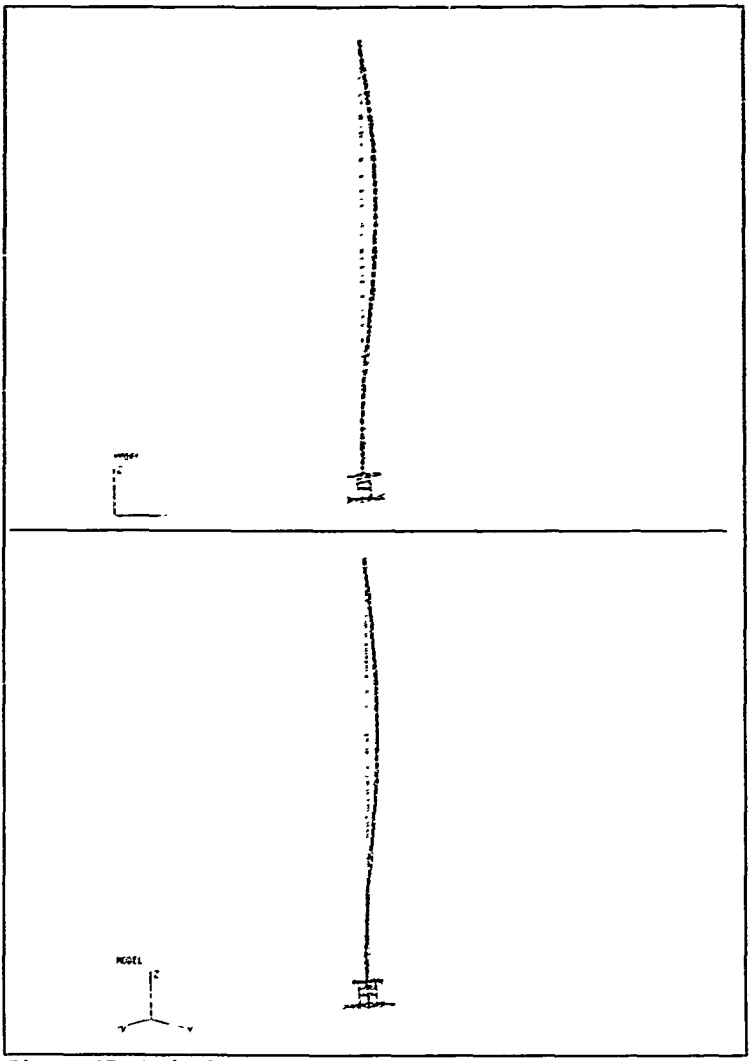

Figure G7. Mode 3, υ = .03535 Hz, GIFTS COMPLEX MODEL

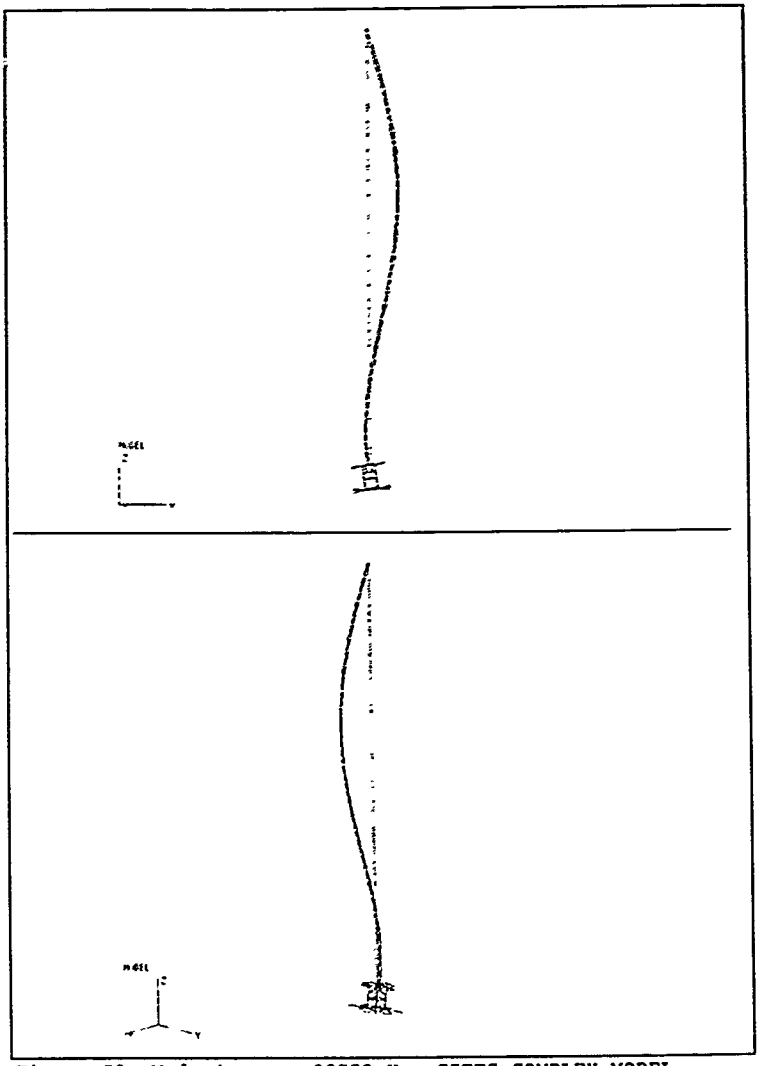

Figure G8. Mode 4, υ = .03552 Hz, GIFTS COMPLEX MODEL

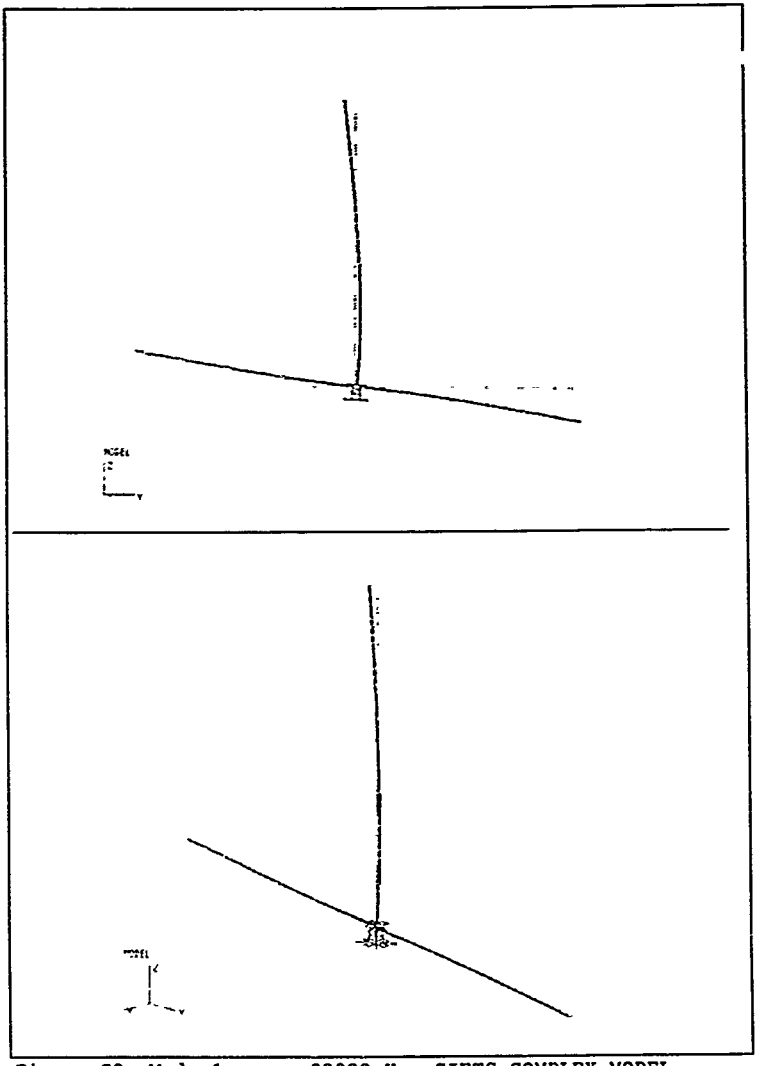

Figure G9. Mode 1, υ = .02322 Hz, GIFTS COMPLEX MODEL

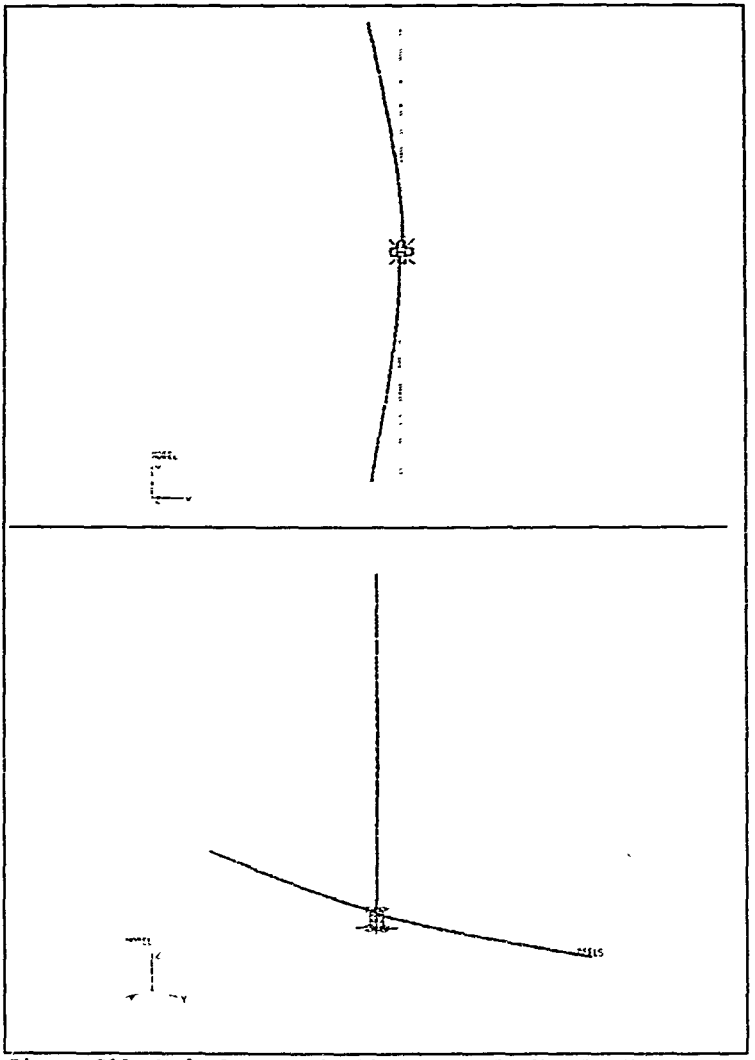

Figure G10. Mode 2, υ = .04294 Hz, GIFTS COMPLEX MODEL

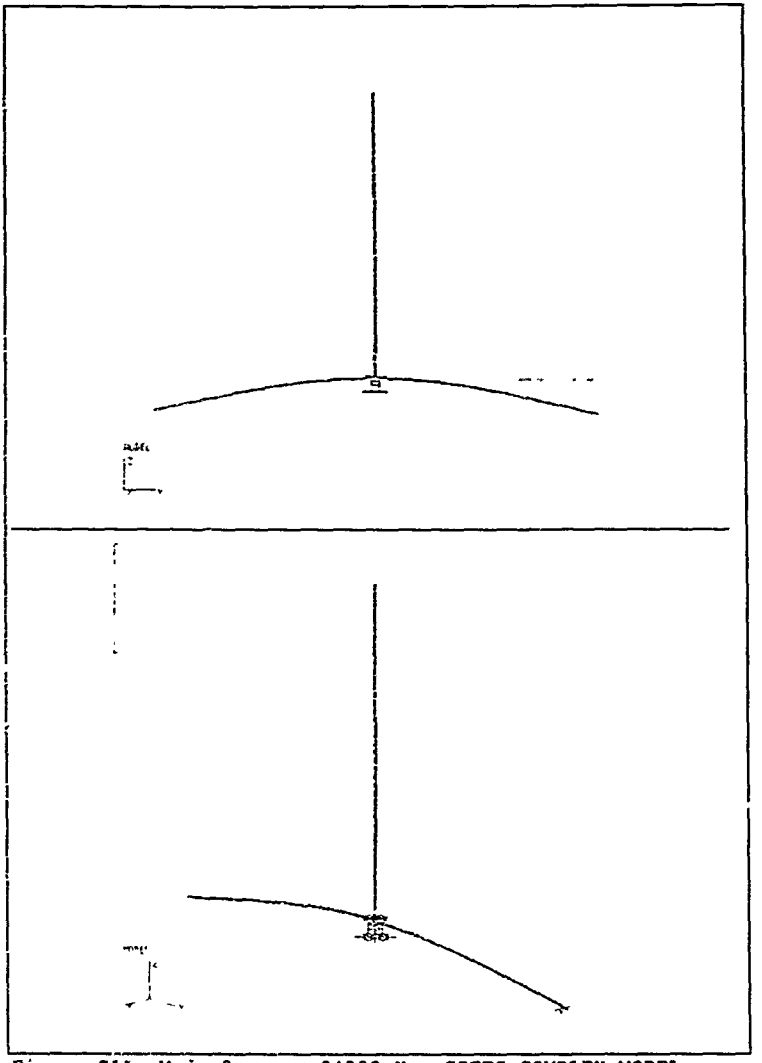

Figure G11. Mode 3, υ = .04302 Hz, GIFTS COMPLEX MODEL

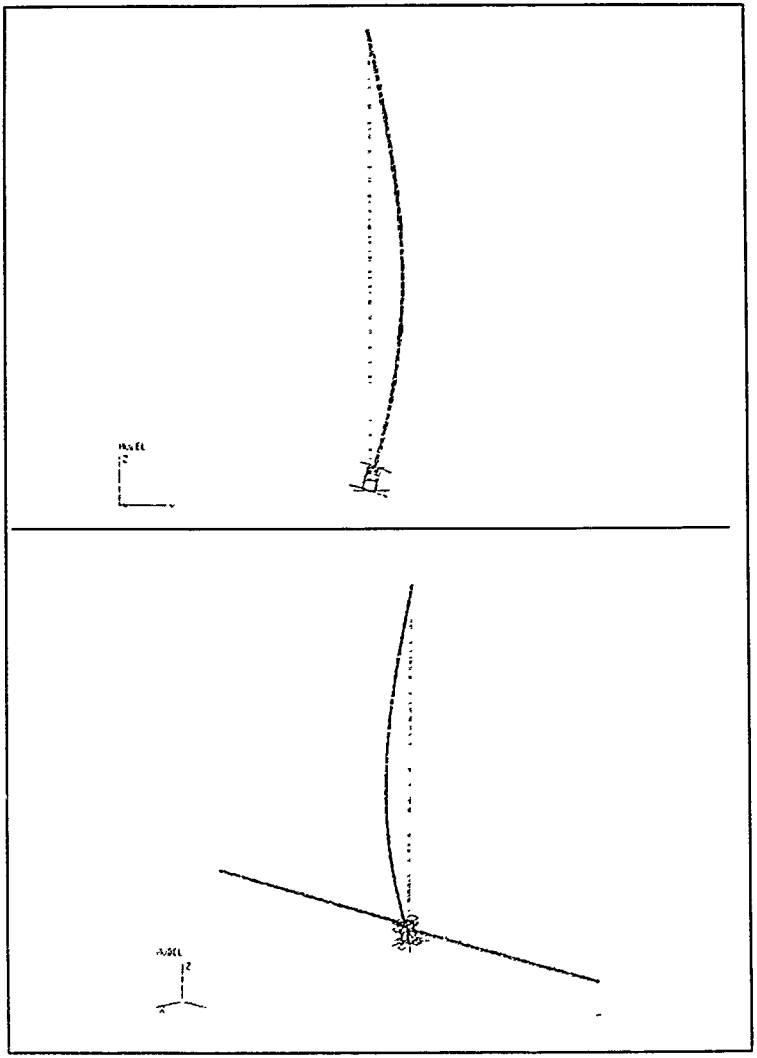

Figure G12. Mode 4, υ = .1349 Hz, GIFTS COMPLEX MODEL

APPENDIX H

A. MAXIMUM TEMPERATURE FOR DIAGONALS

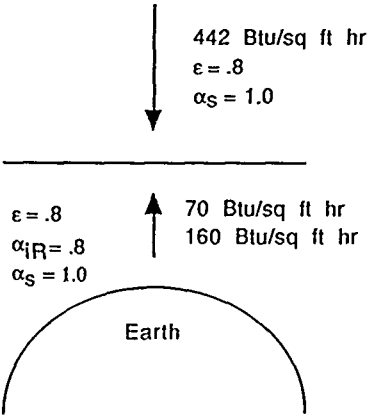

Figure H1. LACE Boom Perpendicular to the Sun

The heat balance equation is

$$\alpha_s sa = \epsilon\sigma T^4 D$$

where s is solar flux intensity, a is surface area and σ is Stefan Boltzman constant.

Heat in = 442 x 1.0 x d + (160 x 1.0 + 70 x .8) x πd/2

$= 781.3\ d$

Heat out $= 0.8 \times \pi d \times \sigma \times T^4$

$781.3 = 0.9 \times \pi \times \sigma \times T^4 = 4.305 \times 10^{-9} T^4$

$T = 652\ R = 193\ F$

B. MINIMUM TEMPERATURE FOR THE DIAGONAL

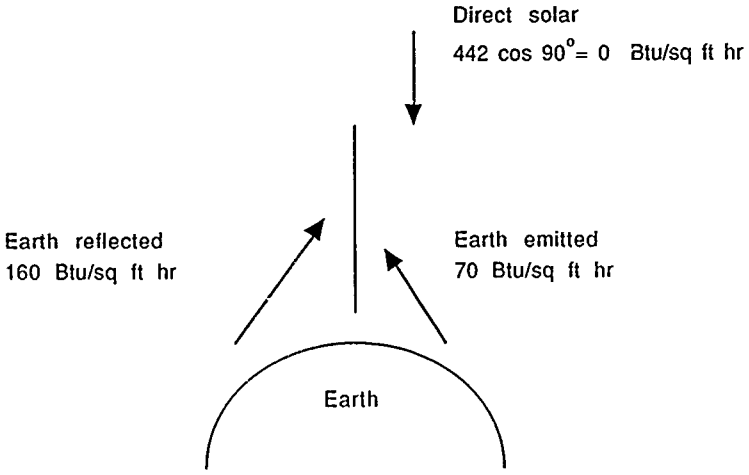

Figure H2. LACE Beam Parallel to the Sun

$F_{d1\text{-}2} = .256$

Reciprocity $F_{d1\text{-}2} dA_2 = F_{2\text{-}d1} A_2 \Rightarrow \quad \frac{F_{2\text{-}d1}}{dA_1} = \frac{.256}{dA_1}$

$$Q_{2\text{-}1} = A_2 F_{2\text{-}d1} (E_{b2})$$

Divide by $dA_1 \quad \frac{Q_{2\text{-}1}}{dA_1} = A_2 \frac{F_{2\text{-}d1}}{dA_1} E_{b2}$

Substitute $\frac{Q_{2\text{-}1}}{dA_1} = A_2 \frac{.256}{A_2} E_{b2} = 0.28\ E_{b2}$

$= (0.256)\ [160 + 70]$ Btu/sq ft hr

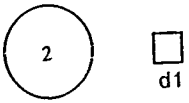

Figure H3. Viewing Factor

= 58.9 Btu/sq ft hr

$$T = \left(\frac{q}{\sigma}\frac{\alpha}{e}\right)^{0.25} = \left(\frac{58.9}{0.1714} x10^{-8} 1.25\right)^{.25} = 455R = -5F$$

[Ref. 13]

APPENDIX I

```
C     ************************
C     *                      *
C     *  WALTERS, W          *
C     *  THESIS RESEARCH     *
C     *  6 JUNE 1990         *
C     *  NONLINEAR SYSTEMS   *
C     *                      *
C     ************************
C
C
C
C     ***PURPOSE***
C
C     THIS PROGRAM COMPUTES DISPLACEMENTS, VELOCITIES,AND
      ACCELERATION
C     USING LINEAR ACCELERATION METHOD
C
C
C
C     ***VARIABLE DEFINITIONS***
C
C     T=        Time
C     A=        Acceleration
C     V=        Velocity
C     U=        Displacement
C     M=        Mass
C     K=        Spring constant
C     C=        Damping
C     P=        Force
C     FS=       Spring force
C     KSTAR=    Delta K*
C     PSTAR=    Delta P*
C     DELT=     Time interval, delta t
C     DELU=     Change in displacement
C     DELV=     Change in velocity
C     DELA=     Change in acceleration
C     DELP=     Change in force
C     A0=       Coefficient of amplitude for force function
C     Omega=    Frequency for force function
C     A1=       Coefficient for X**3 term for stiffness
                function
C     B1=       Coefficient for X**2 term for stiffness
                function
C     C1=      Coefficient for X  term for stiffness function
```

```
C     D1=       coefficient for constant term for stiffness
                function
C     A2=      Coefficient for X**2 term for damping function
C     B2=       Coefficient for X term for damping function
C     C2=       Coefficient for constant term for damping
                function
C     FRAC=     Fraction of linear stiffness term used for
                coeff. of cubic term
C
C     ***VARIABLE DECLARATIONS***
C
      Real*16 T,A,V,U,M,K,C,FS,KSTAR,PSTAR,DELT,DELU,DELV,

*DELA,DELP,A0,Omega,A1,B1,C1,D1,A2,B2,C2,FRAC,MASS,P(5000)
C     DIMENSION P(5000)
      Integer I,N
C
      CHARACTER*7 DUMMY
      CHARACTER NAME*8,FN*8
C     ***INITIAL DATA***
C
      T=0.0
      N=0
C
C     ***MAIN PROGRAM***
C
C
C === CREATE A FILE FOR CHAOTIC COMPUTAIONS
      OPEN (UNIT=1, FILE='ACC.INP', STATUS='OLD')
C
      WRITE (6,*) 'INPUT THE FILE NAME'
      READ (5,'(A)') NAME
      FN = NAME
      OPEN (UNIT = 12, FILE = FN, STATUS = 'NEW')
      WRITE(6,*) 'DO YOU WANT INTERACTIVE INPUT FILE,
      0=YES,1=NO'
      READ(5,*) IYES
      IF (IYES.GT.0) GO TO 500
C
      PRINT *, 'ENTER INITIAL CONDITIONS'
      PRINT *, 'INITIAL DISPLACEMENT ='
      READ *, U
      PRINT *, 'INITIAL VELOCITY ='
      READ *, V
      Print *, 'F(X)=A0*COS(Omega*T)'
      Print *, 'Enter value for A0'
      Read *, A0
      Print *, 'Enter value for Omega'
      Read *, Omega
      Print *, 'K(X)=A1*X**3+B1*X**2+C1*X+D1'
      Print *, 'Enter value for A1'
```

```
      Read *, A1
      Print *, 'Enter value for B1'
      Read *, B1
      Print *, 'Enter value for C1'
      Read *, C1
      Print *, 'Enter value for D1'
      Read *, D1
      Print *, 'C(X)=A2*V**2+B2*V+C2'
      Print *, 'Enter value for A2'
      Read *, A2
      Print *, 'Enter value for B2'
      Read *, B2
      Print *, 'Enter value for C2'
      Read *, C2
      Print *, 'Enter value for mass'
      Read *, M
      Print *, 'Enter value for delt'
      Read *, DELT
      Print *, 'Enter value for n, number of time steps'
      Read *, N
C
      GO TO 550
  500 CONTINUE
      READ(1,*) A0
      READ(1,*) Omega
      READ(1,*) A1
      READ(1,*) C1
      READ(1,*) D1
      READ(1,*) A2
      READ(1,*) B2
      READ(1,*) C2
      READ(1,*) M
C
C     WRITE(*,*) A0,Omega,A1,C1,D1,A2,B2,C2,M
      PRINT *, 'NONLINEAR STIFF TERM B1 IS FRACTION OF LINEAR
      TERM D1'
      PRINT *, 'INPUT FRACTION DESIRED'
      READ *, FRAC
C
      B1= FRAC*D1+D1
C
      PRINT *, 'ENTER INITIAL CONDITIONS'
      PRINT *, 'INITIAL DISPLACEMENT ='
      READ *, U
      PRINT *, 'INITIAL VELOCITY ='
      READ *, V
      Print *, 'Enter value for delt'
      Read *, DELT
      Print *, 'Enter value for n, number of time steps'
      Read *, N
  550 CONTINUE
```

```
      DUMMY='WALTERS'
      Do 20 I=1,N
      Call Force(A0,Omega,T,I,P)
      Call Damp(A2,B2,C2,V,C)
      Call FSPRING(A1,B1,C1,D1,U,I,K,FS)
      CALL DFORCE(T,DELP,I,P)
C
C     Solve for A
C
      A=(1/M)*(P(I)-(C*V)-FS)
C
C     Solve for KSTAR
C
      KSTAR=K+((3*C)/DELT)+((6*M)/DELT**2)
C
C     Solve for PSTAR
C
      PSTAR=DELP+(((6*M)/DELT)+(3*C))*V+((3*M)+C*(DELT/2))*A
C
C     Solve for DELU
C
      DELU=PSTAR/KSTAR
C
C     Solve for DELV
C
      DELV=(3/DELT)*DELU-(3*V)-A*(DELT/2)
C
C     Solve for DELA
C
      DELA=(6/DELT**2)*DELU-((6/DELT)*V)-(3*A)
C
C     Write output file
C
C *** OUTPUT TO THE CHAOTIC FILE
      WRITE(11,6000) DUMMY,T,U,V,A
 6000 FORMAT(A7,F6.3,E11.4,4E12.4)

C     Update U,V,T for next iteration
C
      U=U+DELU
      V=V+DELV
      T=T+DELT
   20 Continue
C
      Write(*,*)T,U,V
      CLOSE(UNIT=1)
      CLOSE(UNIT=11)
      Stop
      End
C
C
```

```
C
*****************************************************************
C
      Subroutine Force(A0,Omega,T,I,P)
C
C     Assigns a value to force based on time
C     Input argument
C     A0-Coefficient,Omega-frequency,T-Time, I-Counter
C     Output argument
C     P-Force
C
      Real*16 A0,Omega,T,P
      Integer I
      DIMENSION  P(5000)
C
C
C     Define results
C
      P(I)=A0*COS(Omega*T)
C     Write(*,*)I,P(I)
      Return
      End
C
C
*****************************************************************
C
      Subroutine Damp(A2,B2,C2,V,C)
C
C     Assigns a value for damping
C     Input argument
C     A2,B2,C2 - Coefficients of damping function
C     U-Displacement
C     Output argument
C     C-Damping
C
      Real*16 A2,B2,C2,V,C
C     Define results
C
      C=A2*V**2+B2*V+C2
      Return
      End
C
C
*****************************************************************

C
      Subroutine FSPRING(A1,B1,C1,D1,U,I,K,FS)
C
C     Calculates the value for FS
C
C     Input arguments
```

```
C
C     U-Displacements
C     A1,B1,C1,D1- Coefficients for stiffness function
C     I-counter
C
C     Output arguments
C
C     FS-Force of spring
C
      Real*16 A1,B1,C1,D1,U,FS,K
      Integer I
C
C     Define results
C
      K=A1*U**3+B1*U**2+C1*U+D1
      FS=K*U
      Return
      End
C
C
*****************************************************************
C
      Subroutine DFORCE(T,DELP,I,P)
C
C     Defines the value for the change in force
C
C     Input argument
C     T-Time,P-Force
C     Output argument
C     DELP-Change in force
      Real*16 T,DELP,F,P(5000)
      INTEGER I
C     DIMENSION P(5000)
C
C
      IF (I.EQ.1) Then
         DELP =0
      ELSE
         DELP=P(I)-P(I-1)
      Endif
      Return
      End
C
*****************************************************************
```

APPENDIX J

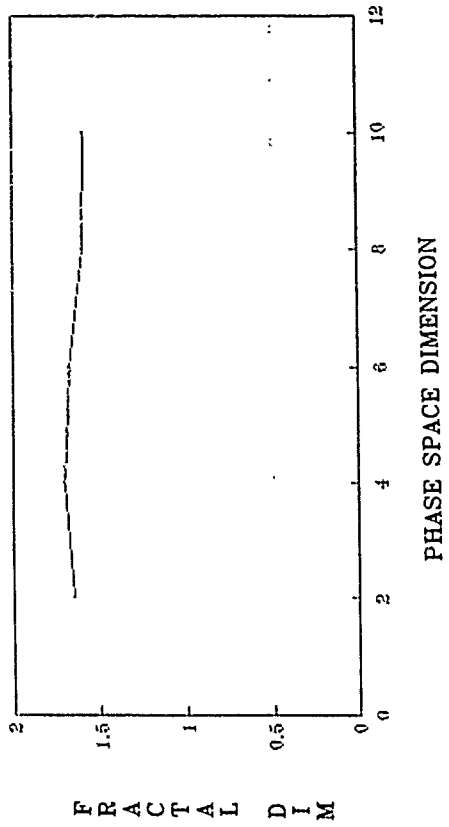

Figure J1. Fractal Dimension. F=41.68, Ω=1.53, C=.177

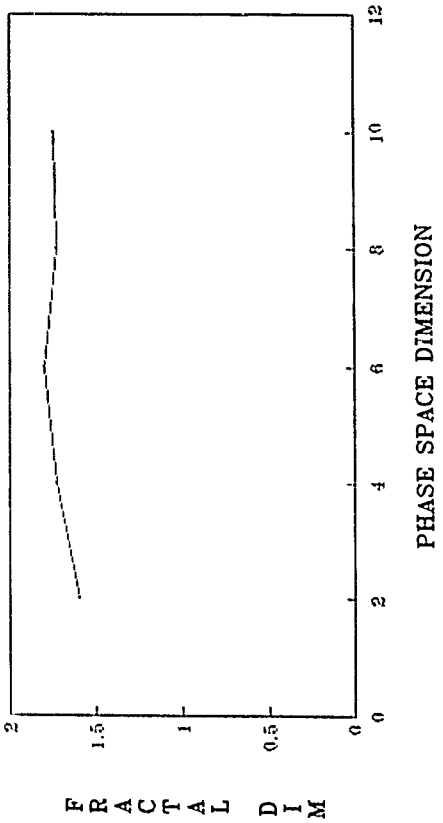

Figure J2. Fractal Dimension. F=83.35, Ω=1.53, C=.177

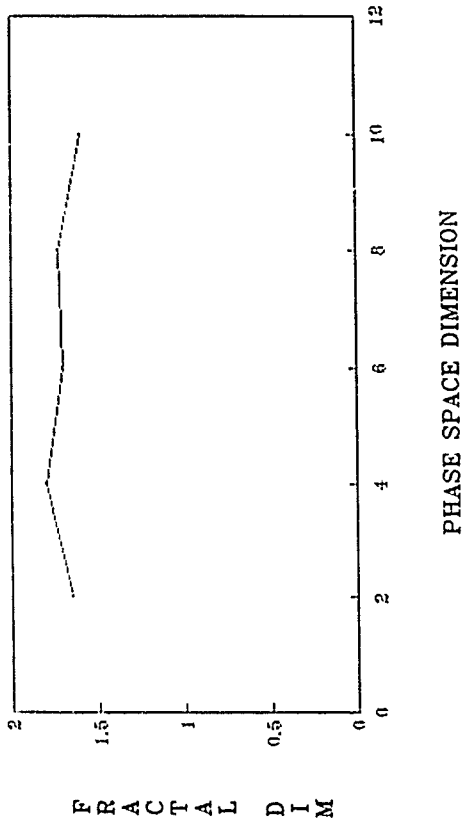

Figure J3. Fractal Dimension. F=166.7, Ω=1.53, C=.177

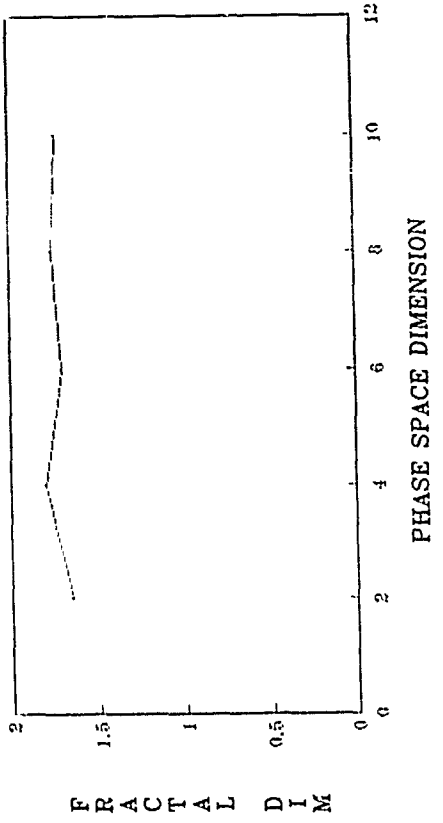

Figure J4. Fractal Dimension. F=208.4, Ω=1.53, C=.177

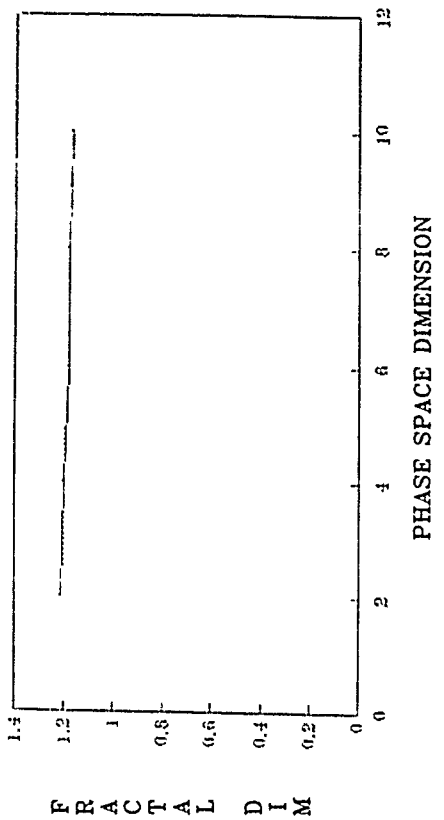

Figure J5. Fractal Dimension. F=20.8, Ω=13.8, C=.177

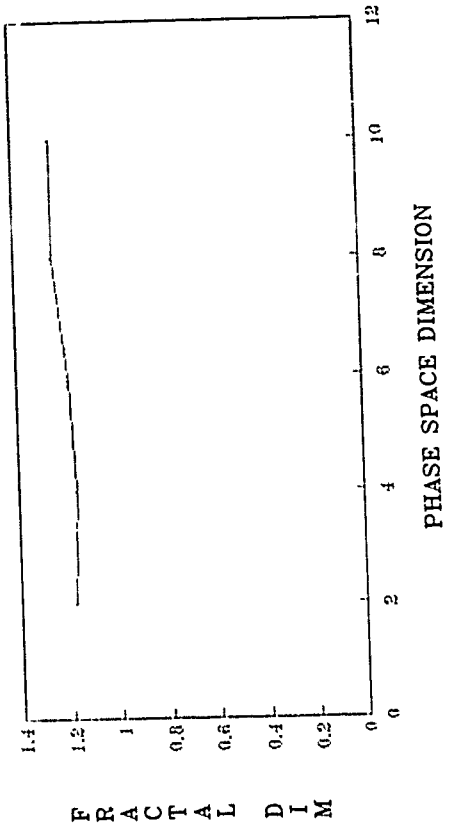

Figure J6. Fractal Dimension. F=41.68, Ω=13.8, C=.177

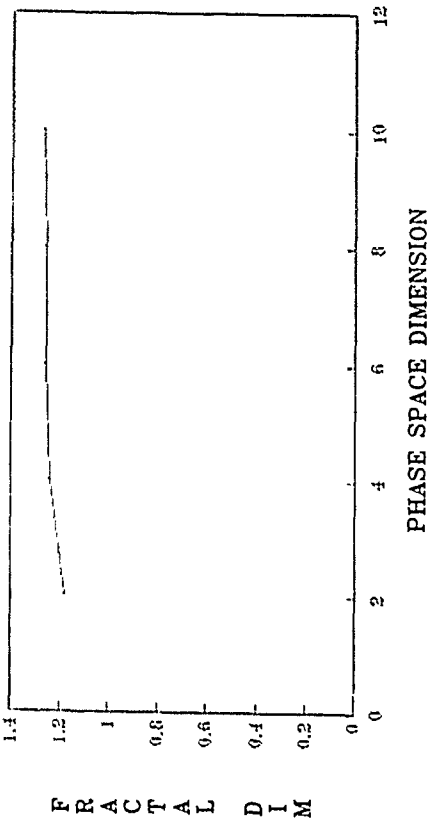

Figure J7. Fractal Dimension. F=83.35, Ω=13.8, C=.177

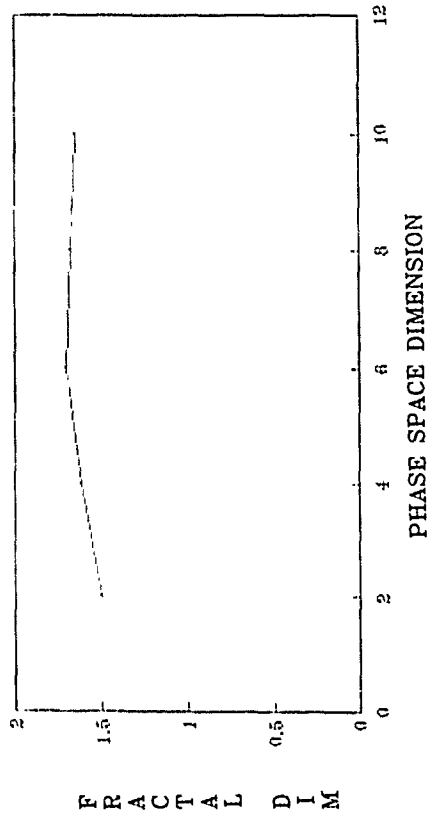

Figure J8. Fractal Dimension. F=166.7, Ω=13.8, C=.177

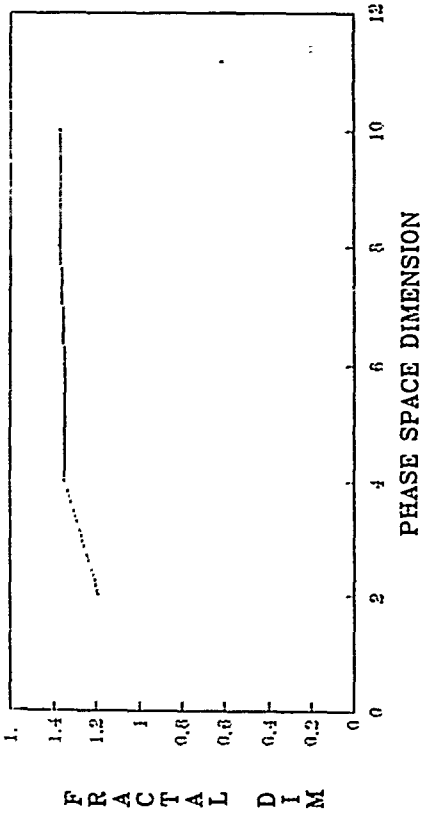

Figure J9. Fractal Dimension. F=208.4, Ω=13.8, C=.177

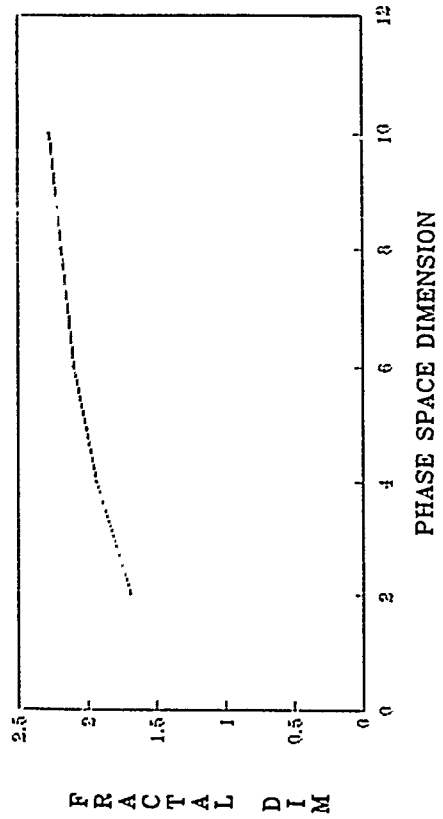

Figure J10. Fractal Dimension. F=41.68, Ω=1.53, C=.0454

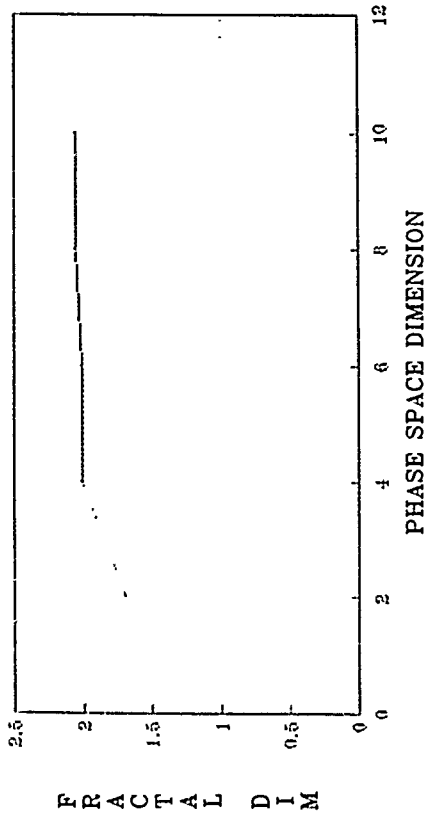

Figure J11. Fractal Dimension. F=83.35, Ω=1.53, C=.0454

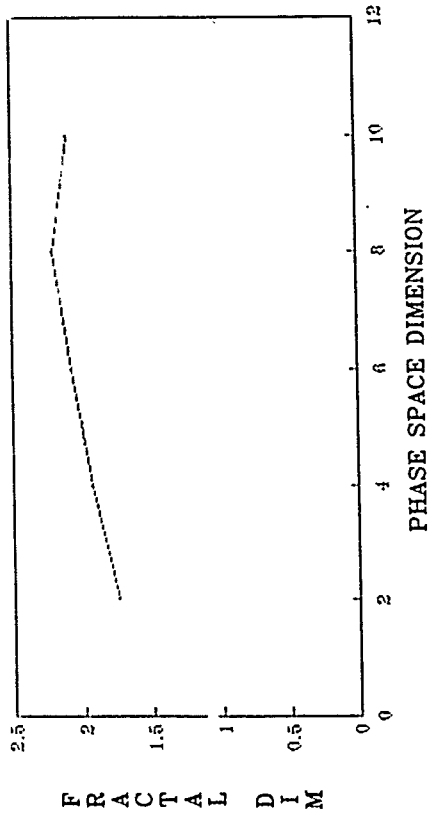

Figure J12. Fractal Dimension. F=166.8, Ω=1.53, C=.0454

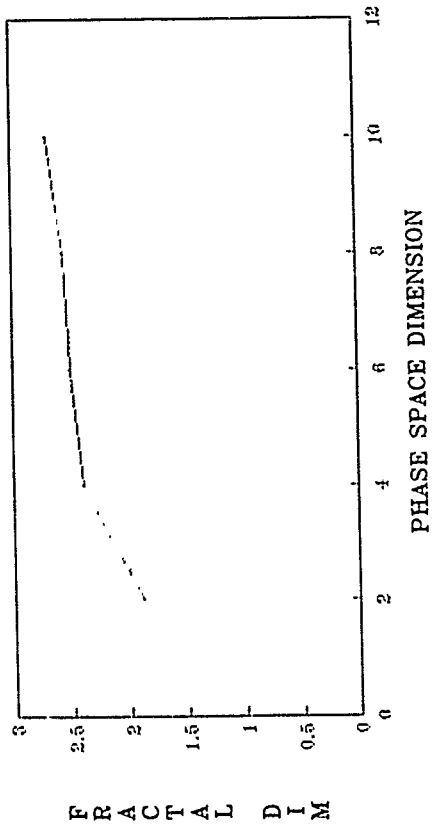

Figure J13. Fractal Dimension. F=208.4, Ω=1.53, C=.0454

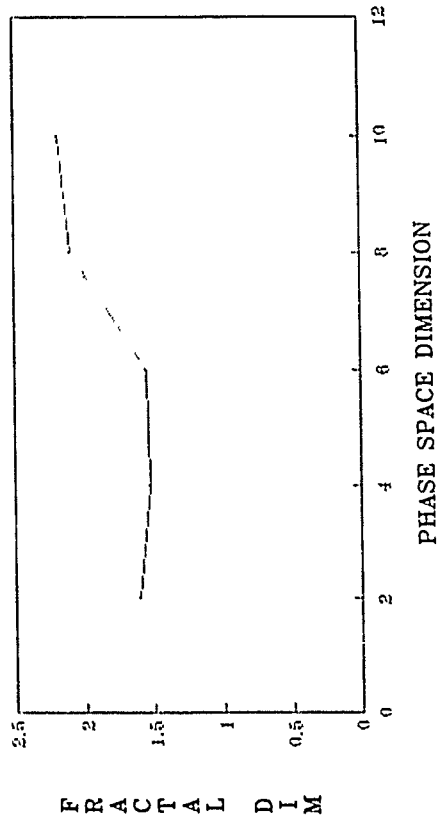

Figure J14. Fractal Dimension. F=20.8, Ω=13.8, C=.0454

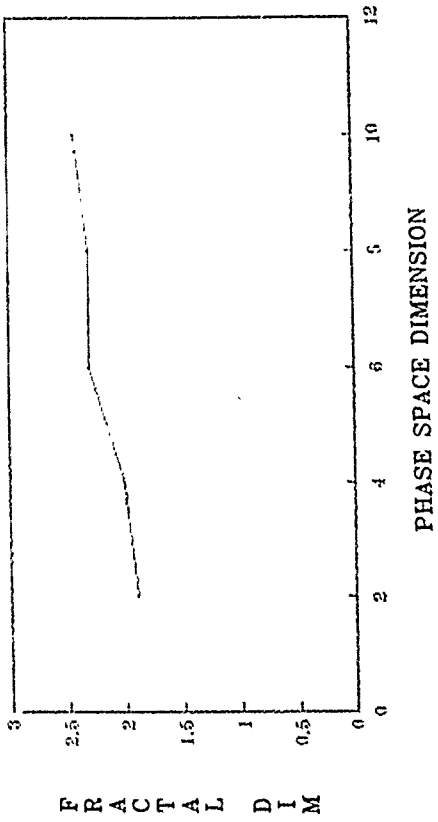

Figure J15. Fractal Dimension. F=41.68, Ω=13.8, C=.0454

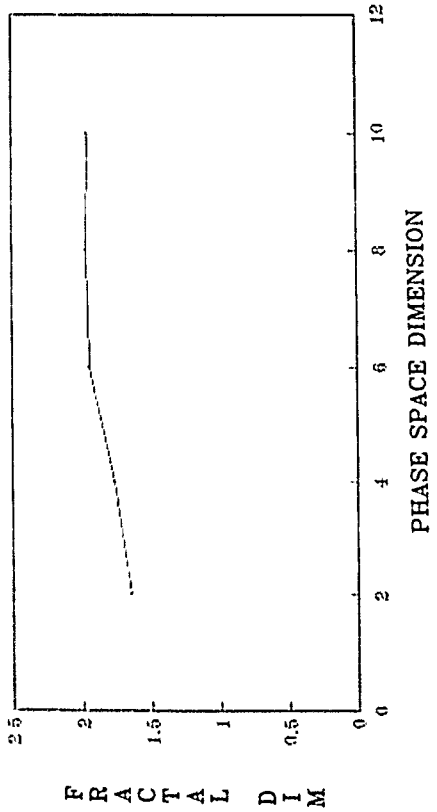

Figure J16. Fractal Dimension. F=83.35, Ω=13.8, C=.0454

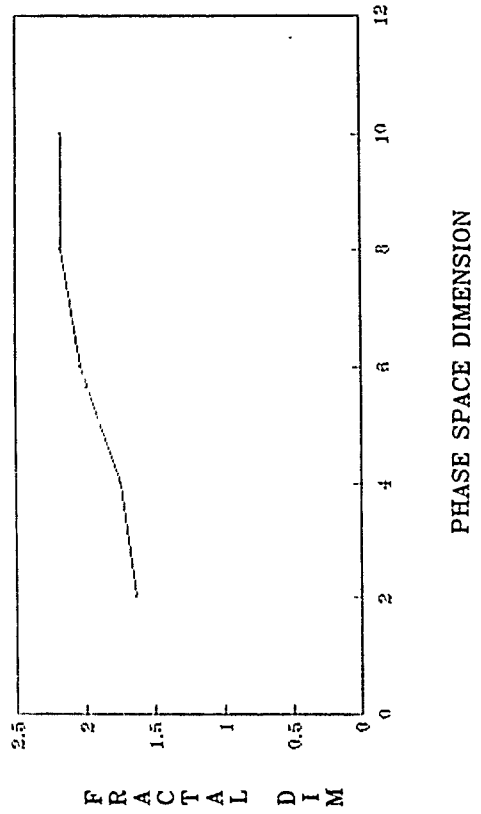

Figure J17. Fractal Dimension. F=166.7, Ω=13.8, C=.0454

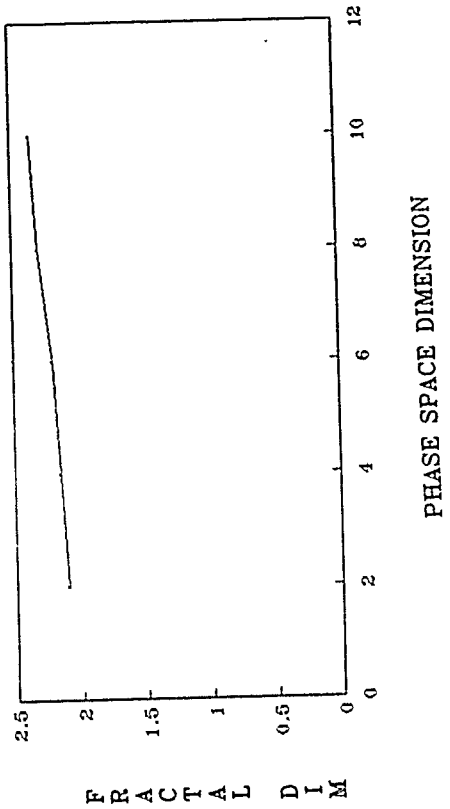

Figure J18. Fractal Dimension. F=208.4, Ω=13.8, C=.0454

LIST OF REFERENCES

1. Fisher, S., "Status of LACE Spacecraft," presented at Second USAF/NASA workshop, Pasadena, CA, (27 March 1990.)

2. Fisher, S., "LACE Flight Dynamics Experiment," presented at Third NASA/DOD CSI Technology Conference, San Diego, CA, (29 January 1990).

3. Denman, E., *et al.*, "Identification of Large Space Structures on Orbit," AFRPL-TR-86-054, Air Force Rocket Propulsion Laboratory, (September 1986).

4. Allen, D.H., and Haisler, W.E., *Introduction to Aerospace Structural Analysis*, John Wiley & Sons, Inc., 1985.

5. Cook, R.D., Malkus, D.S., and Plesha, M.E., *Concepts and Applications of Finite Element Analysis*, John Wiley & Sons, Inc., 1989.

6. Craig, R.R., *Structural Dynamics - An Introduction to Computer Methods*, John Wiley & Sons, Inc., 1981.

7. Bathe, K-J., and Wilson, E.L., *Numerical Methods in Finite Element Analysis*, Prentice Hall, Inc., 1976.

8. Bathe, K-J, *Finite Element Procedures in Engineering Analysis*, Prentice Hall, Inc., 1982.

9. *Computer Aided Structural Analysis/Graphical Interactive Finite Element Total System - Users Reference and Primer Manuals*, Tuscon, AZ: CASA/GIFTS, Inc., 1987.

10. "Automatically Deployable ABLE Booms," Goleta, CA: AEC-ABLE Engineering.

11. Agrawal, B.N., *Design of Geosynchronous Spacecraft*, Prentice Hall, Inc., 1986.

12. Kamel, H., Liu, D., McCabe, M., and Phillipoulos, V., "Some Developments in the Analysis of Complex Ship Structures," *Advances in Computational Methods in Structural Mechanics and Design*, J.T. Oden, *et al.*, (eds), University of Alabama Press, University of Alabama, 1972, pp. 703-726.

13. Ikeda, P.J., Brogren, E.W., "LACE Thermal Deformation," Information paper presented to NRL, (1 November 1989).

14. Hurty, W.C., "Dynamic Analysis of Structural Systems Using Component Modes," *AIAA Journal,* vol. 3, no. 4, (1965), 678-684.

15. Craig, R.R., and Bampton, M.C.C., "Coupling of Substructures for Dynamic Analysis," *AIAA Journal,* vol. 6, no. 7, (1968), 1313-1319.

16. Rubin, S., "Improved Component-Mode Representation for Structural Dynamics Analysis," *AIAA Journal,* vol. 13, no. 8, (1975), 995-1006.

17. MacNeal, R.H., "A Hybrid Method of Component Mode Synthesis," *Computers and Structures,* vol 1, (1971), 581-601.

18. Martina, D.R., and Miller, K.A., "Combined Experimental, Analytical Modeling of Dynamic Structural Systems," *The American Society of Mechanical Engineer,* (1985), 1-18.

19. Singh, R.P., VanderVoort, R.J., and Likins, P.W., "Dynamics of Flexible Bodies in TREE Topology - A Computer Oriented Approach," *Journal of Guidance, Control and Dynamics,* vol. 8, no. 5, (Sept.-Oct. 1985), 584-589.

20. "TREETOPS User Manual," Dynacs Engineering Co., Inc., Clearwater, FL.

21. Moon, F.C., *Chaotic Vibrations,* John Wiley & Sons, Inc., 1987.

22. Sarigul-Klijn, M.M., "Application of Chaos Methods to Helicopter Vibration Reduction Using Higher Harmonic Control,", Doctoral Dissertation, Naval Postgraduate School, Monterey, CA, (March 1990).

23. Thompson, M.T., and Steward,H.B., *Nonlinear Dynamics and CHAOS,* John Wiley & Sons, Inc., 1986

24. Guckenheimer, J., and Holmes, P., *Nonlinear Oscillations, Dynamical Systems and Bifurcations of Vector Fields,* Springer-Verlag, 1983

25. Grassberger, P., and Proccucia,I., "Characterization of Strange Attractors," Physics Review Letters, No. 50, (1983), 364-379.

26. Walters, Wesley F., AE4900 Report, "Parametric Study of Chaotic Vibrations in the LACE Spacecraft Boom," (1990)

27. Moon, F.C., and Li, G.X., "Experimental Study of Chaotic Vibrations in a Pin-Jointed Space Truss Structure," *AIAA Journal*, vol. 28, no. 5, (1990)

BIBLIOGRAPHY

Gere, J.M. and Timoshenko, S.P., *Mechanics of Materials,* PWS Publishers, 1984.

Hurty, W.C. and Rubinstein, M.F., *Dynamics of Structures,* Prentice-Hall, 1964.

Koffman, E.B., and Friedman, F.L., *Problem Solving and Structural Programming in Fortran 77,* Addison-Wesley Publishing Company, Inc., 1987.

Levy, S., and Wilkinson, J.P., *The Component Element Method in Dynamics,* McGraw-Hill Book Co., 1976.

Meirovitch, L., *Elements of Vibration Analysis,* McGraw-Hill Book Co., 1975.

Segerlind, L.J., *Applied Finite Element Analysis,* John Wiley & Sons, Inc., 1976.

Thomson, W.T., *Theory of Vibration with Applications,* Prentice-Hall, 1988.

INITIAL DISTRIBUTION LIST

1. Defense Technical Information Center — 2
   Cameron Station
   Alexandria, Virginia 22304-6145

2. Superintendent — 2
   Attn: Library, Code 1424
   Naval Postgraduate School
   Monterey, California 93943-5000

3. Department Chairman, Code AA — 1
   Department of Aeronautics and Astronautics
   Naval Postgraduate School
   Monterey, California 93943-5000

4. Department of Aeronautics and Astronautics — 20
   Attn: Professor Ramesh Kolar, Code AA/Kj
   Naval Postgraduate School
   Monterey, California 93943-5000

5. Department of Aeronautics and Astronautics — 1
   Attn: Professor Brij Agrawal, Code AA/Ag
   Naval Postgraduate School
   Monterey, California 93943-5000

6. Space Systems Academic Group — 1
   Attn: Professor Rudolph Panholzer, Code SP
   Naval Postgraduate School
   Monterey, California 93943-5000

7. Major Wesley F. Walters — 2
   293 Skinner Dr.
   Redstone Arsenal, AL 35808

8. Naval Research Laboratory — 2
   Attn: Dr. Shalom Fisher, Code 8240.1
   Washington, D.C., 20375